(2)

THE OHIO STATE UNIVERSITY

Relegation for Decentralized Control

Ü. Özgüner
Department of Electrical Engineering

Air Force Office of Scientific Research
Bolling Air Force Base
Washington, D.C. 20332-6448

Contract No. F49620-89-C-0046
Final Report
For the Period: March 1, 1989 - September 30, 1992

February 1993

REPORT DOCUMENTATION PAGE

Form Approved
OMB No. 0704-0188

1. AGENCY USE ONLY *(Leave blank)*	2. REPORT DATE	3. REPORT TYPE AND DATES COVERED
	February 1993	Final (March 1, 1989 - Sept. 30, 1992)

4. TITLE AND SUBTITLE

Relegation for Decentralized Control

5. FUNDING NUMBERS

Contract No.
F49620-89-C-0046

6. AUTHOR(S)

U. Ozguner

7. PERFORMING ORGANIZATION NAME(S) AND ADDRESS(ES)

The Ohio State University
Research Foundation
1960 Kenny Rd.
Columbus, OH 43210

8. PERFORMING ORGANIZATION REPORT NUMBER

RF 767334/721886

9. SPONSORING/MONITORING AGENCY NAME(S) AND ADDRESS(ES)

Air Force Office of Scientific Research
Bolling Air Force Base
Washington, D.C. 20332-6448

10. SPONSORING/MONITORING AGENCY REPORT NUMBER

11. SUPPLEMENTARY NOTES

12a. DISTRIBUTION/AVAILABILITY STATEMENT

Approved for public release,
distribution unlimited

12b. DISTRIBUTION CODE

13. ABSTRACT *(Maximum 200 words)*

14. SUBJECT TERMS	15. NUMBER OF PAGES 145
	16. PRICE CODE

17. SECURITY CLASSIFICATION OF REPORT	18. SECURITY CLASSIFICATION OF THIS PAGE	19. SECURITY CLASSIFICATION OF ABSTRACT	20. LIMITATION OF ABSTRACT

THE OHIO STATE UNIVERSITY

Relegation for Decentralized Control

Ü. Özgüner
Department of Electrical Engineering

Air Force Office of Scientific Research
Bolling Air Force Base
Washington, D.C. 20332-6448

Contract No. F49620-89-C-0046
Final Report
For the Period: March 1, 1989 - September 30, 1992
RF Project No. 767334/721886

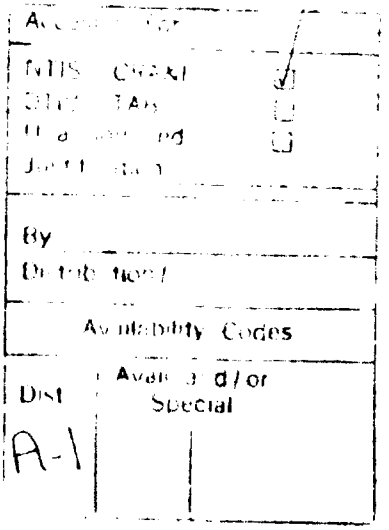

February 1993

OVERVIEW

In this report, we describe the total effort at Ohio State on the Project **Relegation for Decentralized Control**, initiated on March 1, 1989, sponsored by the Air Force Office of Scientific Research (AFSC), under Contract F49620–89–C–0046.

The first part of this report reflects on one of the primary research topics which was considered in the first year of research. This work performed in the first year concentrated on optimal relegation. In the second part of the report, we concentrate on circuit analogies for large flexible space structures. Many large-scale systems such as flexible spacecraft appendages are nonlinear in behavior. But their large scale makes centralized control difficult. Thus, we propose several methods for designing decentralized control laws that take system nonlinearities into account. Equally important is the task of modeling large-scale systems. This motivated research on applying well-known circuit theory techniques to the problem of modeling flexible structures. The third part of this report describes work performed on another primary research topic which was considered in the first year of research—the use of singular perturbations for multi–time scale analysis of two–link structures. This work was developed for use in embedding active materials into the links and relegating the control tasks. (That is, slewing was relegated to torque actuators at the joints and vibration damping was relegated to the film type materials along the links.) In the fourth part of the report, we focus on the problem of decentralized control of nonlinear systems. The next two parts of the report discusses results of using sliding–mode control on structures with closed chain kinematics and sampled–data systems, respectively. Finally, preliminary work was performed in using neural networks in the control of rigid-flexible structures. We then discuss example configurations being considered for application of the results in relegation, including new results on a specific configuration of interest which provides a set of new problems in structures with coupled rigid and flexible dynamics. This is the class of structures with closed chain kinematics. The specific example we have initiated work on is that of a planar truss. Extensive effort has been spent on modeling issues, leading to the utilization of decentralized sliding–mode (variable structure) control techniques.

Contributors to this three-year research effort were:
Students:
Dr. D. Schoenwald
Peter Dix
Mathew Boesch

Layne Lenning
Wu-Chung Su

Post-doctoral researchers:
Dr. Ken-Shin Xu
Dr. S. Drakunov

Principal Investigator:
Prof. Ü. Özgüner

Two book chapters and three journal publications have appeared based on research on this project. Twenty-six presentations were made at conferences and the papers appeared in the respective proceedings. Five papers are presently under review in various journals. The publications resulting from this research are listed in Appendix A.

Contents

List of Figures

List of Tables

1. INTRODUCTION

In this report, we describe the total effort at Ohio State on the Project **Relegation for Decentralized Control**, initiated on March 1, 1989, sponsored by the Air Force Office of Scientific Research (AFSC), under Contract F49620–89–C–0046.

The main thrust of our effort has been to consider the control of interconnected rigid and flexible structures. In order to accomplish this, we have utilized different analysis approaches, ranging from partial differential equations representing simple substructures, to finite element models representing complex structures. We have also initiated work in exploiting the analogies between circuits and systems. Much work remains to be done in this area. We have used different techniques for control. Apart from the basic linear quadratic regulator, we used series expansion techniques and singular perturbation in simplifying and decomposing high dimensional control problems and we have considered feedback linearization and variable structure control, in handling nonlinearities.

The following chapters will provide details of the results obtained through the tenure of the project.

In **Chapter 2** the work on the concept of *relegation* is outlined. Here we provide the basis for assigning control tasks to multiple coupled systems so that some some total criterion is minimized.

Chapter 3 is on our initial work on *circuit analogies*. This approach is even further developed at this time in a new project.

In **Chapter 4** the use of singular perturbations for multi–time scale analysis of two–link structures is developed. This technique was developed for use in imbedding active materials into the links and relegating the control tasks. (That is, slewing was relegated to torque actuators at the joints and vibration damping was relegated to the film type materials along the links.)

In **Chapter 5** we focus on the problem of decentralized control of nonlinear systems. Many large-scale systems such as flexible spacecraft appendages are nonlinear in behavior. But their large scale makes centralized control difficult. Thus, we propose several methods for designing decentralized control laws that take system nonlinearities into account.

Chapter 6 discusses results on a specific configuration of interest which provides a set of new problems in structures with coupled rigid and flexible dynamics. This is the class of structures with closed chain kinematics. The specific example we have initiated work on is that of a planar truss. Extensive effort has been spent on modeling issues, leading to the utilization of decentralized sliding–mode (variable

structure) control techniques. Recent results (produced jointly with Dr. D. Young of LLNL) on frequency shaping for sliding–mode control, have provided a means of handling the "chattering" phenomena, earlier thought to be a deterrent to the use of sliding–mode control with flexible structures.

In **Chapter 7** we provide initial results on the control of sampled systems with the sliding–mode control technique. This highly innovative approach is presently being further developed.

Finally in **Chapter 8** the utilization of neural networks for the identification and control is considered. This research was also partially supported by a NASA Doctoral Fellowship.

Chapter 9 provides some applications and examples of how and where our research results may be utilized. It especially outlines an experimental configuration (LIVE) which was developed for experiments on coupled rigid and flexible structures.

2. RELEGATION

In the control of large systems, the notion of decentralization plays an important role. The decentralization constraint enters into large-scale systems because it may be impractical or even impossible to communicate signals from one controller to another. Moreover, decentralization may be required by the control designer to achieve reliability and a degree of redundancy. It may also impose a structure to the control implementation by relegating control authority to separate channels. This chapter introduces and analyzes the concept of relegation for the design of decentralized controllers for large systems.

Relegation is the assignment of control tasks and information channels in view of control effectiveness, on-line computational complexity, controller capabilities, and physical and structural constraints [1, 2, 3]. In this chapter, one particular form of relegation will be introduced–namely *decentralized set–point relegation.* One is often faced with the task of selecting output set-points for subsystems given some physical constraints. Relegation is the idea of choosing these set-points in a rigorous, optimal fashion such that each subsystem's goals have been chosen to minimize the performance criterion of the overall system. This implies that the set-points are chosen to satisfy a constraint equation such that the performance index of the system is minimized. Redundancy in the choice of feasible set-points is exploited by choosing them to minimize the cost functional while maintaining a decentralized feedback structure. This is a unique approach to the decentralized quadratic regulator problem that will enable the choosing of system set-points optimally instead of using *ad hoc* methods.

The decentralized control utilized here consists of proportional state feedback and integral output error feedback for each input/output channel. The feedback gain matrix is obtained via the solution of two coupled Lyapunov equations. The optimal cost will then contain a term which is quadratic in the output set-points, and it is the minimization of this term subject to a linear or nonlinear constraint function which leads to the solution of the optimal choice of output set-points. In Section 2.1, we briefly consider the Decentralized Quadratic Regulator problem and introduce the idea of Decentralized Set–Point Relegation. In Section 2.2, we point out how set–points are incorporated into the quadratic regulator setting. We then indicate how these can be assigned to uncoupled subsystems while further minimizing the cost in Section 2.3. In Section 2.4, we outline the interconnected system configuration and advocate a series expansion method for calculation of the control. We also introduce an iterative linearization approach for use when the constraint equations are nonlinear. Section 9.2 contains an example of an optical tracking system on which the concept of relegation is demonstrated.

2.1 The Decentralized Quadratic Regulator

Consider the basic *decentralized quadratic regulator problem*:

$$\dot{x} = Ax + \sum_{i=1}^{N} B_i u_i, \quad x(0) = x_0 \tag{2.1}$$

$$y_i = C_i x, \quad i = 1, \ldots, N. \tag{2.2}$$

where N is the number of input/output channels, n is the dimension of x, m_i is the dimension of u_i, and p_i is the dimension of y_i. We wish to minimize the cost criterion

$$J = \int_0^\infty (x^T Q x + \sum_{i=1}^{N} u_i^T R_i u_i)\, dt \tag{2.3}$$

and the following feedback structure constraint

$$u_i = K_i\, y_i, \quad i = 1, \ldots, N. \tag{2.4}$$

It can be shown [4, 5, 6, 7, 8] that the necessary conditions for minimizing J given by (2.3) with the controller structure (2.4) imply the solution of the following system of nonlinear algebraic equations:

$$\begin{aligned} A_c^T P + P A_c + \bar{Q} &= 0 \\ A_c L + L A_c^T + X_0 &= 0 \end{aligned} \tag{2.5}$$

and

$$\nabla_{K_i} J = B_i^T P L C_i^T + R_i K_i C_i L C_i^T = 0 \tag{2.6}$$

where

$$\begin{aligned} A_c &= A + \sum_{i=1}^{N} B_i K_i C_i \\ \bar{Q} &= Q + \sum_{i=1}^{N} C_i^T K_i^T R_i K_i C_i \\ X_0 &= x_0\, x_0^T. \end{aligned}$$

Now consider the situation when each control channel has a set of variables y_{ri} to be regulated and these have been assigned output *set-points* y_i^d, $i = 1, .., N$. Note that we differentiate here between the local measurements and the local variables to

be regulated. If the set-points are pre-determined and fixed, fairly straightforward extensions to the decentralized regulator problem are possible to find the associated controllers. However, in many problems of interest, e.g. large space structures, robotics, and manufacturing, these set-points jointly satisfy a constraint equation. Their one-to-one assignment to channels is not obvious. We shall call this *the decentralized set-point relegation problem* (see Figure 2.1). Depending on the type of

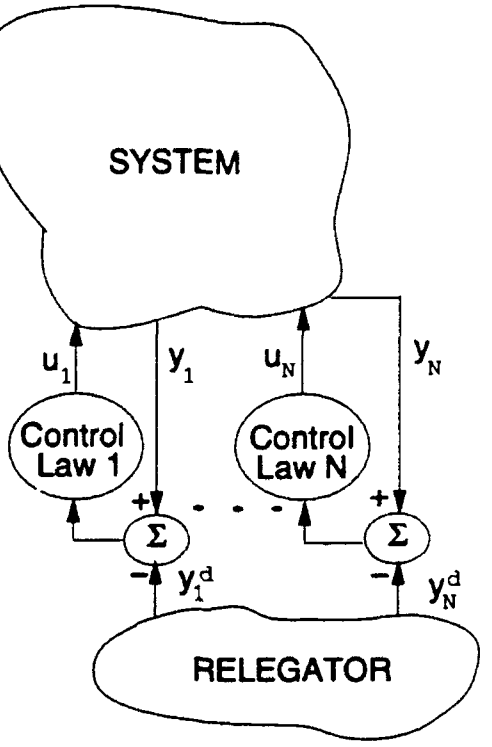

Figure 2.1: Set Point Relegation

constraints the set–points need to satisfy, there are a number of distinct special cases of interest in decentralized set–point relegation:

1. Linear constraints
2. Nonlinear constraints
3. Time–varying constraints

In this chapter, we shall consider the first two cases above. The third case represents a trajectory relegation problem which is not specifically addressed here. The three types of constraints above may arise due to physical considerations of the problem but may also be due to computational aspects of the problem as well. It is assumed

that these constraints do not uniquely specify the set-points, but rather allow a choice of feasible set-points possibly even an infinite number of choices.

2.2 Incorporation of Set–Points

We first outline the incorporation of set–points into the standard centralized quadratic regulator problem. To motivate this, we consider the multi-input, multi-output system

$$\begin{aligned} \dot{x} &= Ax + Bu \\ y_r &= Cx\,, \end{aligned} \tag{2.7}$$

under the cost criterion

$$J = \int_0^\infty (z^T Q z + \dot{u}^T R \dot{u}) dt\,, \tag{2.8}$$

where $z(t)$ is defined as

$$z(t) \triangleq \begin{bmatrix} \dot{x} \\ \Delta y \end{bmatrix} \tag{2.9}$$

$$\Delta y(t) \triangleq y_r(t) - y^d\,, \tag{2.10}$$

and y^d, a constant set point, has been specified.

The state equations for the system with $\dot{u}$ as input and z as state vector can now be written. If Q =block-diag$\{Q_1, Q_2\}$ then the solution of the above problem takes the form

$$u = K^1 x + K^2 \int_0^t (y_r(\tau) - y^d) d\tau \tag{2.11}$$

where the $\{K^1, K^2\}$ pairs are calculated from the associated Riccati equations.

Let the matrix solution to the Riccati equation be partitioned as

$$P = \begin{bmatrix} P_1 & P_3 \\ P_3^T & P_2 \end{bmatrix}$$

and let

$$S = BR^{-1}B^T.$$

Then the Riccati equation decouples into three equations:

$$-P_3^T S P_3 + Q_2 = 0$$

$$P_3^T A + P_2 C - P_3^T S P_1 = 0$$

$$A^T P_1 + C^T P_3^T + P_1 A + P_3 C - P_1 S P_1 + Q_1 = 0\,.$$

As can be seen, P_3 can be calculated from the first equation. Then

$$P_2 = P_3^T (A - S P_1) C^T (C C^T)^{-1}\,, \tag{2.12}$$

and P_1 can be calculated from the Riccati equation

$$A^T P_1 + P_1 A - P_1 S P_1 + (Q + C^T P_3^T + P_3 C) = 0\,. \tag{2.13}$$

The optimal cost is given by

$$J^* = z^T(0) P z(0)\,. \tag{2.14}$$

Since $z(0)$ contains y^d , the optimal cost J^* is a function of the value of the set-point. In problems where there is some freedom in choosing these set-points, it is easily seen that one set of y_d can produce a lower J^* than another set. Therefore, we look at ways in which the set-points can be chosen to minimize J^* while maintaining the decentralized nature of the control laws.

2.3 Relegation for Uncoupled Systems

Consider the set of dynamically uncoupled linear subsystems

$$\begin{aligned} \dot{x}_i &= A_i x_i + B_i u_i \\ y_{ri} &= C_i x_i \qquad i = 1, 2, \ldots, N, \end{aligned} \tag{2.15}$$

under the cost criterion

$$J = \sum_{i=1}^{N} \int_0^\infty (z_i^T Q_i z_i + u_i^T R_i u_i) dt\,. \tag{2.16}$$

The state z_i is defined as

$$z_i(t) \triangleq \begin{bmatrix} \dot{x}_i \\ \Delta y_i \end{bmatrix} \tag{2.17}$$

$$\Delta y_i(t) \triangleq y_{ri}(t) - y_i^d, \tag{2.18}$$

where y_i^d is a constant set point.

The solution of the above problem takes the form

$$u_i = K_i^1 x_i + K_i^2 \int_o^t (y_{ri}(\tau) - y_i^d) d\tau \quad , \quad i = 1, 2, \ldots, N \tag{2.19}$$

where neither the relative feedback nor the solution for $\{K_i^1, K_i^2\}$ are coupled. In fact, the $\{K_i^1, K_i^2\}$ pairs are calculated from uncoupled Riccati equations which provide the matrix pairs $\{P_1^i, P_2^i\}$ such that the optimal cost is given by

$$J^* = \sum_{i=1}^{N} z_i^T(0) P^i z_i(0). \tag{2.20}$$

We now assume that one step above on the hierarchy there exists a *relegator* (see Figure 2.1) which must specify the $\{y_i^d\}$ set points, constrained with a set of linear, static equations of the general form

$$\sum_{i=1}^{N} F_i y_i^d = G. \tag{2.21}$$

The question now is whether the relegator can pick a specific set $\{y_i^d\}$ that satisfies the constraints (2.21) while further minimizing J^*. Thus, we consider the problem

$$\min_{y_i^d} J^* = \min_{y_i^d} \sum_{i=1}^{N} (y_{ri}(0) - y_i^d)^T P_2^i (y_{ri}(0) - y_i^d) \tag{2.22}$$

such that (2.21) holds. This is equivalent to minimizing

$$\hat{J} = \sum_{i=1}^{N} (y_i^d)^T P_2^i y_i^d - 2 y_{ri}^T(0) P_2^i y_i^d + \Lambda^T (F_i y_i^d) - \Lambda^T G, \tag{2.23}$$

where Λ is a vector of Lagrange multipliers. In such a minimization exercise, we obtain

$$\frac{\partial \hat{J}}{\partial y_i^d} = 2P_2^i y_i^d - 2P_2^i y_{ri}(0) + F_i^T \Lambda = 0 \tag{2.24}$$

for $i = 1, \ldots, N$. In view of this and (2.21),

$$y_i^d = y_{ri}(0) - 0.5(P_2^i)^{-1} F_i^T \Lambda \,, \tag{2.25}$$

and

$$\Lambda = 2[\sum_{i=1}^{N} F_i (P_2^i)^{-1} F_i^T]^{-1} [\sum_{i=1}^{N} F_i y_{ri}(0) - G] \tag{2.26}$$

to give

$$y_i^d = y_{ri}(0) - (P_2^i)^{-1} F_i [\sum_{i=1}^{N} F_i (P_2^i)^{-1} F_i^T]^{-1} [\sum_{i=1}^{N} F_i y_{ri}(0) - G] \tag{2.27}$$

for $i = 1, \ldots, N$. Equation (2.27) represents the decisions taken by the relegator to satisfy (2.21) while minimizing J^*.

2.4 Relegation for Coupled Systems

We now consider the special case of interconnected systems with local state measurements available for feedback. We shall furthermore assume that a local output vector is to be regulated to a given set point. Consider the set of dynamically coupled linear subsystems,

$$\begin{aligned} \dot{x}_i &= \sum_{j=1}^{N} A_{ij} x_j + B_i u_i \\ y_{ri} &= C_i x_i \,, \quad i = 1, 2, \ldots, N \end{aligned} \tag{2.28}$$

where N is the number of input/output channels, n_i is the dimension of x_i , m_i is the dimension of u_i , and p_i is the dimension of y_{ri} . We wish to minimize the cost criterion

$$J = \frac{1}{2} \sum_{i=1}^{N} \int_0^\infty (z_i^T Q_i z_i + \dot{u}_i^T R_i \dot{u}_i)\, dt \tag{2.29}$$

where $z_i(t)$ is the $n_i + p_i$ dimension vector defined as

$$z_i(t) = \begin{bmatrix} \dot{x}_i \\ \Delta y_i \end{bmatrix} \tag{2.30}$$

$$\Delta y_i = y_{ri} - y_i^d \tag{2.31}$$

$$z_i(0) = \begin{bmatrix} \dot{x}_i(0) \\ \Delta y_{ri}(0) \end{bmatrix} = z_{i0} \tag{2.32}$$

with Q_i positive semi-definite and R_i positive definite matrices of appropriate dimensions. A more compact cost criterion is defined as

$$J = \frac{1}{2}\int_0^\infty \left(z^T Q z + \dot{u}^T R \dot{u}\right) dt \tag{2.33}$$

where $Q = \text{block-diag}\,[Q_1 \cdots Q_N]$ and $R = \text{block-diag}\,[R_1 \cdots R_N]$.
We redefine (2.28) in the state z as

$$\dot{z} = \begin{bmatrix} A_{11} & 0 & A_{12} & 0 & \dots & A_{1N} & 0 \\ C_1 & 0 & 0 & 0 & \dots & 0 & 0 \\ A_{21} & 0 & A_{22} & 0 & \dots & A_{2N} & 0 \\ 0 & 0 & C_2 & 0 & \dots & 0 & 0 \\ & & & \vdots & & & \\ A_{N1} & 0 & A_{N2} & 0 & \dots & A_{NN} & 0 \\ 0 & 0 & 0 & 0 & \dots & C_N & 0 \end{bmatrix} z + \begin{bmatrix} B_1 & \dots & 0 \\ 0 & \dots & 0 \\ 0 & \dots & 0 \\ 0 & \dots & 0 \\ & \vdots & \\ 0 & \dots & B_N \\ 0 & \dots & 0 \end{bmatrix} \dot{u} \tag{2.34}$$

or more compactly,

$$\dot{z} = \hat{A}z + \hat{B}\dot{u}\,, \tag{2.35}$$

with decentralized feedback

$$\begin{aligned} \dot{u}_i &= K_i z_i = K_i^1 \dot{x}_i + K_i^2 \Delta y_i\,, \quad K_i = [K_i^1 \;\; K_i^2] \\ \dot{u} &= Kz\,, \quad K = \text{Block-diag}[K_1, K_2, \dots, K_N] \end{aligned} \tag{2.36}$$

such that each channel input has the form

$$u_i = K_i^1 x_i + K_i^2 \int_0^t (y_{ri}(\tau) - y_i^d)\, d\tau\,, \quad i = 1, 2, \dots, N\,. \tag{2.37}$$

The optimal solution for the decentralized feedback gain matrix K to the minimization of the quadratic cost criterion J is known to involve the iterative solution of two coupled Lyapunov equations as mentioned before. It is well known that the cost associated with any stabilizing feedback is, in fact, $z^T(0)Pz(0)$ where P is the solution of the related Lyapunov equation

$$A_c^T P + P A_c + \bar{Q} = 0\,. \tag{2.38}$$

In the event of weakly coupled subsystems (ϵ-coupling), a series expansion method [9, 10] is advocated to solve for the feedback gain matrix K. This series expansion will also give an approximation to the weighting factors $\{P_2^i\}$ to be used in the set-point distribution.

We use the series expansion (ϵ-coupling) method to generate the local feedback solution for weakly coupled systems where the local states are available at the subsystem level. We shall embed a coupling parameter ϵ between the subsystems so that the equations satisfying the necessary condition of optimality are as given below:

$$\bar{A}_c = \begin{bmatrix} A_{11} + B_1 K_1 & \epsilon A_{12} \\ \epsilon A_{21} & A_{22} + B_2 K_2 \end{bmatrix}$$

$$\bar{Q}_c = \begin{bmatrix} Q_1 + K_1^T R_1 K_1 & 0 \\ 0 & Q_2 + K_2^2 R_2 K_2 \end{bmatrix}$$

Partition P and L as

$$P = \begin{bmatrix} P_1 & P_3 \\ P_3^T & P_2 \end{bmatrix}$$

$$L = \begin{bmatrix} L_1 & L_3 \\ L_3^T & L_2 \end{bmatrix}$$

The gradients (2.6) are then

$$\nabla_{K1} J = 2[B_1^T(P_1 L_1 + P_3 L_3^T) + R_1 K_1 L_1] = 0 \tag{2.39}$$

$$\nabla_{K2} J = 2[B_2^T(P_3 L_3 + P_2 L_2^T) + R_2 K_2 L_2] = 0\,. \tag{2.40}$$

The coupled Lyapunov equations (2.5) become

P equations

$$(A_{11}+B_1K_1)^TP_1+\epsilon A_{21}^TP_3^T+\epsilon P_3A_{21}+P_1(A_{11}+B_1K_1) +(Q_1+K_1^TR_1K_1)=0 \tag{2.41}$$

$$(A_{22}+B_2K_2)^TP_2+\epsilon A_{12}^TP_3^T+\epsilon P_3A_{12}+P_2(A_{22}+B_2K_2) +(Q_2+K_2^TR_2K_2)=0 \tag{2.42}$$

$$(A_{11}+B_1K_1)^TP_3+\epsilon A_{21}^TP_2+\epsilon P_1A_{12}+P_3(A_{22}+B_2K_2)=0 \tag{2.43}$$

L equations

$$(A_{11}+B_1K_1)L_1+\epsilon A_{12}L_3^T+\epsilon L_3A_{12}^T+L_1(A_{11}+B_1K_1)^T +X_{01}=0 \tag{2.44}$$

$$(A_{22}+B_2K_2)L_3+\epsilon A_{21}L_3^T+\epsilon L_3A_{21}^T+L_2(A_{22}+B_2K_2)^T +X_{02}=0 \tag{2.45}$$

$$(A_{11}+B_1K_1)L_3+\epsilon A_{12}L_2+\epsilon L_1A_{21}^T+L_3(A_{22}+B_2K_2)^T=0\,. \tag{2.46}$$

Consider now the power series expansion in terms of ϵ for P and L

$$P=P^0+\epsilon P^1+\frac{1}{2}\epsilon^2P^2+\cdots$$

$$L=L^0+\epsilon L^1+\frac{1}{2}\epsilon^2L^2+\cdots$$

resulting in the power series for K.

$$K=K^0+\epsilon K^1+\frac{1}{2}\epsilon^2K^2+\cdots$$

We shall henceforth use the superscript to indicate both the order of the derivative and the term in the series expansion.

0'th order terms:

Setting $\epsilon = 0$ Eq. (2.43) becomes

$$(A_{11}+B_1K_1^0)^TP_3^0+P_3^0(A_{22}+B_2K_2^0)=0\,. \tag{2.47}$$

We temporarily assume the following assertion to be true:

Assertion I : K_1^0 and K_2^0 asymptotically stabilize the subsystems $\{A_{11},B_1\}$ and $\{A_{22},B_2\}$.

With Assertion I applied to the unique solution of Eq. (2.47) (and similarly from Eq. (2.46)), we obtain

$$P_3^0 \equiv 0\,, \quad L_3^0 \equiv 0\,.$$

With $\epsilon = 0$ Eq. (2.44) is a Lyapunov equation and under Assertion I admits a positive definite solution for L_1^0. Thus Eq. (2.39) simplifies to

$$B_1^T P_1^0 + R_1 K_1^0 = 0\,.$$

Substituting into Eq. (2.41) at $\epsilon = 0$ we obtain the standard subsystem Riccati equation:

$$A_{11}^T P_1^0 + P_1^0 A_{11} - P_1^0 B_1 R_1^{-1} B_1^T P_1^0 + Q_1 = 0\,.$$

Similar arguments result in the Riccati equation for the second subsystem. Therefore, if $\{A_{11}, B_1\}$ and $\{A_{22}, B_2\}$ are stabilizable pairs, Assertion I is indeed true.

1'st order term

Under Assertion I and the solution of the 0'th order equation we will find that $K_1^1, K_2^1, P_1^1, P_2^1, L_1^1, L_2^1$ are all zero. The terms P_3^1 and L_3^1 can be calculated from the linear equations

$$(A_{11} + B_1 K_1^0)^T P_3^1 + P_3^1 (A_{22} + B_2 K_2^0) + A_{21}^T P_2^0 + P_1^0 A_{12} = 0$$

$$(A_{11} + B_1 K_1^0) L_3^1 + L_3^1 (A_{22} + B_2 K_2^0)^T + A_{12}^T L_2^0 + L_1^0 A_{21}^T = 0\,.$$

2nd order terms

P_1^2 is solved from

$$(A_{11} + B_1 K_1^0)^T P_1^2 + P_1^2 (A_{22} + B_1 K_1^0) + A_{21}^T P_3^{1T} + P_3^1 A_{21} = 0\,.$$

Then K_1^2 is

$$K_1^2 = -R_1^{-1} B_1^T P_1^2 - 2 R_1^{-1} P_3^1 L_3^{1T} (L_1^0)^{-1}\,.$$

The following terms can then be sequentially generated. Note that the odd order terms will give no local feedback, yet one intermediate set of linear matrix equations will still have to be solved. After the 0'th order term the local feedbacks are calculated from Lyapunov equations.

At this point we assume there exists a *relegator* whose function is to specify the y^d set-points subject to the following set of nonlinear constraints

$$H_i(y^d) = 0\,, \quad i = 1, 2, \ldots, N \tag{2.48}$$

where $H_i(y^d)$ is a scalar function of the output set-points vector y^d. Because general nonlinear functions are difficult to solve, we shall expand $H_i(y^d)$ about a point $\bar{y}$ that represents the current estimate of y^d. The power series is carried to quadratic terms in y^d

$$H_i(y^d) = H_i(\bar{y}) + \frac{\partial H_i(\bar{y})}{\partial y^d}(y^d - \bar{y}) + \frac{1}{2}(y^d - \bar{y})^T \frac{\partial^2 H_i(\bar{y})}{\partial (y^d)^2}(y^d - \bar{y}) \tag{2.49}$$

for $i = 1, 2, \ldots, N$, where the gradients are defined as

$$\frac{\partial H_i(\bar{y})}{\partial y^d} = \left[\begin{array}{cccc} \frac{\partial H_i(\bar{y})}{\partial y_1^d} & \frac{\partial H_i(\bar{y})}{\partial y_2^d} & \cdots & \frac{\partial H_i(\bar{y})}{\partial y_N^d} \end{array} \right], \tag{2.50}$$

and the Hessians are defined as

$$\frac{\partial^2 H_i(\bar{y})}{\partial (y^d)^2} = \left[\begin{array}{ccc} \frac{\partial^2 H_i(\bar{y})}{\partial (y_1^d)^2} & \cdots & \frac{\partial^2 H_i(\bar{y})}{\partial y_N^d y_1^d} \\ \vdots & & \vdots \\ \frac{\partial^2 H_i(\bar{y})}{\partial y_1^d y_N^d} & \cdots & \frac{\partial^2 H_i(\bar{y})}{\partial (y_N^d)^2} \end{array} \right]. \tag{2.51}$$

We wish to minimize the following cost criterion with respect to y^d

$$\begin{aligned} \hat{J} &= y^{dT} P_2 y^d - 2y_r(0)^T P_2 y^d + \sum_{i=1}^{N} \Lambda_i [H_i(\bar{y}) \frac{\partial H_i(\bar{y})}{\partial y^a}(y^d - \bar{y}) \\ &+ \frac{1}{2}(y^d - \bar{y})^T \frac{\partial^2 H_i(\bar{y})}{\partial (y^d)^2}(y^d - \bar{y})] \end{aligned} \tag{2.52}$$

where Λ_i are a set of Lagrange multipliers. We proceed by setting the gradient of $\hat{J}$ equal to zero and solving for y^d obtaining

$$y^d = [2P_2 + \sum_{i=1}^{N} \frac{\partial^2 H_i(\bar{y})}{\partial (y^d)^2} \Lambda_i]^{-1} [2P_2 y_r(0) - \sum_{i=1}^{N} (\frac{\partial H_i(\bar{y})^T}{\partial y^d} - \frac{\partial^2 H_i(\bar{y})}{\partial (y^d)^2} \bar{y}) \Lambda_i] \tag{2.53}$$

where Λ_i, $i = 1, 2, \ldots, N$, are solved for by substituting (2.53) into (2.49). This motivates the following algorithm to solve for y^d [3]:

1.) Choose $\bar{y} = 0$ initially and some tolerance δ.
2.) Evaluate $H_i(\bar{y})$, $\frac{\partial H_i(\bar{y})}{\partial y^d}$, and $\frac{\partial^2 H_i(\bar{y})}{\partial (y^d)^2}$ for $i = 1, 2, \ldots, N$.
3.) Solve for Λ_i, $i = 1, 2, \ldots, N$ by substituting (2.53) into (2.49).

4.) Using above, solve for y^d by solving (2.53) for its p components.
5.) If $\| y^d - \bar{y} \| \leq \delta$ then stop; otherwise set $\bar{y} = y^d$ and go to step 2.

It should be noted that with some sacrifice in accuracy one can linearize (2.49) instead of expanding to second order and obtain the following simpler equations for Λ_i and y^d

$$\frac{\partial H_i(\bar{y})}{\partial y^d} P_2^{-1} \sum_{i=1}^{N} \frac{\partial H_i(\bar{y})^T}{\partial y^d} \Lambda_i = 2[H_i(\bar{y}) + \frac{\partial H_i(\bar{y})}{\partial y^d}(y_r(0) - \bar{y})], \tag{2.54}$$

for $i = 1, 2, \ldots, N$. Then y^d is computed using

$$y^d = y_r(0) - 0.5 P_2^{-1} \sum_{i=1}^{N} \frac{\partial H_i(\bar{y})^T}{\partial y^d} \Lambda_i . \tag{2.55}$$

The algorithm above is still followed to find y^d except Hessian information is no longer needed. This algorithm represents the action of the relegator in choosing the set-points for each subsystem. An example of this algorithm is presented in Section 9.2.

A number of comments can be made regarding the problem outlined:

1. Note that y_i^d depends on $y_{ri}(0)$ which may be assumed known. Also, y_i^d can be solved for assuming $y_{ri}(0) = 0$.
2. Equation (2.21) may be generalized to (slowly) time varying constraints. In this case, one could implement the relegation scheme described in this chapter at a series of operating points.
3. The quadratic regulator problem can be generalized to accommodate frequency weighting. Note that the interesting and intuitively obvious conclusion that a band limited actuator will be given a "closer" set point to achieve.

In conclusion, it can be observed that decentralized setpoint relegation provides the hierarchical framework that couples a version of resource allocation with the dynamics of the controlled system. This is accomplished in a globally optimal manner, that is, both the high-level resource allocation (or target allocation) and the lower level dynamic control problem have a single goal. We believe this to be a very general framework that can be utilized in many large scale system problems.

3. MODELING AND CONTROL OF FLEXIBLE STRUCTURES USING CIRCUIT ANALOGIES

Large space structures (LSS) may be viewed as an interconnection of several substructures or networks. Essentially, the vibration control problem of flexible structures can be approached as a power transfer problem—similar to problems in transmission line theory or electrical circuits. The propagation of disturbances in LSS with light damping is mathematically similar to the electrical characteristics of a lossless transmission line. Thus, each of the substructures may be described in terms of scattering parameters similar to those of an electrical network.

The scattering parameters can be derived from either a partial differential equation (PDE) model of the structure or from the finite element model (FEM) of the structure. Like transmission lines, LSS are distributed parameter systems; therefore, they exhibit wave modes similar to those encountered in the PDE approach. FEMs are merely approximations of PDE models. For lumped parameter models such as FEMs, lumped parameter circuit analogies of LSS may be obtained directly from the FEM equations. Therefore, the scattering parameters of the structures may be obtained using circuit analysis techniques. As an example, a FEM of a beam can be broken into an interconnection of passive four-port networks.

The PDE models have been used in various control approaches such as the traveling wave approach. In the traveling wave approach to flexible structure control, the disturbances to a structure are viewed as waves traveling through a medium. These waves can be reflected, partially reflected, or dissipated as they travel across the structure. At interfaces within the structure, scattering properties may be examined—how much of an incoming wave is reflected and how much is absorbed. With this perspective, the flow of these disturbances through the structure may be more easily understood.

Since the propagation of disturbances in a mechanical system is mathematically similar to that of electrical or microwave circuits, the motivation for this work is to reconsider circuit analogies of mechanical systems and use existing results from circuit theory and network theory in the analysis and design of LSS.

The scattering parameters of a flexible structure have been determined both from the wave formulation from the PDE model and from a circuit analogy of the FEM. The coupling of structures has been analyzed from an impedance matching (circuit) and a substructure synthesis (FEM) viewpoint. Component Mode Synthesis (CMS) techniques for modeling LSS and active vibration damping have also been considered in the framework of scattering parameters.

3.1 Circuit Analogies of Mechanical Systems

Circuit analogies of mechanical systems have existed for many years. When the history of mechanical and electrical systems is considered, the complementary progress of the two areas is evident. Results of electrical network theory have many applications to acoustical, mechanical, and electromechanical systems. Included in these applications is vibration control of large flexible structures.

Typical examples of circuit analogies for mechanical systems are shown in Table 3.1.

Table 3.1: Electrical / Mechanical System Analogies

ELECTRICAL	MECHANICAL (LINEAR)	MECHANICAL (ROTATIONAL)
voltage, V	velocity, v, $\dot{x}$	angular velocity, ω, $\dot{\theta}$
current, I, $\dot{q}$	force, F	torque, τ
charge, q	momentum, P	angular momentum, h
flux linkage, λ	displacement, x	angular displacement, θ
capacitance, C	mass, M	moment of inertia, J
inverse of inductance, $\frac{1}{L}$	stiffness, K	rotational stiffness, K
inverse of resistance, $\frac{1}{R}$	viscous damping, β	viscous damping, β

Using these circuit analogies, the the analogous systems of equations for electrical and mechanical systems are:

$$I_{ext} = C\dot{V} + \frac{1}{R}V + \frac{1}{L}\int V\,dt \tag{3.1}$$

$$F_{ext} = M\ddot{x} + \beta\dot{x} + Kx \tag{3.2}$$

$$\tau_{ext} = J\ddot{\theta} + \beta\dot{\theta} + K\theta \tag{3.3}$$

For a general n-port network as shown in Figure 3.1, the *port-voltage* and *port-current vectors* are defined as

$$v(t) = [v_1(t), v_2(t), \ldots, v_N(t)]^T \tag{3.4}$$

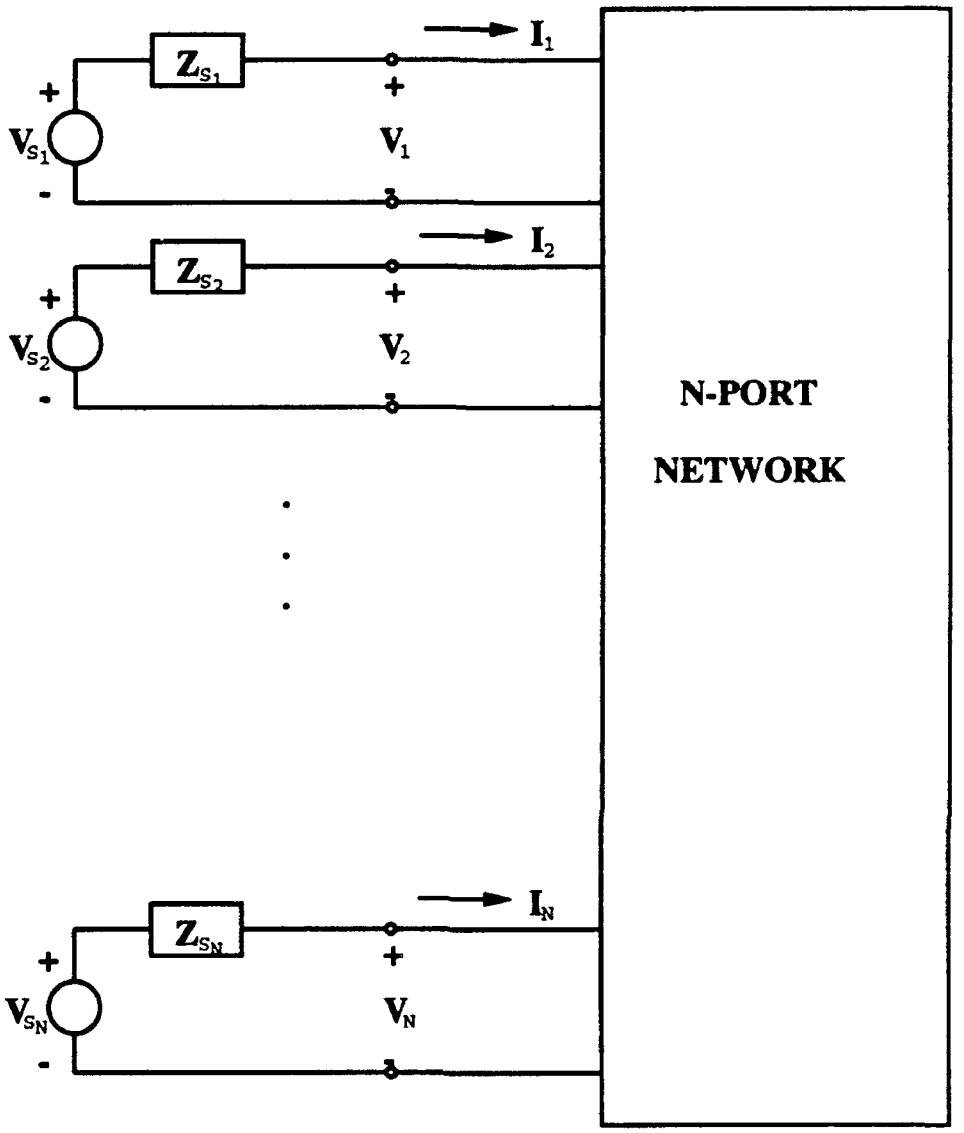

Figure 3.1: General representation of an N-port network.

$$i(t) = [i_1(t), i_2(t), \ldots, i_N(t)]^T \tag{3.5}$$

The *open circuit impedance matrix*, $Z(s)$, is defined such that

$$V(s) = Z(s)I(s) \tag{3.6}$$

where

$$Z_{ij} = \left.\frac{V_i}{I_j}\right|_{I_k=0 \ \forall \ k\neq j} \tag{3.7}$$

Similarly, the *short circuit admittance matrix*, $Y(s)$, is defined such that

$$I(s) = Y(s)V(s) \tag{3.8}$$

where

$$Y_{ij} = \left.\frac{I_i}{V_j}\right|_{V_k=0 \ \forall \ k\neq j} \tag{3.9}$$

These impedance and admittance matrices do not always exist because they are defined in terms of zero or infinite loading at the ports. Alternatively, scattering matrices may be used to characterize the network because they:

- *exist* for all "nonpathological" passive LTI networks (lumped or distributed parameter systems)
- are defined in terms of some *finite stable loadings* at the ports
- have *widely known properties* (much literature exists)
- are closely related to *power transfer properties* of a network; thus, several quantities of interest are simply and concisely represented in terms of scattering parameters
- are particularly useful in problems concerning power transfer, lossless networks, and network matching
- can be derived from either a *PDE* model or a *FEM* of the structure

3.2 Scattering Parameters

Again, consider the n-port shown in Figure 3.1. The normalized port-voltage and port-current vectors, V and I, are defined as

$$\begin{aligned} V &= \sqrt{R_o}^{-1} V' \\ I &= \sqrt{R_o} I' \end{aligned}$$

where V' and I' are the "ordinary" voltage and current vectors, which would actually be *measured* at the ports, and R_o is a normalizing matrix. The incident and reflected

voltage vectors, V_i and V_r, are defined to satisfy

$$V_i = \frac{1}{2}(V + I) \tag{3.10}$$

$$V_r = \frac{1}{2}(V - I) \tag{3.11}$$

where $V_s = 2V_i$ and V_s and Z_s are the voltage vector at the source and the input (source) impedance matrix, respectively.

The scattering matrix, S, is defined such that

$$V_r = SV_i \tag{3.12}$$

where

$$0 \leq |S_{ij}| \leq 1 \tag{3.13}$$

Further, if the normalized impedance matrix, Z, is defined such that

$$V = ZI \tag{3.14}$$

then

$$S = (Z + U)^{-1}(Z - U) = (Z - U)(Z + U)^{-1} \tag{3.15}$$

where U is the identity matrix. This is equivalent to

$$S = (Z' + R_o)^{-1}(Z' - R_o) = (Z' - R_o)(Z' + R_o)^{-1} \tag{3.16}$$

where Z' is the "ordinary" open circuit impedance matrix.

As an example, the impedance and scattering parameters at the end of a cantilevered beam were calculated from a PDE model and an eight-element FEM. Assuming unit source impedance, the open circuit impedance and the scattering parameter from the PDE approach were determined numerically, using a FORTRAN program to generate the Bode plots in Figures 3.2 and 3.3.

Using the circuit analogies, the *impedance matrix* from the FEM is defined as

$$Z(s) = (sM + \frac{K}{s})^{-1} \tag{3.17}$$

where M and K are the mass and stiffness matrices, respectively. The *scattering matrix* is then defined as

$$S(s) = \frac{Z(s) - R}{Z(s) + R} \tag{3.18}$$

Plots of the Bode responses for $Z_{11}(s)$ and $S_{11}(s)$, assuming unit input impedances, are shown in Figures 3.4 and 3.5. These parameters correspond to the impedance and scattering parameters at the tip of the beam.

Circuit synthesis techniques can be applied to structure synthesis. Connecting substructures is analogous to connecting circuit networks. The impedance or scattering parameter of the entire structure can be determined from the impedances of the interconnected substructures as one would determine the impedance of a circuit. CMS methods have been studied in this context.

The circuit equivalent of a linear proof-mass actuator has been developed. This can now be used for controller design. Controllers may be inserted at a substructure interface or at some other location on the substructure for decentralized control. The use of feedback for structural vibration control is analogous to the use of dependent current sources in the circuit equivalent of the structure. Another interesting approach is to represent actuators or substructures with their Thevenin or Norton equivalents.

Using overlapping decomposition, the circuit/structure can be separated for decentralized controller design. Controllers may be designed to achieve certain scattering properties or to achieve certain voltage/velocity properties. H_2 or H_∞ design techniques could be used in these designs.

In conclusion, circuit analogies of mechanical systems have been used to establish a framework for analyzing LSS. Using these analogies, the scattering properties of LSS can be characterized in terms of the scattering parameters. These scattering parameters may be found from either a PDE model or a FEM. This method of modeling provides insight into the scattering properties which can be exploited for controller design.

Using this approach, work is in progress to explore applications to Controlled Component Synthesis and Overlapping Decomposition. Furthermore, controller designs which "shape" scattering parameters as desired are being considered. Existing broadband matching and network synthesis techniques may be used in actuator and controller design–for both active and passive damping. Established circuit parameter sensitivity results may also be used to analyze structure parameter sensitivity.

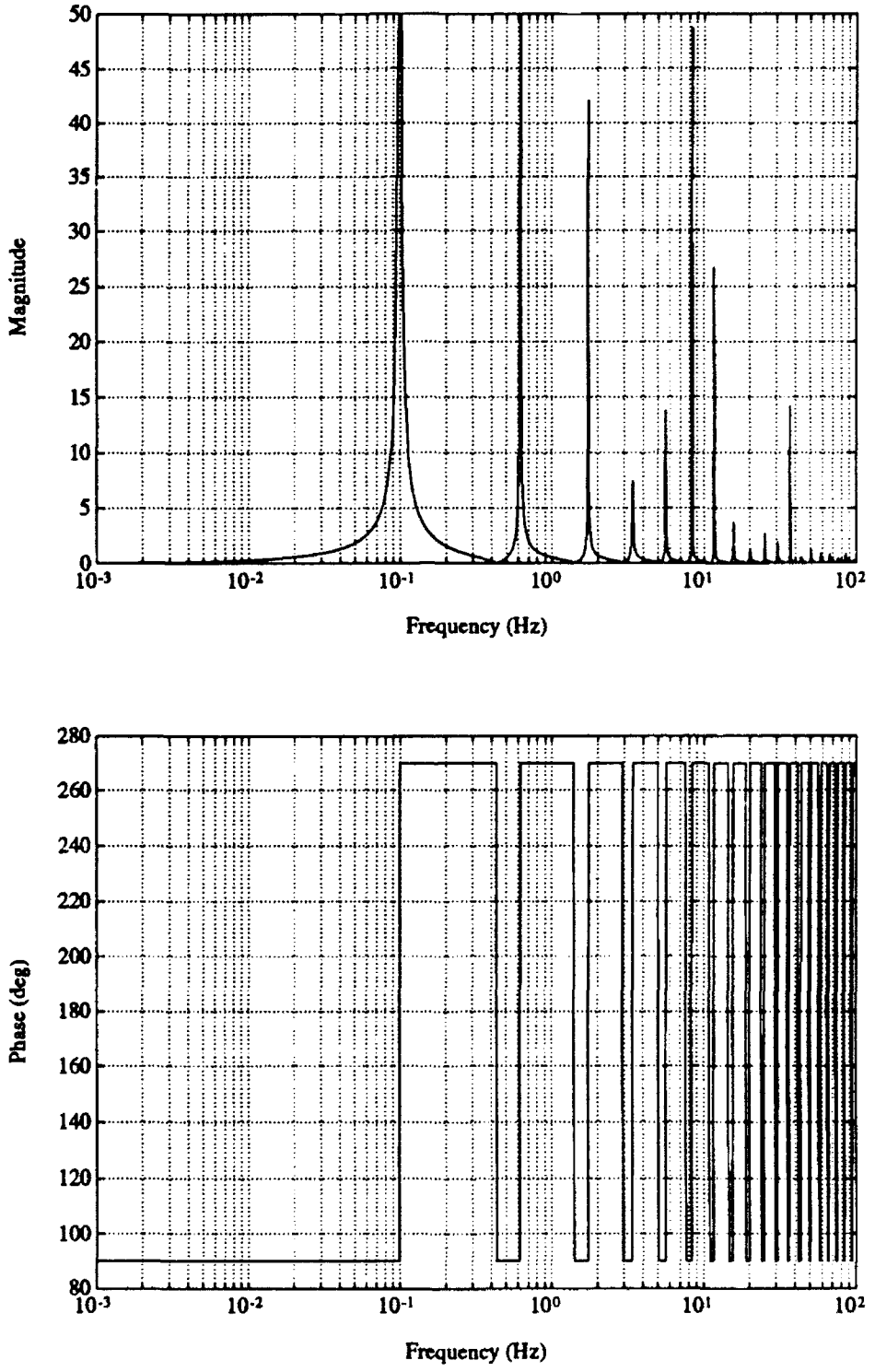

Figure 3.2: Input impedance of cantilevered beam at tip (PDE).

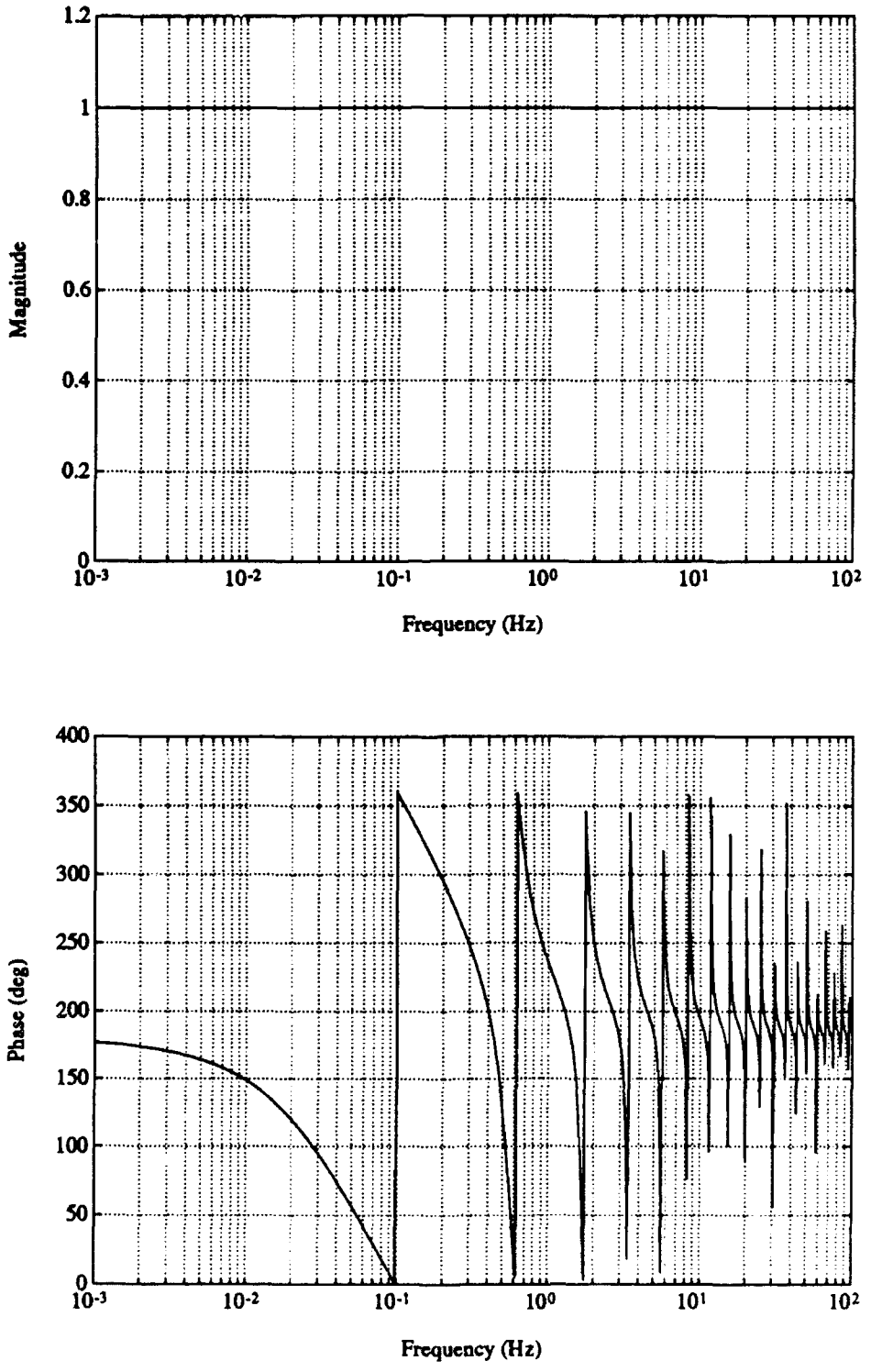

Figure 3.3: Scattering parameter of cantilevered beam at tip (PDE).

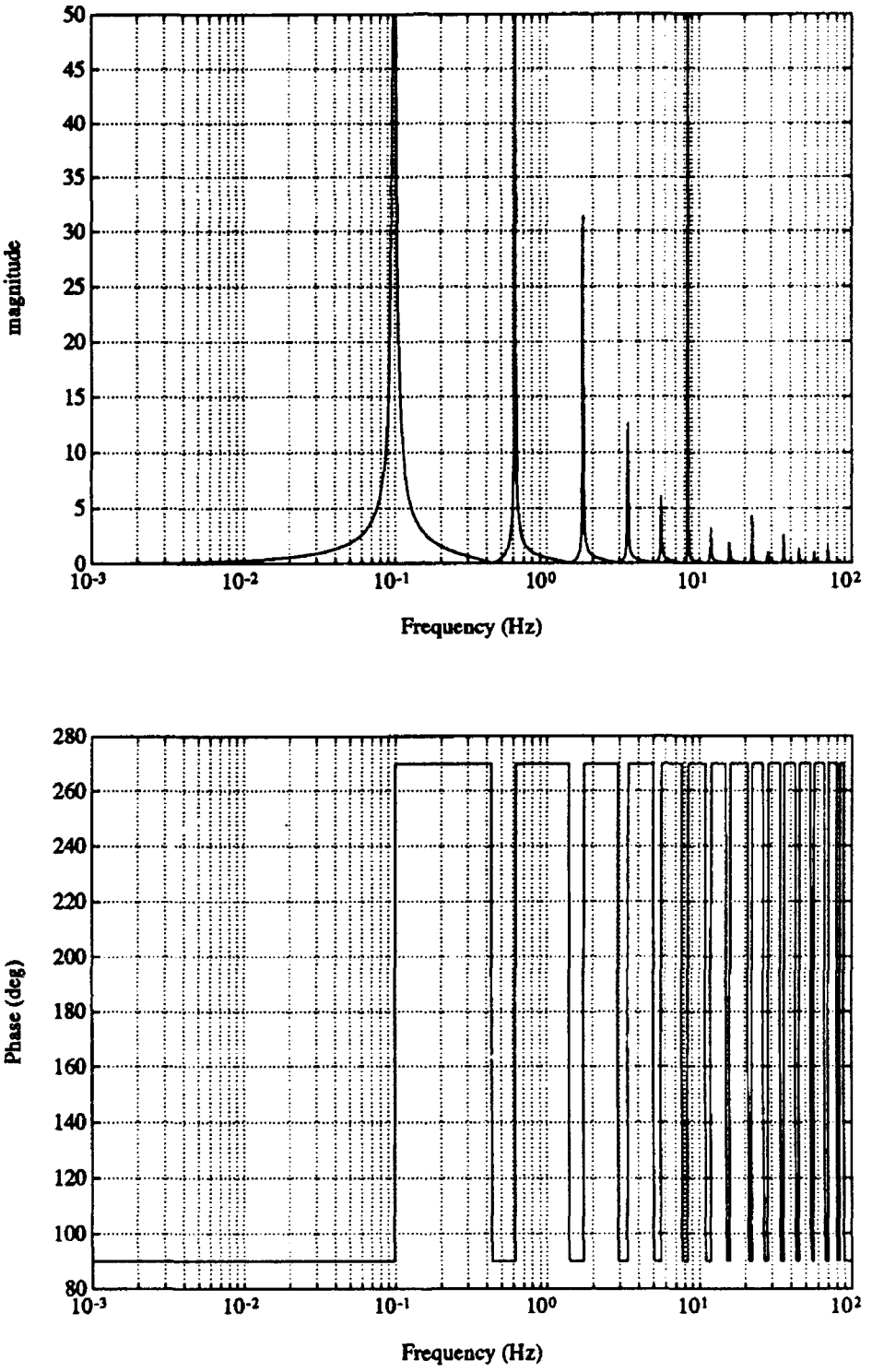

Figure 3.4: Input impedance of cantilevered beam at tip (FEM).

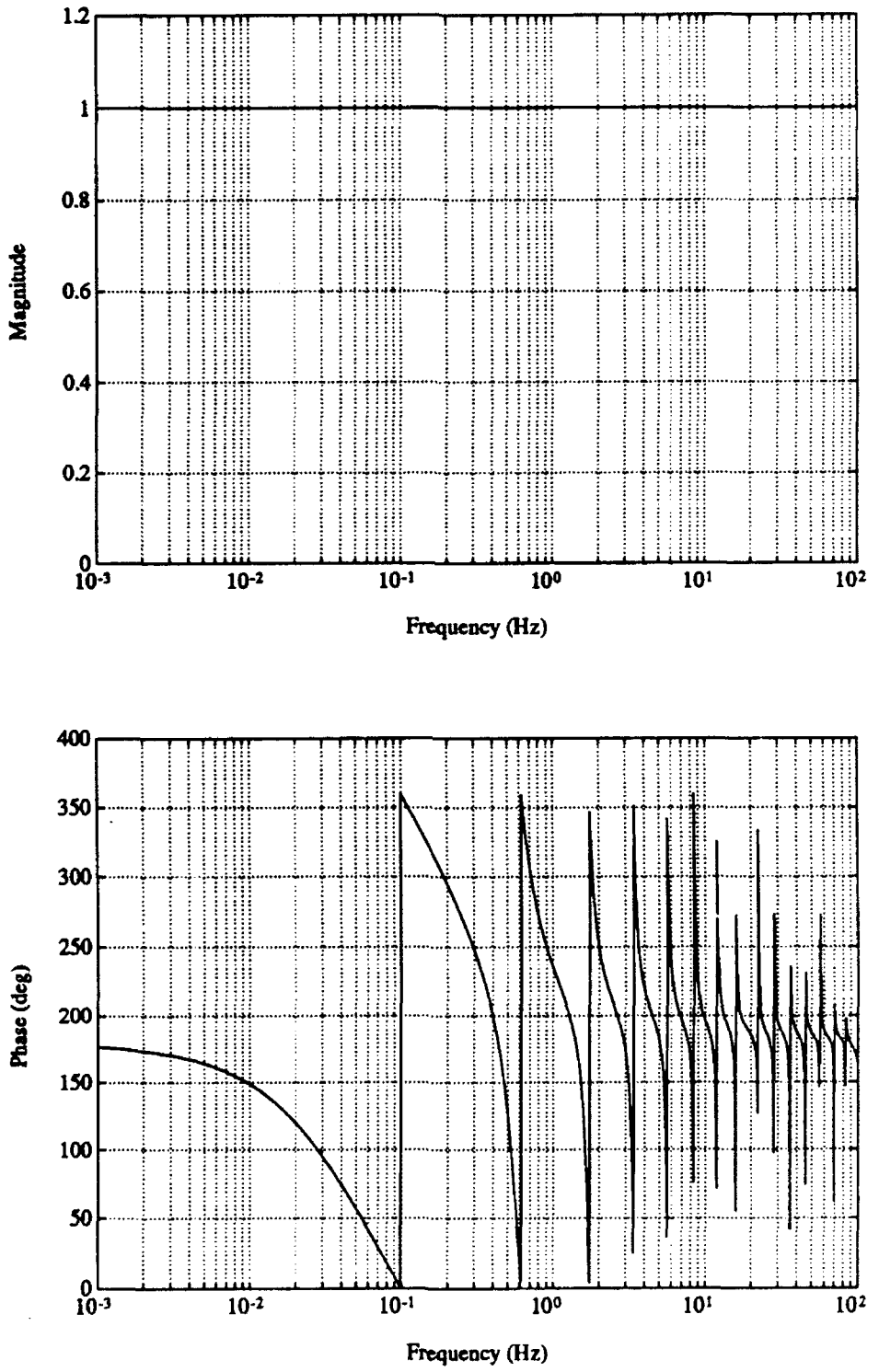

Figure 3.5: Scattering parameter of cantilevered beam at tip (FEM).

4. MULTI-LINK FLEXIBLE MANIPULATORS

In many applications that involve slewing of mechanical structures such as in spacecraft and robotics, performance is limited by the mass and rigidity of the moving appendages. The use of lightweight materials and slender appendages can enhance speed and mobility while reducing energy consumption but inevitably lead to flexibility. The principal drawback to flexibility in structures is the issue of control. This is due to the tremendous increase in complexity of the system dynamics as a result of the elasticity in the links. There is a wealth of literature on rigid link control, but additional control strategies are needed to deal with the more complex dynamics of flexible links. This chapter addresses the strategy of combining two methods for handling structural elasticity: perturbation techniques and distributed vibration damping.

Several works in particular, Spong *et al.* [11], Khorrami and Özgüner [7], and Siciliano and Book [12], apply perturbation techniques to flexible joint and flexible link manipulators. In [11], the integral manifold approach is employed to decompose the dynamics into a fast subsystem representing the elastic forces at the joints and a slow subsystem representing the rigid body motion. The control strategy is then an approximate feedback linearization which allows the use of rigid link control ideas. In [7], a two-time-scale approach is used to design a low order controller for the rigid system that can also compensate for the flexibility effects. In [12], a singular perturbation approach is utilized to achieve an approximate linearization strategy for manipulators with elastic links.

In these perturbation methods, the system dynamics are a function of a small parameter ϵ which represents stiffness of the joints or links. As ϵ tends to zero the slow subsystem (integral manifold) tends to the rigid link manipulator model. The integral manifold is then expanded as a power series in ϵ about $\epsilon = 0$. The primary advantage of the integral manifold approach is that it enables one to linearize the system dynamics to an arbitrary order of ϵ via the torque controllers. Other approximate linearization strategies have been proposed for flexible-link manipulators such as pseudo-linearization [13] and input-output inversion [14]. But the integral manifold approach facilitates the incorporation of approximate linearization (for the slow subsystem) and distributed actuation (for the fast subsystem) as is done in this chapter.

The primary goal of distributed vibration damping is to add thin material (e.g. polymer films) to an elastic beam and apply control signals to effect a dampening of the modes of vibration. No particular distributed actuator is proposed but instead analysis undertaken here is applicable to a wide variety of thin film actuators whose characteristics are very similar in how they impact the equations but may differ in

hardware implementation. The purpose of this analysis is to provide a description of how film actuators can reduce bending effects in flexible manipulators. The basic idea behind film actuators is that they produce a strain along the longitudinal axis of the links when applied with a voltage distributed along the link. It is shown that feedback of various measured variables to this voltage can produce a strain which dampens the modes of vibration.

Our controller design is based upon a distributed parameter model of the two-link manipulator which is derived via the Hamiltonian formulation. The dynamical equations of this model are omitted due to their length. For details on this model, the reader is referred to Khorrami [15], Schoenwald *et al.* [16], and Schoenwald and Özgüner [17]. Computer simulations are provided which show the results of the feedback linearizing torque control and the improvement in vibrational damping obtained with the distributed actuator. The computer simulation model is obtained from the distributed parameter model via the assumed modes method.

4.1 Control via the integral manifold approach

It has been shown in Ding *et al.* [18] and Khorrami and Zheng [19] among others that the necessary and sufficient conditions for exact feedback linearizability of flexible link robots are not satisfied. That is, torque control alone cannot exactly linearize the full-order dynamic system since there are not as many control inputs as output variables. The purpose of applying integral manifold theory to the above structure is to be able to reduce the dynamics of the system to the rigid body motion. This reduced order system will account for the flexibility of the links. In addition, the effects of the rigid body motion on the flexure are given by a manifold condition.

According to Sobolev [20], a manifold M_ϵ is an integral manifold for a dynamic system if it is invariant under solutions of the system. That is, if the system lies on the manifold M_ϵ at some time t_0 then the solution trajectories must remain on the manifold M_ϵ for all $t > t_0$. If the fast dynamics as represented by the flexural vibration equations are asymptotically stable then the solution of the full system will rapidly converge to the integral or slow manifold M_ϵ and remain there for all time.

Consider the two-link flexible manipulator depicted in Figure 4.1. The joint angles, θ_i, are measured as the angle between the axes X_i and X_{i-1}. The elastic deformation, $\alpha_i(\ell_i, t)$, is measured as the deflection between the link at length=ℓ_i and the axis tangent to the link at the hub, X_i. The torque inputs, $\hat{u}_i$, are applied at the ith hub. Gravity, shear deformation, torsion, and axial displacement have been neglected in the model. The mass of the ith hub and mass per unit length of the ith link are M_i and ρ_i, respectively. The mass moment of inertia of hub 1 is I_h.

In order to apply integral manifold theory, the full system model must be in singularly perturbed form. This model has been shown to be singularly perturbed in Khorrami

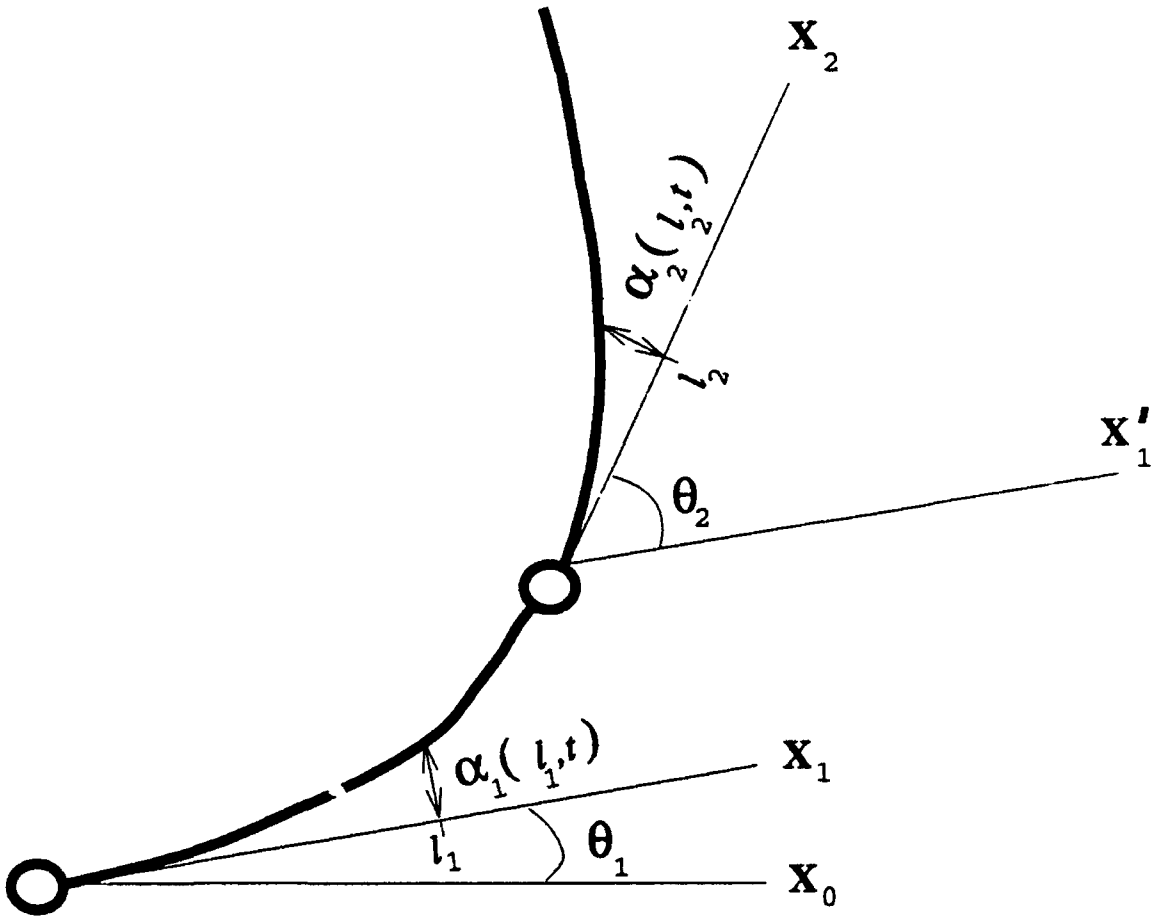

Figure 4.1: Geometry of two-link flexible manipulator.

and Özgüner [7] for the one-link case and Khorrami [15] for the two-link case. Thus, we concentrate on deriving the slow and fast manifold equations describing the two-link manipulator's behavior. These equations have not been developed previously. To do this, a normalized model of the system is derived.

First, we normalize the link deviations and spatial variables with respect to link lengths. That is

$$x_1 = \frac{\ell_1}{L_1}, \quad x_2 = \frac{\ell_2}{L_2}, \quad y_1 = \frac{\alpha_1}{L_1}, \quad y_2 = \frac{\alpha_2}{L_2}. \tag{4.1}$$

With the above normalization, our control variables become

$$u_1 = \frac{\hat{u}_1}{L_1^3 L_2^3} \quad \text{and} \quad u_2 = \frac{\hat{u}_2}{L_1 L_2^3}, \tag{4.2}$$

and we define

$$J = \frac{I_h}{L_1^3 L_2^3} + \frac{\rho_1}{3L_2^3} + \frac{M_2}{L_1 L_2^3} + \frac{\rho_2}{L_1 L_2^2}. \tag{4.3}$$

The small parameter ϵ is introduced in the following manner: Since ϵ must be related to the stiffness properties of the links, a natural choice [7, 15, 21, 22] is to let ϵ be inversely proportional to the square of the lowest frequency of oscillation due to flexure of the links. Because there are two links, there are two such parameters, ϵ_1 and ϵ_2:

$$\epsilon_i = \frac{\rho_i L_i^4}{E_i I_i}, \quad i = 1, 2. \tag{4.4}$$

This choice of ϵ shows that as the bending stiffness $E_i I_i$ becomes larger ϵ_i becomes smaller which implies that the links behave more rigidly. Since the y_i terms represent the flexure effects, it can be shown that [7, 15] y_i is of order ϵ_i. Thus, we let

$$y_i = \epsilon_i z_i, \quad i = 1, 2 \tag{4.5}$$

where z_i is our new variable for flexure effects. It can also be verified [7, 15] that as ϵ_i vanishes, the dynamics of the rigid body motion are recovered. Working with two different small parameters greatly increases the complexity of the integral manifold equations. Thus, we make the following assumption:

A1.) $O(\epsilon_1) = O(\epsilon_2) = O(\epsilon)$.

This allows us to deal with just one small parameter representing the flexibility of the two links. It is important to note that this does not mean that $\epsilon_1 = \epsilon_2$. Indeed, these two parameters can differ significantly provided they are of the same order for approximation purposes.

With the terms from above, we can now define the integral manifold:

$$M_\epsilon = \{\theta_1, \theta_2, \dot{\theta}_1, \dot{\theta}_2, z_1, z_2, \dot{z}_1, \dot{z}_2 | z_i = h_i(\theta_i, \dot{\theta}_i, u_i, x_i, \epsilon), \dot{z}_i = \dot{h}_i(\theta_i, \dot{\theta}_i, u_i, x_i, \epsilon)\} \tag{4.6}$$

for $i = 1, 2$ where h_i represents the effects of flexure on the rigid body motion. The h_i variables are obtained by solving a manifold condition which is simply the substitution of $z_i = h_i$ into the transverse motion equation for link i. However, these equations are very difficult to solve so the manifold terms h_i and the torque control terms u_i are expanded in the parameter ϵ as follows:

$$u_i = u_{i0} + \epsilon u_{i1} + O(\epsilon^2) \tag{4.7}$$

$$h_i = h_{i0} + \epsilon h_{i1} + O(\epsilon^2) \tag{4.8}$$

where $h_{ij} = h_{ij}(\theta_i, \dot{\theta}_i, u_i, x_i)$. It should be noted that in the equations to follow, we simplify notation by writing $h_{ij} = h_{ij}(x_i, t)$ to reflect h_{ij}'s dependence on length (x_i) and time $(\theta_i,\ \dot{\theta}_i,\ u_i)$. The h_{ij} terms do not depend on ϵ since this is now assumed in the power series expansion.

Substituting (4.1), (4.2), (4.4)-(4.8) into the flexural vibration equations and equating like powers of ϵ, we obtain the following manifold conditions:

Manifold equations for link 1:

$$\begin{aligned} O(1): &\quad x_1\tilde{\theta}_1 = -h_{10,x_1x_1x_1x_1} \\ O(\epsilon): &\quad \tilde{h}_{10} = -h_{11,x_1x_1x_1x_1} + h_{10}\dot{\theta}_1^2 \end{aligned} \tag{4.9}$$

Manifold equations for link 2:

$$\begin{aligned} O(1): &\quad \tfrac{1}{L_1}\, x_2(\tilde{\theta}_1 + \tilde{\theta}_2) + \tfrac{1}{L_2}\,\tilde{\theta}_1 \cos\theta_2 = -\tfrac{1}{L_1}\, h_{20,x_2x_2x_2x_2} - \tfrac{1}{L_2}\,\dot{\theta}_1^2 \sin\theta_2 \\ O(\epsilon): &\quad \tfrac{1}{L_1}\,\tilde{h}_{20} + \tfrac{1}{L_2}\, h_{10}(1,t)\tilde{\theta}_1 \sin\theta_2 = -\tfrac{1}{L_1}\, h_{21,x_2x_2x_2x_2} + \tfrac{1}{L_1} h_{20}(\dot{\theta}_1 + \dot{\theta}_2)^2 \\ &\quad -\tfrac{1}{L_2}\,\tilde{h}_{10}(1,t)\cos\theta_2 + \tfrac{1}{L_2} h_{10}(1,t)\dot{\theta}_1^2 \cos\theta_2 - \tfrac{2}{L_2}\dot{h}_{10}(1,t)\dot{\theta}_2 \sin\theta_2 \end{aligned} \tag{4.10}$$

where $O(\epsilon^2)$ terms have been ignored.

Substituting (4.1)-(4.8) into the rigid body motion equations, and again equating like powers of ϵ, we obtain the following corrected slow manifold equations representing the rigid body motion on the slow manifold. These equations are corrected in the sense that the flexibility effects from the manifold equations are included to increasingly higher powers in ϵ.

Corrected slow manifold equations for link 1:

$$
\begin{aligned}
O(1): \quad & \left[J + \tfrac{\rho_2}{2L_1^2L_2}\cos\theta_2\right]\bar{\theta}_1 + \left[\tfrac{\rho_2}{3L_1^3} + \tfrac{\rho_2}{2L_1^2L_2}\cos\theta_2\right](\bar{\theta}_1 + \bar{\theta}_2) \\
& = \tfrac{\rho_2}{2L_1^2L_2}(2\dot{\theta}_1 + \dot{\theta}_2)\dot{\theta}_2\sin\theta_2 + u_{10} \\
O(\epsilon): \quad & \left[\tfrac{\rho_2}{2L_1^2L_2}\, h_{10}(1,t)\sin\theta_2 - \tfrac{\rho_2}{L_1^2L_2}\sin\theta_2 \int_0^1 h_{20}dx_2\right]\bar{\theta}_1 + \\
& [\tfrac{\rho_2}{2L_1^2L_2}\, h_{10}(1,t)\sin\theta_2 - \tfrac{\rho_2}{L_1^2L_2}\sin\theta_2 \int_0^1 h_{20}dx_2](\bar{\theta}_1 + \bar{\theta}_2) + \\
& \left(\tfrac{M_2}{L_1L_2^3} + \tfrac{\rho_2}{L_1L_2^2}\right)\bar{h}_{10}(1,t) + \tfrac{\rho_2}{2L_1^2L_2}\,\bar{h}_{10}(1,t)\cos\theta_2 + \\
& \tfrac{\rho_1}{L_2^3}\int_0^1 x_1\bar{h}_{10}dx_1 + \tfrac{\rho_2}{L_1^2}\int_0^1\left[\tfrac{x_2}{L_1} + \tfrac{\cos\theta_2}{L_2}\right]\bar{h}_{20}dx_2 \\
& = -\tfrac{\rho_2}{2L_1^2L_2}(2\dot{\theta}_1 + \dot{\theta}_2)h_{10}(1,t)\dot{\theta}_2\cos\theta_2 - \\
& \tfrac{\rho_2}{L_1^2L_2}\dot{\theta}_2\dot{h}_{10}(1,t)\sin\theta_2 + \tfrac{2\rho_2}{L_1^2L_2}(\dot{\theta}_1 + \dot{\theta}_2)\sin\theta_2\int_0^1 \dot{h}_{20}dx_2 + \\
& \tfrac{\rho_2}{L_1^2L_2}\dot{\theta}_2\left[2\dot{\theta}_1 + \dot{\theta}_2\right]\cos\theta_2\int_0^1 h_{20}dx_2 + u_{11}
\end{aligned}
\tag{4.11}
$$

Corrected slow manifold equations for link 2:

$$
\begin{aligned}
O(1): \quad & \left(\tfrac{\rho_2}{2L_2}\cos\theta_2 + \tfrac{\rho_2}{3L_1}\right)\bar{\theta}_1 + \tfrac{\rho_2}{3L_1}\,\bar{\theta}_2 = -\tfrac{\rho_2}{2L_2}\,\dot{\theta}_1^2\sin\theta_2 + u_{20} \\
O(\epsilon): \quad & \left[-\tfrac{\rho_2}{L_2}\sin\theta_2\int_0^1 h_{20}dx_2 + \tfrac{\rho_2}{2L_2}\,h_{10}(1,t)\sin\theta_2\right]\bar{\theta}_1 + \\
& \tfrac{\rho_2}{L_1}\int_0^1 x_2\bar{h}_{20}dx_2 + \tfrac{\rho_2}{2L_2}\,\bar{h}_{10}(1,t)\cos\theta_2 \\
& = -\tfrac{\rho_2}{L_2}\,\dot{\theta}_1^2\cos\theta_2\int_0^1 h_{20}dx_2 + \tfrac{\rho_2}{2L_2}\,\dot{\theta}_1^2 h_{10}(1,t)\cos\theta_2 - \\
& \tfrac{\rho_2}{L_2}\,\dot{h}_{10}(1,t)\dot{\theta}_1\sin\theta_1 + u_{21}
\end{aligned}
\tag{4.12}
$$

where again the $O(\epsilon^2)$ terms have been ignored. It should be noted that the $O(1)$ equations of the slow manifold represent the equations of a two-link rigid manipulator as expected. These equations are the slow subsystem of the flexible manipulator, and in Section 4.3 we explain the strategy for asymptotically stabilizing the slow subsystem. This terminology is important since it is the slow subsystem that must be stabilized to ensure stability of the full system for small enough ϵ provided the fast dynamics are asymptotically stable.

Also of interest are the fast manifold equations. To derive this, we introduce the fast or stretched time scale $\tau = t/\sqrt{\epsilon}$. We also define the deviation of the flexure variables from the integral manifold as

$$\eta_i = z_i - h_i. \tag{4.13}$$

Substituting (4.13) and the fast time scale into the flexible dynamics and letting

$\epsilon \to 0$ [23] we get the boundary layer system

$$\frac{d^2\eta_1}{d\tau^2} = -\eta_{1,x_1x_1x_1x_1} - h_{1,x_1x_1x_1x_1} - x_1(\tilde{\theta}_1)^0 \tag{4.14}$$

$$\begin{aligned}\frac{d^2\eta_2}{d\tau^2} &= -\eta_{2,x_2x_2x_2x_2} - h_{2,x_2x_2x_2x_2} - x_2((\tilde{\theta}_1)^0 + (\tilde{\theta}_2)^\upsilon) \\ &- \frac{L_1}{L_2}(\tilde{\theta}_1)^0 \cos\theta_2^0 - \frac{L_1}{L_2}(\dot{\theta}_1^2)^0 \sin\theta_2^0\end{aligned} \tag{4.15}$$

with initial conditions

$$\eta_1^0 = z_1^0 - h_1(\theta_1^0, (\dot{\theta}_1)^0, u_1^0, x_1, 0) \tag{4.16}$$

$$\eta_2^0 = z_2^0 - h_2(\theta_2^0, (\dot{\theta}_2)^0, u_2^0, x_2, 0)\,. \tag{4.17}$$

The above system describes the trajectories (θ_i, η_i), which, for every given initial condition $(\theta_i^0, \dot{\theta}_i^0, \tilde{\theta}_i^0)$, lie on a fast manifold defined by $\theta_i = \theta_i^0$ =const, and rapidly descend to the slow manifold M_0 (i.e., M_ϵ with $\epsilon = 0$).

4.2 Distributed actuator control

Though flexible manipulators have advantages in terms of speed, mobility, and reduced energy consumption, their vibrational characteristics make control more difficult. Passive damping of flexible robot arms is not adequate due to its additional mass and its inability to adjust to changing flexibility effects. Hence, some kind of active damping is desirable to control the vibrations. In Spong *et al.* [11] and Siciliano *et al.* [21], only torque control is used to cancel the vibrational motion. But because of the dynamical complexity of flexible links versus flexible joints, it would appear additional control effort is needed. Current design practice in general flexible structures is to use discrete or point actuators to actively dampen vibrations. However, these flexible systems have an infinite number of degrees of freedom forcing most designs to truncate the system model to a finite number of discrete modes. Choosing which modes to represent the system and where to put the actuators is a difficult problem. Chassiakos and Bekey [24]propose an optimal scheme for locating ideal point actuators on a vibrating beam and Barbieri [25] incorporates the dynamics of a particular proof mass actuator into the system model.

But in Bailey and Hubbard [26], Burke and Hubbard [27, 28], and Crawley and de Luis [29], a distributed actuator which has the possibility of controlling an infinite number of vibrational modes and adds a minimum of dynamical complexity to the system model is proposed. The actuator is spatially distributed and makes use of a polymer film. When a voltage is applied spatially across the faces of the film, it results in a longitudinal strain over the entire plated area of the film, making it

a distributed parameter actuator. If this voltage is varied spatially, the strain will also vary spatially and in Bailey and Hubbard [26] candidate voltage functions are revealed as able to control all the vibrational modes of flexible beams with many different boundary conditions.

The dynamics and hardware details of various film actuators are explained in Bailey and Hubbard [26], Burke and Hubbard [27, 28] and Crawley and de Luis [29] and will not be repeated here. Instead, the new equations of the two-link structure with distributed actuator control are derived by adding the polymer actuator to the manifold equations which are essentially Euler-Bernoulli beam models with slewing effects [16, 30]. The film type distributed actuator will affect the manifold equations as well as the boundary conditions. This actuator will also impact the corrected slow manifold via the solution of the manifold equations (i.e., the h_{ij} terms). But it will not affect the rigid link motion (i.e., the O(1) corrected slow manifold equations). The primary difference between the work presented in this chapter and the work of Bailey and Hubbard [26], Burke and Hubbard [27, 28], and Crawley and de Luis [29] in implementation of the film is that the flexible links are slewing (rigid body motion) as well as vibrating. The new manifold equations can be stated as follows:

O(1) manifold equation for link 1:

$$x_1\bar{\theta}_1 = -h_{10,x_1x_1x_1x_1} + \frac{m_1}{\rho_1 L_1^3}\hat{V}_{1,x_1x_1} \tag{4.18}$$

O(1) manifold equation for link 2:

$$\frac{1}{L_1}x_2(\bar{\theta}_1+\bar{\theta}_2)+\frac{1}{L_2}\bar{\theta}_1\cos\theta_2 = -\frac{1}{L_1}h_{20,x_2x_2x_2x_2} - \frac{1}{L_2}\dot{\theta}_1^2\sin\theta_2 + \frac{m_2}{\rho_2 L_1 L_2^3}\hat{V}_{2,x_2x_2} \tag{4.19}$$

where $\hat{V}_i(x_i,t)$ is the voltage applied to the film on the ith link which can vary in both space and time and m_i is a physical constant representing stiffness and other parameters of the film. The boundary conditions with the addition of the film actuator can be found in Schoenwald and Özgüner [17].

Bailey and Hubbard [26] show that a uniformly spatially varying voltage distribution fails to control even-numbered modes of many types of vibrating beams. But we have proposed a uniform distribution for the film since our assumed geometric boundary conditions are clamped-free which are controllable via this distribution [28]. The shape of the actuator's spatial component is obtained by cutting the film into the desired shape and adhering it to the longitudinal faces of the beams. This implies that only the temporal component of the film voltage can be varied since the shape of the film must be determined *a priori*. Thus, our control strategy focuses on the

type of control that would be most effective for the temporal component of the film distribution.

It is proposed here that feedback for this time-varying voltage will enhance the damping properties of the actuator. There are two primary types of feedback currently being considered: (a.) feedback of position error obtained from hub angle measurements and (b.) feedback of the endpoint acceleration of each link. Strategy (a.) showed the most encouraging results of the two, however, both methods proved feasible. Results of these simulations appear in Section 4.4.

4.3 Approximate feedback linearization

From (4.11) and (4.12), we choose the control terms u_{i0} to linearize the O(1) corrected slow manifold equations. This is simply the linearization of the rigid manipulator dynamics and can be done via the well-known computed torque method as is suggested by Spong *et al.* [11] and Siciliano and Book [12]. Because of the reliance on the rigid link angles and their derivatives in the calculations, the following assumption is made:

A2.) θ_i, $\dot{\theta}_i$ are assumed to be measurable.

Assumption A2 is quite reasonable since fairly inexpensive hardware is available for such purposes, e.g., shaft encoders and tachometers. The computed torque method will not require the measurement or estimation of joint acceleration, $\ddot{\theta}_i$, thus negating the need for differentiation of measured signals. With the rigid linearizing control law, the O(1) equations for the corrected slow manifold (i.e. the slow subsystem) are as follows:

O(1) rigid body motion equation for link 1:

$$\left(J + \frac{\rho_2}{3L_1^3}\right)\ddot{\theta}_1 + \frac{\rho_2}{3L_1^3}\ddot{\theta}_2 = v_1 \tag{4.20}$$

O(1) rigid body motion equation for link 2:

$$\frac{\rho_2}{3L_1}\ddot{\theta}_1 + \frac{\rho_2}{3L_1}\ddot{\theta}_2 = v_2 \tag{4.21}$$

where v_i are the external inputs needed to implement the desired slewing behavior.

The above equations imply that the $O(1)$ feedback linearization strategy results in two double integrators which are well known to be controllable through PD feedback (i.e., joint angle and velocity feedback). We now briefly discuss how the PD control

gains can be chosen from the linearized model. First, we put the linearized model into state space form by defining the following states

$$\xi_1 = \theta_1 - \theta_1^* \,, \quad \xi_2 = \dot{\theta}_1 \,, \quad \xi_3 = \theta_2 - \theta_2^* \,, \quad \xi_4 = \dot{\theta}_2 \tag{4.22}$$

where θ_i^* is the desired slewing angle for the ith link. Next, we define two physical constants

$$m_1 = I_h + \frac{1}{3}\rho_1 L_1^3 + \frac{1}{3}\rho_2 L_2^3 + M_2 L_1^2 + \rho_2 L_1^2 L_2 \,, \quad m_2 = \frac{1}{3}\rho_2 L_2^3 \tag{4.23}$$

which allows us to express the linearized model as

$$\begin{bmatrix} \dot{\xi}_1 \\ \dot{\xi}_2 \\ \dot{\xi}_3 \\ \dot{\xi}_4 \end{bmatrix} = \begin{bmatrix} 0 & 1 & 0 & 0 \\ 0 & 0 & 0 & 0 \\ 0 & 0 & 0 & 1 \\ 0 & 0 & 0 & 0 \end{bmatrix} \begin{bmatrix} \xi_1 \\ \xi_2 \\ \xi_3 \\ \xi_4 \end{bmatrix} + \begin{bmatrix} 0 & 0 \\ \frac{1}{m_1 - m_2} & \frac{-1}{m_1 - m_2} \\ 0 & 0 \\ \frac{-1}{m_1 - m_2} & \frac{m_1}{m_2(m_1 - m_2)} \end{bmatrix} \begin{bmatrix} v_1 \\ v_2 \end{bmatrix} . \tag{4.24}$$

This system has four poles at the origin and its controllability matrix has full rank. Now we define the decentralized feedback laws

$$v_1 = g_{11}\xi_1 + g_{12}\xi_2 \,, \quad v_2 = g_{21}\xi_3 + g_{22}\xi_4 \tag{4.25}$$

where the goal is to choose the gains to obtain moderately damped poles without choosing the gains too high so as to excite vibrational modes through the effect of the higher order nonlinearities.

Following standard pole placement design techniques, it was decided to place the poles such that two of them are a complex conjugate pair with approximately 3% damping with the other two on the negative real axis. With physical constants of $m_1 = 2.02$ kg-m^2 and $m_2 = 0.0046$ kg-m^2, the gains obtained were $g_{11} = g_{12} = -10$, $g_{21} = -0.5$, and $g_{22} = -0.02$. Other pole placements were analyzed, however as damping increases so do the gains which results in the excitation of higher order nonlinearities. The oscillations in the joint trajectories were particularly sensitive to the velocity gains g_{i2}. Smaller gains resulted in longer settling times. Thus, to achieve greater damping without exciting higher order nonlinearities, the corrective ($O(\epsilon)$) control is needed.

The remainder of the feedback linearization strategy is to choose the control terms u_{ij} to cancel nonlinearities in the $O(\epsilon^j)$ equations. This can be done to an arbitrary power of ϵ. A detailed description of the $O(\epsilon)$ linearizing controller is presented in [17]. This control law represents a higher order correction to the rigid linearizing

controller. The decision as to when to incorporate the higher order control law will depend upon the particular structure involved. Generally, flexible structures with principal vibratory modes under 10 Hz will benefit from higher order control laws. But, only very flexible structures (ϵ's greater than 0.1) would require anything more than the $O(\epsilon)$ control law. The addition of the distributed actuator will alleviate much of the elasticity problem, but the higher order control law may reduce the amount of energy the distributed actuator is required to add to the system.

4.4 Simulation results

In this section, results of our computer simulations on a two-link flexible manipulator are presented. The computer program which handles the simulations implements a finite-dimensional model of the system using the assumed modes method. This method and the derivation of the finite-dimensional model as well as structural dimensions of the OSU two-link flexible manipulator are detailed in [17]. Gravity effects are not incorporated in the model, but viscous damping of the links is included. The simulated sampling time was 10 milliseconds and a 5th order Runge-Kutta differential equation solver with adaptive stepsize was utilized for solving the system differential equations.

The program simulates a one-mode expansion for each link. The first link is modeled as clamped at one end with a mass and moment of inertia at the other end representing the second joint/link assembly. The second link is modeled as clamped-free. These assumed mode shapes represent our effort to accurately include the analytical boundary conditions. The details of these mode shapes are discussed in [17]. The experimental results of the structure in Yurkovich *et al.* [31] indicate only one mode is apparent in each link, thus a one-mode approximation is justified. The modal frequencies obtained from FFT plots of tip position are 1.6 Hz for the first link and 1.5 Hz for the second link. From (4.4), $\epsilon_1 = 0.0282$ and $\epsilon_2 = 0.0315$ using structural data from Schoenwald and Özgüner [17]. Since $\epsilon_i \propto \frac{1}{\omega_i^2}$, the ratio predicted by the ϵ values is $\frac{\omega_2}{\omega_1} = 0.946$ which is very close to the simulation results of $\frac{\omega_2}{\omega_1} = 0.938$.

The torque control consisted of a PD component plus the O(1) linearizing control described in the last section. The PD controller consists of constant feedback of the shaft velocities and constant feedback of the position error of the rigid link angles. The procedure for choosing the gains for the PD control was explained in Section 4.3. The distributed actuator control consists of a spatially uniform component and a temporal component consisting of constant position error feedback as described in Section 4.2. Several other types of feedback were implemented including tip acceleration and tip deflection, however the position error feedback achieved the most encouraging results and in a physical system it would be easy to measure. The boundary conditions are

incorporated in the distributed control law via distribution theory since the uniform spatial distribution must be differentiated twice at the boundaries (which involves taking derivatives of delta distributions).

In all plots the first link is initially displaced 45 degrees above a reference line and the second link is initially displaced yet another 45 degrees from the first link. All angular velocities and accelerations are initially zero and so is the initial tip deflection, velocity, and acceleration. The desired final position is for the two links to be on a straight line with each other at the reference line, i.e., $\theta_1 = \theta_2 = 0$ and both links at rest. That is, both links are slewed through an angle of 45 degrees. The film actuator simulated here is a normalized model of the one described in Bailey and Hubbard [26] and Burke and Hubbard [27, 28]. This implies that the film physical constants are simply embedded in the applied voltage. Thus, the results obtained are applicable to many types of film actuators.

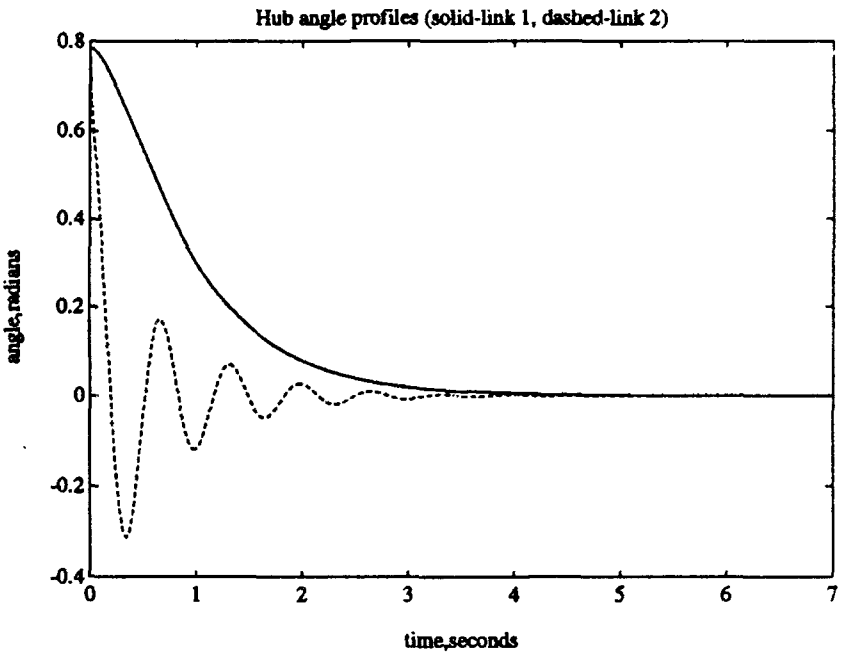

Figure 4.2: Joint angle plots with PD feedback and O(1) linearizing control.

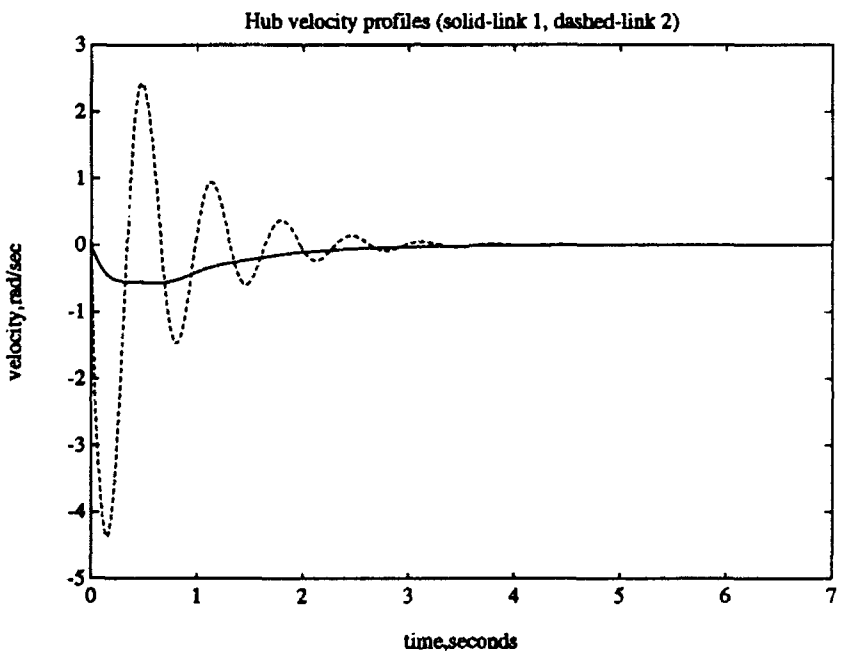

Figure 4.3: Joint velocity plots with PD feedback and O(1) linearizing control.

Figures 4.2 and 4.3 show the joint angles and velocities vs. time for the above described torque control and slewing maneuvers but without the film actuator. It can be seen that the links achieved their desired positions in about 3 seconds. The joint angle and velocity responses of link 2 oscillate as is seen in Figures 4.2 and 4.3, but this is not the case for link 1. The first link has a much heavier mass than the second link (about 10 times as heavy as link 2) making it more difficult to oscillate. Also, nonlinearities of $O(\epsilon)$ (which are not canceled by the torque law) create a more overdamped response at the joint of link 1. Figure 4.2 shows the hub angle responses with PD control and the O(1) linearizing control. Plots not shown here indicate that PD control by itself has a very similar response to Figure 4.2, but the responses take approx. 0.5 seconds longer to settle down. Thus, the linearization helps but not substantially. The addition of the distributed actuator has little effect on the hub angle profiles.

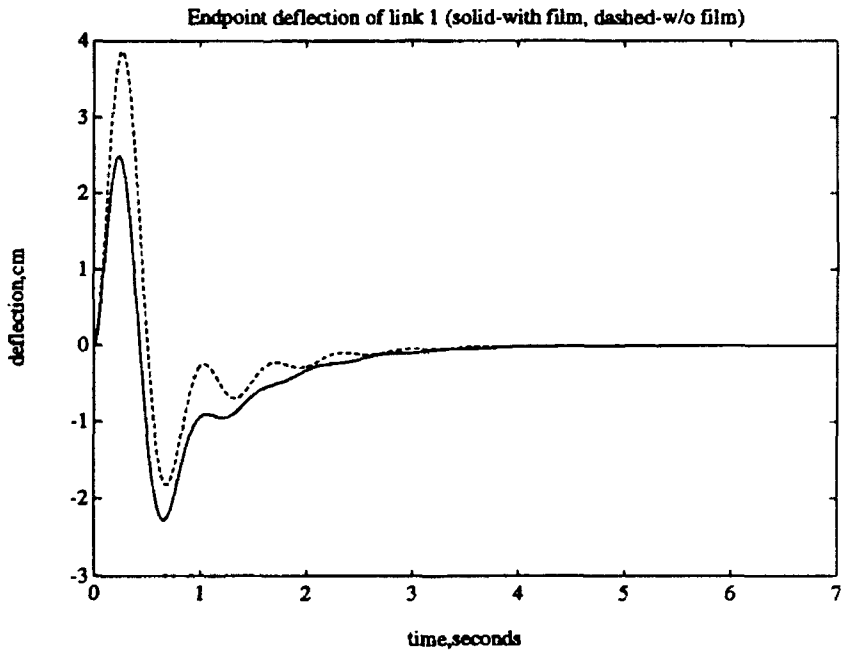

Figure 4.4: Endpoint deflections of link 1 with and without distributed actuator.

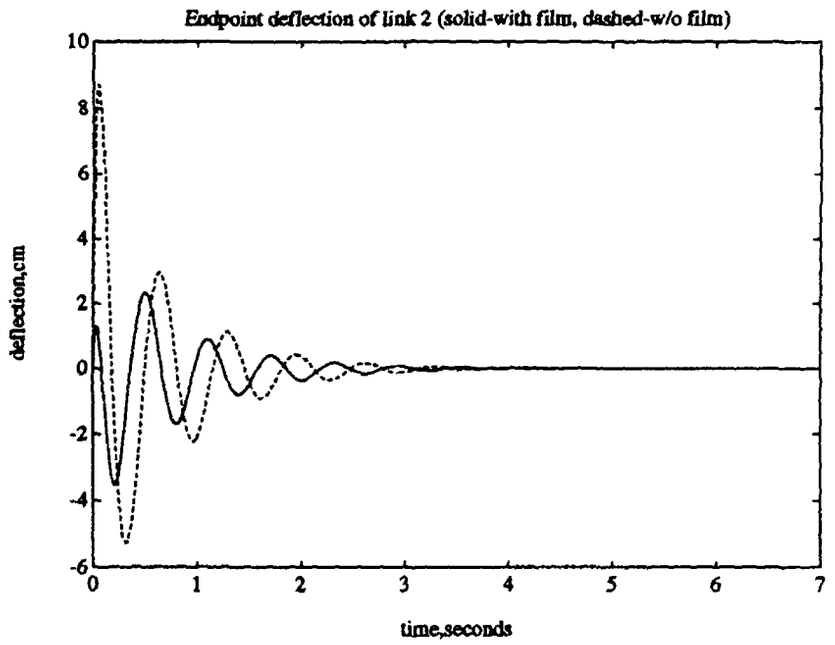

Figure 4.5: Endpoint deflections of link 2 with and without distributed actuator.

Figures 4.4 and 4.5 illustrate the tip deflections with and without the film actuator. The torque control applied is exactly the same as in Figures 4.2 and 4.3. As can be seen, the maximum absolute deflection has been reduced in the first link from 3.9 cm to 2.4 cm, and in the second link from 8.7 cm to 3.7 cm. The improvement is most noticeable in the second link (approx. 60% reduction) which would normally be the payload-carrying link. The distributed actuator force for link 1 is overdamped, thus the reason for the reduction of deflection in link 1 on the positive side but not on the negative side as is apparent in Figure 4.4. The small phase shift evident in the tip deflections of the second link is due to the position error feedback of the film actuator. The film feeds back the position error in a decentralized fashion, i.e., the ith link's film feeds back the ith link's joint angle error. Because of the nonlinearities in the flexure equations (which are of $O(\epsilon)$ and are not linearized by the torque controller here), there is a small phase shift between the joint angles and tip deflection.

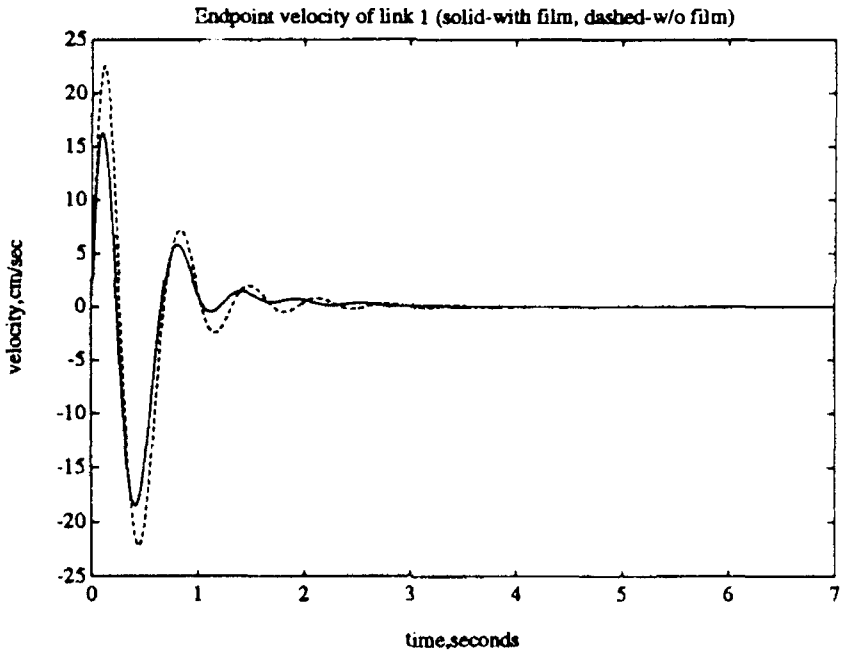

Figure 4.6: Endpoint velocities of link 1 with and without distributed actuator.

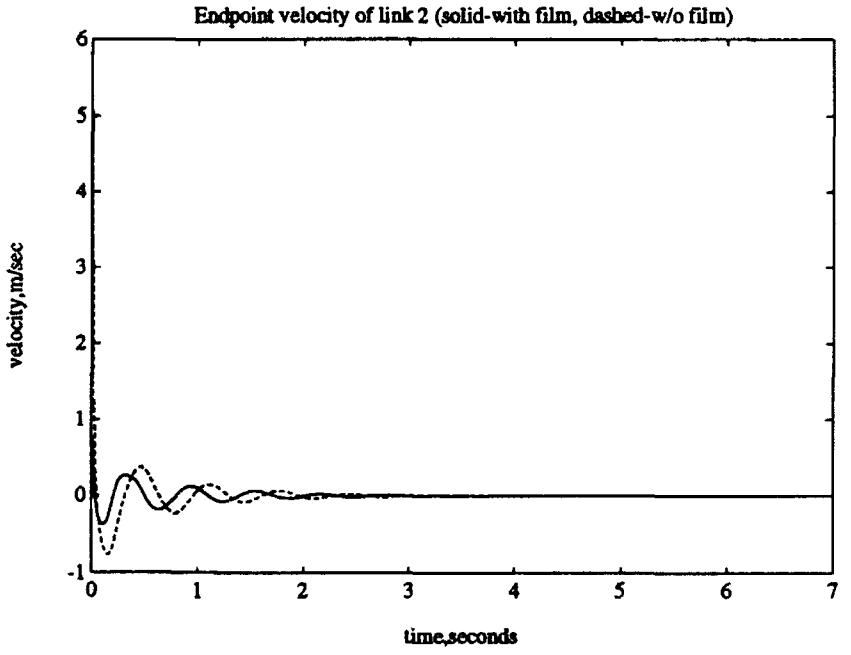

Figure 4.7: Endpoint velocities of link 2 with and without distributed actuator.

Also important in vibrational dampening is the reduction of tip velocity. One can imagine a payload on the tip of the 2nd link and the importance of keeping the endpoint speed at a minimum. The plots in Figures 4.6 and 4.7 indicate that the tip velocities are reduced, particularly in the second link whose maximum endpoint velocity has been slowed by a factor of 6. The tip velocities also settle faster with the film actuator than without it.

5. DECENTRALIZED FEEDBACK LINEARIZATION

Many nonlinear control strategies exist (variable structure control, perturbation methods, sensitivity analysis, and Lyapunov methods) for systems with full state information. In the effort presented in this chapter, we focus on feedback linearization due to its ability to transform a nonlinear system into a linear one, thus allowing the wealth of linear control techniques to be utilized. Figure 5.1 shows the basic idea behind feedback linearization. The tools needed are a nonlinear change in coordinates, $z = \Phi(x)$, to transform the system into its normal form. Then a linearizing control law in the new coordinates renders the system's state space as well as its input-output response linear in these new coordinates. The transfer function of the closed loop system is $H(s) = \frac{1}{s^r}$ where r is the relative degree of the nonlinear system.

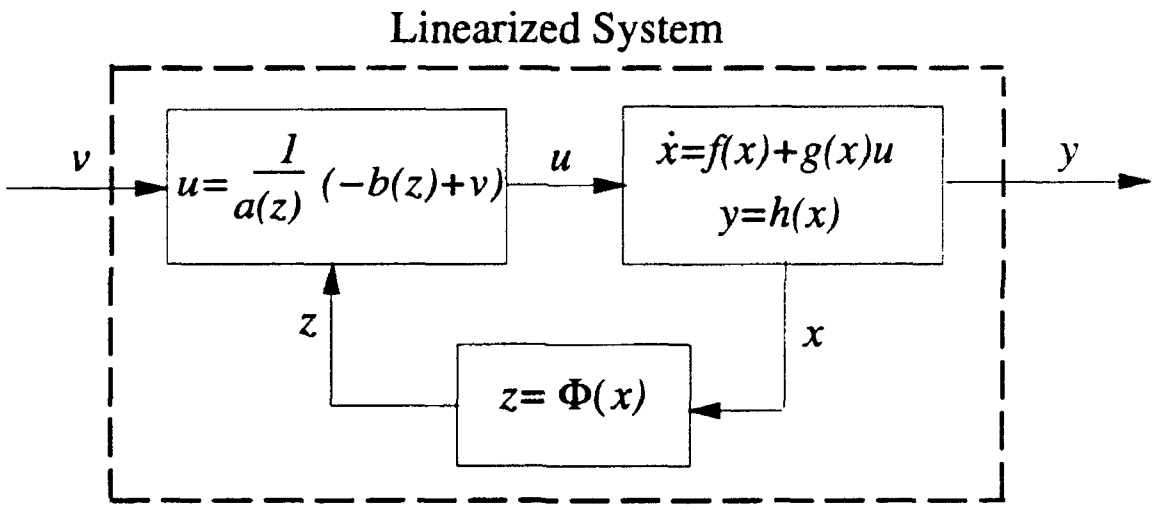

Figure 5.1: Concept of feedback linearization.

Much work has been done on centralized feedback linearization for MIMO systems, but decentralized feedback linearization has received little prior attention. In the centralized MIMO feedback linearization approach, each input is assumed to have the full system state available for feedback. Restricting each input to use only its local state generally makes the problem unsolvable because nonlinear interactions between states or subsystems cannot be canceled. Thus, decentralized feedback linearization must focus on the observer problem as well as looking at specific classes of systems for which the problem may be solvable. In the last year, we have developed four methods for use in various aspects of the decentralized feedback linearization problem which we describe in this report. We also propose two structures for applying these methods.

We begin by looking at the observer problem. If just one input-output pair is successfully able to observe the full state then this pair could be used to linearize the system. The idea then is to close all but one of the input-output ports with output feedback and choose these output feedback functions such that the conditions for solving the observer problem at the one remaining open input-output port are met. This procedure is illustrated in Figure 5.2 which shows a block diagram of a MIMO nonlinear system with m input/output ports. All but one of these ports is closed with local output feedback. If these feedback laws are chosen appropriately then the last port will be able to construct an observer for the full state.

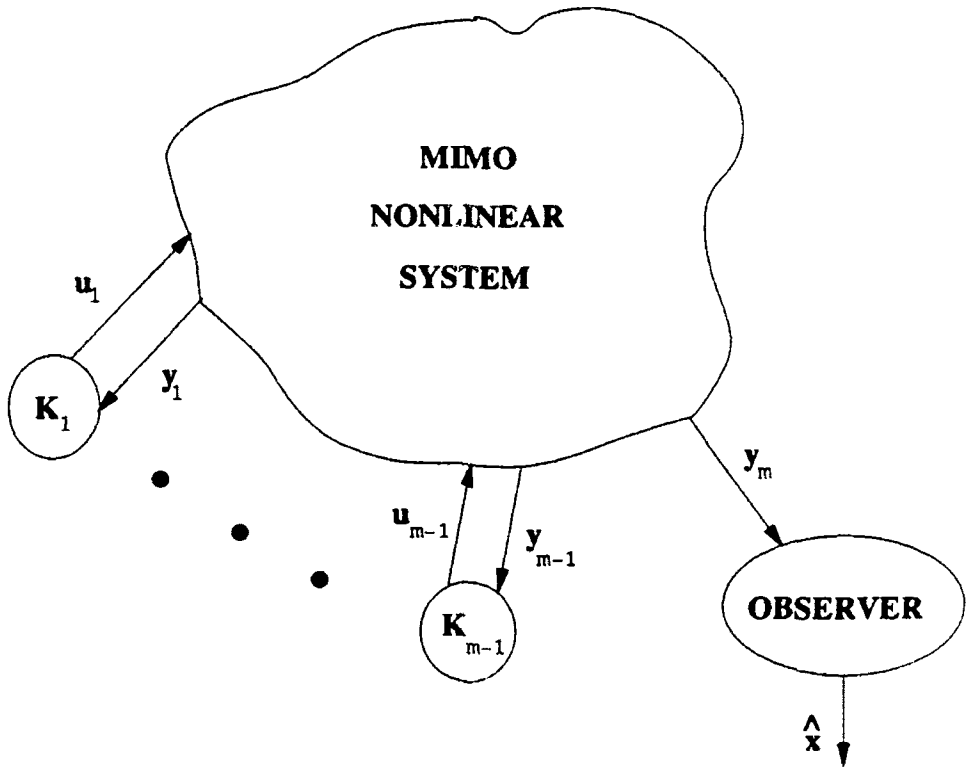

Figure 5.2: Decentralized strategy to observer design.

As an example, consider the following system consisting of two nonlinear coupled subsystems with linear interconnections

$$\begin{aligned} \dot{x}_1 &= f_{11}(x_1) + A_{12}x_2 + g_1(x_1)u_1\,, \quad y_1 = C_1x_1 \\ \dot{x}_2 &= A_{21}x_1 + f_{22}(x_2) + g_2(x_2)u_2\,, \quad y_2 = C_2x_2\,. \end{aligned} \tag{5.1}$$

An observer can be constructed at port 2 (we could have just as easily chosen port 1), if the following two conditions hold:
i.) $C_2 \neq 0$, $C_2A_{21} \neq 0$.

ii.)The feedback function $u_1 = K_1(y_1)$ must be a solution to the partial differential equation

$$\frac{\partial^2 f_{11}}{\partial x_1^2} + \frac{\partial^2 g_1}{\partial x_1^2} K_1(y_1) + 2\frac{\partial g_1}{\partial x_1}\frac{\partial K_1}{\partial x_1} + g_1(x_1)\frac{\partial^2 K_1}{\partial x_1^2} = 0\,. \tag{5.2}$$

Specifically, if $f_{11}(x_1) = x_1^2$ and $g_1(x_1) = x_1$ then (5.2) becomes

$$x_1\frac{\partial^2 K_1}{\partial x_1^2} + 2\frac{\partial K_1}{\partial x_1} = -2 \tag{5.3}$$

which gives us the linear output feedback $u_1 = K_1(y_1) = -C_1^{-1}y_1$.

The next issue to address is the decentralized controllability of the linearized system obtained upon successful feedback linearization. We show that the linearized system (which is in Brunovsky canonical form) can be asymptotically stabilized via decentralized dynamic output feedback. That is, this particular canonical form contains no decentralized fixed modes (modes that are invariant under static decentralized feedback). This result shows that if the decentralized feedback linearization can be solved by one controller then the task of controlling the linearized system can be relegated to another controller.

This approach is illustrated in Figure 5.3. A linearizing controller utilizes state feedback (which may be provided by an observer) to linearize the MIMO system. Then, local control laws employing dynamic output feedback can stabilize the linearized system. This is possible because we have shown that the canonical form one obtains upon linearizing a system contains no decentralized fixed modes. This means that all eigenvalues of the closed loop linear system can be moved via static output feedback, thus dynamic output feedback can stabilize these modes. This result allows us to relegate the linearization of the system to one controller and the stabilization to the remaining controllers. The importance of this result is that we can design stabilizing decentralized control laws for a linear system.

The next issue we address is that of linearizing and stabilizing coupled subsystems, each of which is nonlinear as well as the coupling terms. We assume each subsystem has its own state available for feedback. We show that if the nonlinear subsystem can be linearized except for the coupling terms then a suitably chosen linear state feedback can exponentially stabilize not only the linearized subsystem but the nonlinear interconnections as well.

The system we consider consists of two nonlinear weakly coupled subsystems with nonlinear interconnections as depicted in Figure 5.4. The system equations can be

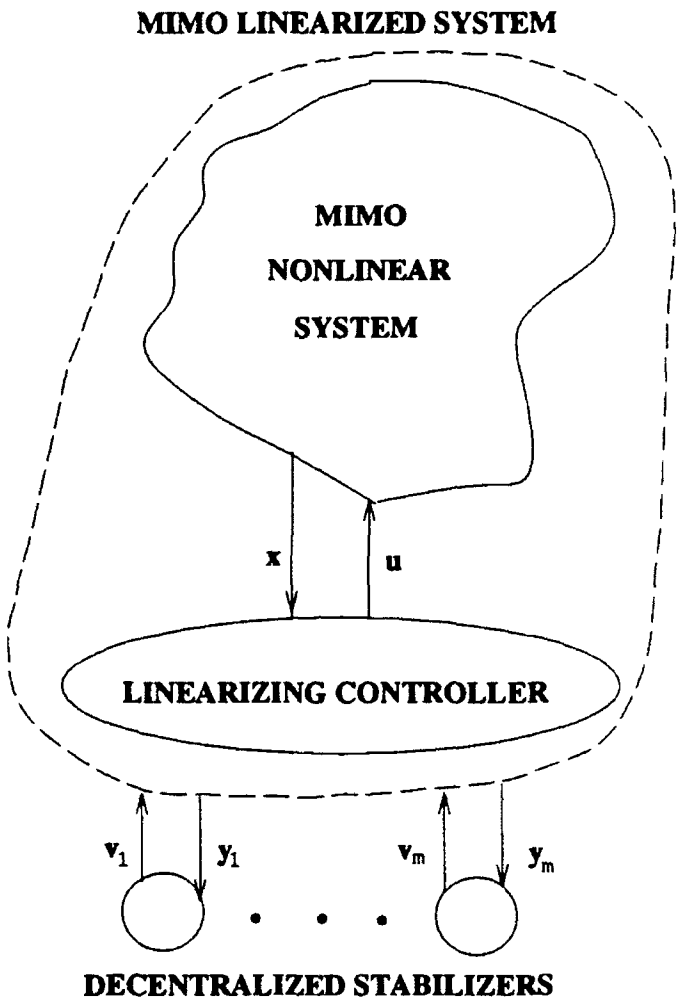

Figure 5.3: Multi-level approach to linearization and stabilization.

written as

$$\begin{aligned} \dot{x}_1 &= f_{11}(x_1) + \epsilon f_{12}(x_2) + g_1(x_1)u_1\,, \quad y_1 = h_1(x_1) \\ \dot{x}_2 &= f_{22}(x_2) + \epsilon f_{21}(x_1) + g_2(x_2)u_2\,, \quad y_2 = h_2(x_2) \end{aligned} \tag{5.4}$$

where ϵ is a small parameter representing the strength of coupling. Each subsystem has its own input and output with the outputs depending on the local state only.

Our result is that if the interaction terms satisfy a Lipschitz condition (the norm of the interconnections is bounded by the norm of the states) then the overall system can be exponentially stabilized to a prescribed degree γ (i.e., $x(t)\exp(-\gamma t) \to 0$ as $t \to \infty$). The control required to achieve this result consists of local feedback linearization which linearizes everything but the coupling terms. Then a local state feedback with

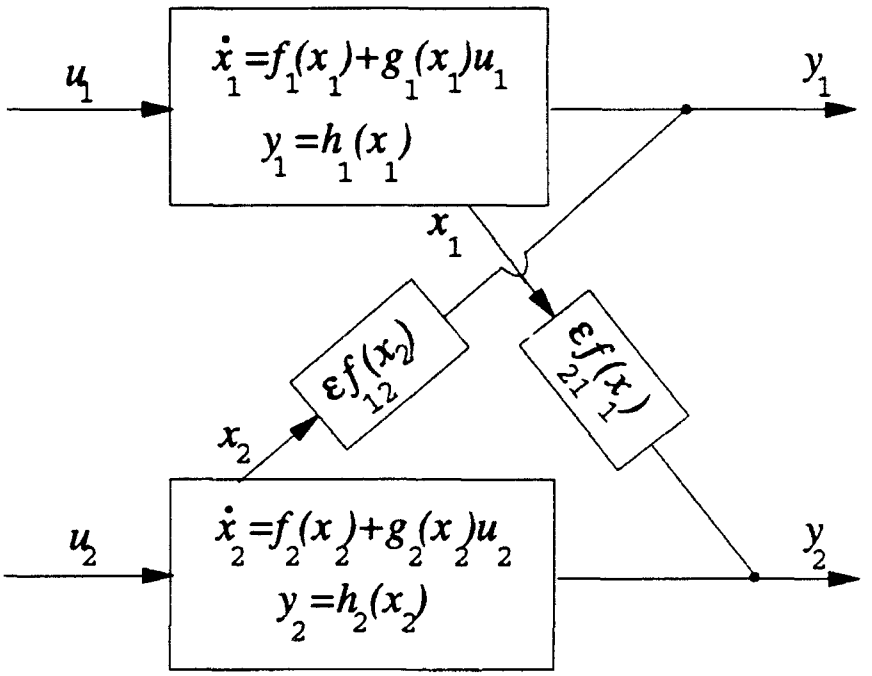

Figure 5.4: Weakly coupled nonlinear system.

gain obtained from an algebraic Riccati equation is designed to exponentially stabilize the system to some prescribed degree. The significance of this result is that using decentralized feedback only, partial linearization of all but the coupling terms and local state feedback are all that is needed to exponentially stabilize these weakly coupled nonlinear systems.

The final result we analyze is that of improving the solvability of the MIMO feedback linearization problem via feedback. That is, we ask the question, can state feedback at all but one of the input/output ports allow one to solve the feedback linearization problem at the remaining input/output port? This is useful for systems that are not feedback linearizable using centralized feedback. Thus, we are interested in feedback laws that can transform a MIMO system that is not feedback linearizable into a single-input single-output (SISO) system that is feedback linearizable. The solvability of the feedback linearization problem depends upon the relative degree, r, of the nonlinear system (the number of times the output can be differentiated before at least one component of the input appears). The relative degree requirement (r must equal the system order, n) is difficult to satisfy. But, if the feedback functions, $u_i = K_i(x)$, $i = 1, \ldots, m$, are chosen to satisfy the partial differential equations that govern the relative degree requirement then the feedback linearization problem is solvable. Essentially, one chooses these feedback functions to satisfy certain partial differential equations so as to *enhance* the relative degree of the nonlinear system.

Then the feedback linearization problem is solvable from the mth input/output port.

6. VARIABLE STRUCTURE CONTROL OF RIGID-FLEXIBLE CLOSED-CHAIN SYSTEMS

This chapter details modeling, control, and regulation characteristics of rigid-flexible closed chain systems in general, and a Rapid Deployment Truss (RDT) in particular. The modeling element unique to this work is extension of holonomic structural constraint modeling to the context of flexible bodies. The control element unique to this work is that the truss deployment be high speed, while not excessively exciting flexible modes. Applications in the large space structures context for such a device include rapid deployment of parabolic dish antenna back-up structures, instrument support platforms, or other space-based devices requiring precise orientation or position.

The obvious motivation for lightweight and rigid large structures in space is reduction in total mass lifted into orbit. However, such structures generally require assembly in orbit, either manually or by teleoperation, both of which can be slow processes. Addition or removal of various segments and modules at a later time would also be as inconvenient. This consideration generates a need for adaptable space structures, those which can vary their configurations.

Previous work on deployable structures emphasizes kinematics of such structures. A flat-folding octahedral truss is experimentally verified in [32], but the system dynamics are dominated by dynamics of lead-screw type actuators. Kinematics of a planar variable geometry truss are formulated in [33], but not dynamics. In these cases, structural vibrations during the deployment phase are not addressed, and in fact the deployment is deliberately slow in an attempt to not excite structural modes excessively.

Motion of flexible structures undergoing large angle, fast slewing maneuvers has been investigated in the context of flexible manipulators. Research on flexible planar manipulators, while fairly mature, has been limited to devices with one or two flexible links, with each link usually modeled as a single flexible beam. Detailed flexible manipulator models have been developed, some based upon Timshenko beam theory, which include higher order effects such as coriolis terms and centrifugal stiffening.

The planar Rapid Deployment Truss considered in this work is shown deployed and during deployment in Figure 6.1 and Figure 6.2. This ladder-like planar frame acts as a static truss when fully deployed, having the desirable truss qualities of low mass and rigidity if joints are locked. In contrast to a manipulator, it has many links or members, and multiple holonomic constraints on allowable configurations, constraints which must be obeyed to maintain structure connectivity. Actuators and sensors are distributed throughout the structure, as are torsion springs which augment rapid deployment. In these ways it is neither a manipulator nor a static truss.

Figure 6.1: Deployed RDT

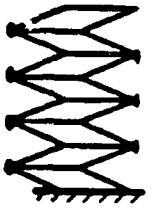

Figure 6.2: RDT During Deployment

As will be shown, the RDT has complicated nonlinear dynamics, its rigid body and flexure motion terms are coupled, and it may be subjected to modeling uncertainties such as tip load variation. A control approach that has met with success for such complicated problems is variable–structure controllers ("VSC") [34, 35, 36, 37]. The VSC philosophy is to use a high gain feedback, which changes structure according to the location of the state vector with respect to a defined surface in the state space. Under conditions that guarantee stability, the state will "slide" to the origin along this surface. A known drawback of this approach is the "chattering" phenomena around the switching surface. In [38] is developed the theory to selectively curtail this chattering, by inserting a filter designed according to the rules of frequency shaped quadratic regulators into the system. The method is summarized and applied to the control design for a simplified RDT in the sequel.

6.1 Modeling of Flexible Rapid Deployment Truss Structure

6.1.1 Modeling Assumptions

The basic truss structure studied in this work is that of a planer n bay box type truss, spring loaded in stowage, and actively dampened in deployment by multiple actuators as in Figure 6.3. Note in this figure that torque springs are chosen to act between

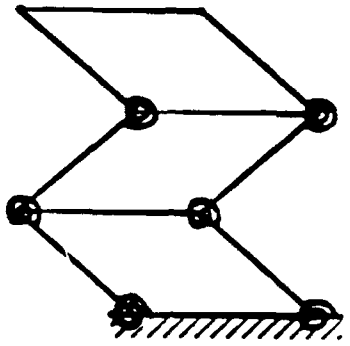

Figure 6.3: RDT with Coil Springs in Place

serially connected longitudinal members, while lateral members ("rungs") are end connected as pinned, and thus no moments can be transferred from the longitudinal to lateral members.

For a static frame-truss, members can be considered much stiffer in the axial direction than in the lateral. In this work, the assumption of zero axial displacements of members in simple static truss bay configurations is assumed extendable to dynamic multi-bay structures such as the RDT.

Since the truss considered is chosen to be deployed by torque actuators augmented with torsional springs, both of which are chosen to act between longitudinal members only, and rungs are connected freely at pin joints, the deflection of longitudinal members, those vertical in Figure 6.1, will occur. If longitudinal members undergo small flexures, little foreshortening of these links from the nominal length should occur. The resulting assumed structure becomes that of two n degree-of-freedom flexible manipulators operating in parallel, with deployment springs and holonomic constraints imposed by lateral members at joints.

The dynamics of the two unconstrained n link flexible open kinematic chains can be found using Timshenko beam theory or Euler-Lagrange formulation. In [39], sin-

gle holonomic constraints between parallel rigid manipulators is considered but constraints between flexible manipulators has not yet been approached. Inclusion and control of rigid body constraint forces in a linearized state space model for dynamics is developed by Hemami in [40].

In modeling flexible links as slender beams, it is both convenient and a valid approximation to restrict the model to finite order by truncating the full set of modes and including only those modes which are considered most important based upon some criterion. For simple slewing structures undergoing small vibrations, the continuous solution to a partial differential equation (PDE) representative of its motion can be found as in [15] for both one- and two-link flexible open kinematic chains (manipulators). However, even when the exact PDE solution is available, it generally must be spatially discretized in some manner for purpose of simulation. In many cases it can be shown by limiting criteria such as controller bandwidth that it is not feasible to attempt to model or control a very large number of modes. Thus some "error indices" might be defined which provide a criterion for exclusion of higher order modes.

6.1.2 General Solution of Holonomic Constraint Forces

In this section, a method proposed by Hemami in [41] is derived which keeps holonomic (configuration dependent) constraint forces in evidence for modeling and control of open- and closed-chain linkages. The derived method is applicable to rigid or flexible linkages, if the flexure variables have been expressed as a finite dimensional summation of modal terms, perhaps based upon the assumed modes modeling method. If vector z is taken as the position state vector of the complete unconstrained system, then the corresponding linkage dynamics can always be expressed as

$$M\ddot{z} + g(z, \dot{z}) = \left(\frac{\partial C}{\partial z}\right)^T \Gamma + u \tag{6.1}$$

where Γ is the vector of constraint forces, and the holonomic constraints are expressed as $C(z) = 0$. To solve (6.1) explicitly for constraint forces Γ, first twice differentiate C with respect to time, giving

$$\ddot{C}(z) = \frac{d}{dt}\left(\frac{\partial C}{\partial z}\right)\dot{z} + \frac{\partial C}{\partial z}\ddot{z} = 0. \tag{6.2}$$

Solve for acceleration $\ddot{z}$ in (6.1) to find

$$\ddot{z} \;=\; M^{-1}\left[-g(z, \dot{z}) + \left(\frac{\partial C}{\partial z}\right)^T \Gamma + u\right]. \tag{6.3}$$

Multiply through (6.3) by $(\frac{\partial C}{\partial z})$ then substitute from (6.2) for $(\frac{\partial C}{\partial z})\ddot{z}$ which gives

$$-\frac{d}{dt}\left(\frac{\partial C}{\partial z}\right)\dot{z} = -\frac{\partial C}{\partial z}M^{-1}g(z,\dot{z}) + \frac{\partial C}{\partial z}M^{-1}\left(\frac{\partial C}{\partial z}\right)^{T}\Gamma + \frac{\partial C}{\partial z}M^{-1}u. \tag{6.4}$$

Solving for Γ yields

$$\Gamma = \left[\frac{\partial C}{\partial z}M^{-1}\left(\frac{\partial C}{\partial z}\right)^{T}\right]^{-1}\left\{-\dot{z}^{T}\frac{\partial}{\partial z}\left[\left(\frac{\partial C}{\partial z}\right)\dot{z}\right] + \frac{\partial C}{\partial z}M^{-1}\left[g(z,\dot{z}) - u\right]\right\}, \tag{6.5}$$

as the expression of constraint forces.

6.1.3 Dynamical Consideration of a Simplified RDT Structure

Consider modeling of a simplified RDT structure, dynamically equivalent to parallel rigid-flex manipulators constrained in position by a rigid pinned-pinned beam ("rung") at the endpoints of the first links only. A detailed structural schematic appears in Figure 6.4. Parameters appearing in the figure are defined in Table 6.2.

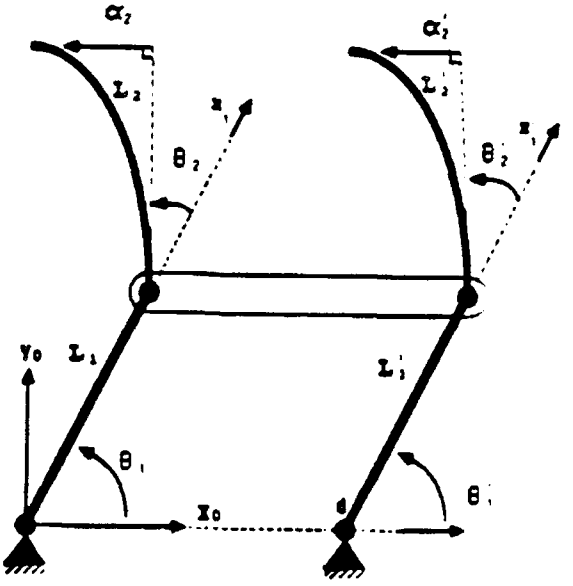

Figure 6.4: Simplified RDT Structural Schematic

For each rigid-flex manipulator individually, equations of motion using the assumed modes constrained expansion will result in

$$M \begin{bmatrix} \ddot{\theta}_1 \\ \ddot{\theta}_2 \\ \ddot{q}_2 \end{bmatrix} + F_r \begin{bmatrix} \dot{\theta}_1^2 \\ \dot{\theta}_2^2 \\ \dot{\theta}_1\dot{\theta}_2 \end{bmatrix} + F_{rf} \begin{bmatrix} \dot{\theta}_1\dot{q}_2 \\ \dot{\theta}_2\dot{q}_2 \end{bmatrix} + \begin{bmatrix} 0 \\ 0 \\ \mu_2\dot{q}_2 \end{bmatrix} + K \begin{bmatrix} \theta_1 \\ \theta_2 \\ q_2 \end{bmatrix} = \begin{bmatrix} 1 & 0 \\ 0 & 1 \\ 0_{N_2} & 0_{N_2} \end{bmatrix} \begin{bmatrix} u_1 \\ u_2 \end{bmatrix}, \quad (6.6)$$

where $q_2 = [q_{21}, q_{22}, ..., q_{2j}, ..., q_{2N_2}]^T$ modal states, j = mode number $(1, \ldots, N_2)$, and M, F_r, F_{rf}, and K are mass, centrifugal, coriolis, and stiffness matrices. A small damping term involving coefficients μ_2 is included for modal states. Control torques u_1 have no direct effect on modal state variables, but affect the rigid body angles θ_1, and through coupling off-diagonal terms in the mass matrix affect modal states.

The rung equations of motion can be written using balance of inertia and constraint forces in the free body diagram of Figure 6.5. Summing horizontal (X_0 direction) and

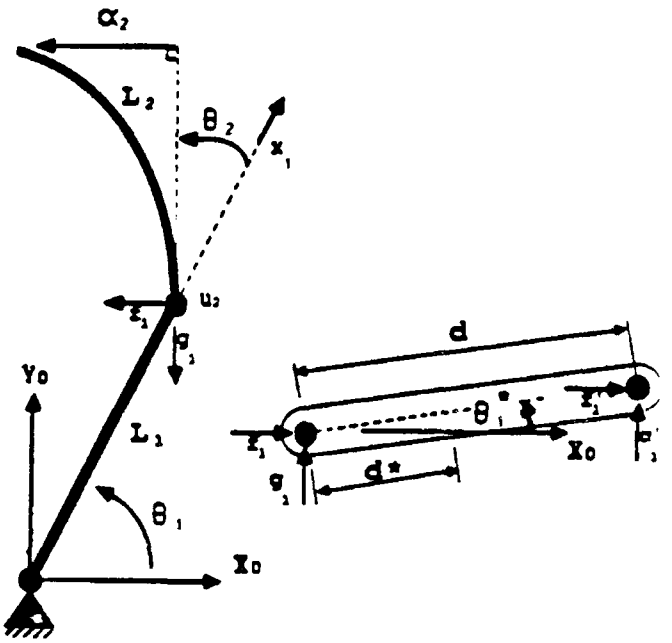

Figure 6.5: Simplified RDT, Rung Free-body Diagram

vertical (Y_0 direction) forces gives

$$f_1 = m_1^* \ddot{x}_1^* - f_1',$$
$$g_1 = m_1^* \ddot{y}_1^* - g_1', \quad (6.7)$$

where $\ddot{x}_1^*$ and $\ddot{y}_1^*$ are the horizontal and vertical acceleration components of the center of mass of rung. Likewise summing moments about the center of mass (θ_1^* direction) gives

$$f_1 d_1^* s_1^* - f_1'(d - d_1^*)s_1^* + g_1'(d - d_1^*)c_1^* - g_1 d_1^* c_1^* = I_1^* \ddot{\theta}_1^*, \tag{6.8}$$

where s_1^* and c_1^* represent $\sin\theta_1^*$ and $\cos\theta_1^*$ respectively, and d_1^* is the distance from left hand pinned joint of rung to its center of mass.

Angular state variable θ_1^* will be maintained explicitly in final equations of motion, as the degree of freedom which allows calculation of explicit constraint forces $\{f_1', g_1'\}$. However, accelerations $\ddot{x}_1^*$ and $\ddot{y}_1^*$ can be expressed in terms of the left hand side manipulator's state variables and θ_1^*, by writing equations for the center of mass position of the rung, then twice differentiating these with respect to time, giving accelerations

$$\begin{aligned} \ddot{x}_1^* &= -L_1\dot{\theta}_1^2 c_1 - d_1^*\dot{\theta}_1^{*2}c_1^* - L_1\ddot{\theta}_1 s_1 - d_1^*\ddot{\theta}_1^* s_1^*, \\ \ddot{y}_1^* &= -L_1\dot{\theta}_1^2 s_1 - d_1^*\dot{\theta}_1^{*2}s_1^* + L_1\ddot{\theta}_1 c_1 + d_1^*\ddot{\theta}_1^* c_1^*. \end{aligned} \tag{6.9}$$

Substitute the preceding accelerations into force balance equations (6.7) to yield

$$\begin{aligned} f_1 &= m_1^*(-L_1\dot{\theta}_1^2 c_1 - d_1^*\dot{\theta}_1^{*2}c_1^* - L_1\ddot{\theta}_1 s_1 - d_1^*\ddot{\theta}_1^* s_1^*) - f_1' \\ g_1 &= m_1^*(-L_1\dot{\theta}_1^2 s_1 - d_1^*\dot{\theta}_1^{*2}s_1^* + L_1\ddot{\theta}_1 c_1 + d_1^*\ddot{\theta}_1^* c_1^*) - g_1'. \end{aligned} \tag{6.10}$$

To write the equations of motion of the rung in terms of left manipulator variables and the explicit constraint forces $\{f_1', g_1'\}$, substitute the right half sides of (6.10) into (6.8) to have

$$\ddot{\theta}_1^*(I_1^* + d_1^{*2}m_1^*) = m_1^* d_1^*[\ddot{\theta}_1(-L_1 c(\theta_1 - \theta_1^*)) + \dot{\theta}_1^2 L_1 s(\theta_1 - \theta_1^*)] - ds_1^* f_1' + dc_1^* g_1'. \tag{6.11}$$

The implicit $\{f_1, g_1\}$ and explicit $\{f_1', g_1'\}$ constraint forces will affect the individual manipulator dynamics through a term added to each manipulator's equation of motion (6.6) to give an equation for the left side manipulator of the form

$$M[\cdot] + F_r[\cdot] + F_{rf}[\cdot] + Damp + K[\cdot] = [\cdot]u - J_1^T \begin{bmatrix} f_1 \\ g_1 \end{bmatrix} \tag{6.12}$$

where the Jacobian matrix J expressed in terms of inertial coordinates $\{ X_0, Y_0 \}$ has the form

$$J_1^T = \begin{bmatrix} -s_1 L_1 & c_1 L_1 \\ 0 & 0 \\ 0_{N_2} & 0_{N_2} \end{bmatrix}. \tag{6.13}$$

In the equation of dynamics for the left side manipulator (6.12) the expressions of forces f_1 and g_1 from (6.10) can be utilized so that these forces are included *implicitly*

in the left manipulator model. Here the term $-J_1^T \begin{bmatrix} f_1 \\ g_1 \end{bmatrix}$ will have only first row nonzero elements of the following form.

$$s_1 L_1 f_1 - c_1 L_1 g_1 \tag{6.14}$$

Expanding this and simplifying the result gives

(6.15)

$$m_1^*(d_1^* \dot{\theta}_1^{*2} L_1 s(\theta_1^* - \theta_1) - \tilde{\theta}_1 L_1^2 - \tilde{\theta}_1^* d_1^* L_1 c(\theta_1^* - \theta_1)) - s_1 L_1 f_1^{'} + c_1 L_1 g_1^{'}. \tag{6.16}$$

The equation (6.16) is easily included in the left side manipulator equations (6.12) by suitably modifying elements of the mass, centrifugal, and coriolis matrices therein. The equation of (6.12) with only explicit constraint forces $\{f_1^{'}, g_1^{'}\}$ takes on the form

$$M[\cdot] + F_r[\cdot] + F_{rf}[\cdot] + Damp + K[\cdot] = [\cdot]u + J_1^T \begin{bmatrix} f_1^{'} \\ g_1^{'} \end{bmatrix}. \tag{6.17}$$

For inclusion of the rung into the system model, equation (6.11) is appended as a row to the dynamics of the left manipulator (6.12).

Similar to the left side, the equation of motion for the right side manipulator has the form

$$M^{'}[\cdot] + F_r^{'}[\cdot] + F_{rf}^{'}[\cdot] + Damp^{'} + K^{'}[\cdot] = [\cdot]u^{'} - J_1^{'T} \begin{bmatrix} f_1^{'} \\ g_1^{'} \end{bmatrix}, \tag{6.18}$$

and the Jacobian

$$J_1^{'T} = \begin{bmatrix} -s_1^{'} L_1^{'} & c_1^{'} L_1^{'} \\ 0 & 0 \\ 0_{N_2^{'}} & 0_{N_2^{'}} \end{bmatrix}. \tag{6.19}$$

In this simplified RDT structure since the constraint loop is made up of only rigid members, the Jacobian is not dependent upon modal terms as would be the case for a flexible link loop. The method is however extendable to flexible members in the constraint loop. as shown in [42].

Prior to solving (6.5) for constraint forces, the method discussed in Section 6.1.2 requires writing constraint equations of the form $C(x) = 0$ where $x = [\theta_1, \theta_2, q_2, \theta_1^*, \theta_1^{'}, \theta_2^{'}, q_2^{'}]^T$

is the position state vector of the complete unconstrained system. If endpoints of left and right side manipulators' first links are expressed as $\bar{x}_1$ and $\bar{x}_1'$ where

$$\bar{x}_1 = \begin{bmatrix} L_1 c_1 \\ L_1 s_1 \end{bmatrix}, \qquad \bar{x}_1' = \begin{bmatrix} d + L_1' c_1' \\ L_1' s_1' \end{bmatrix}, \tag{6.20}$$

then the constraint equation can be written as

$$C(x) = \bar{x}_1' - \bar{x}_1 - d \begin{bmatrix} c_1^* \\ s_1^* \end{bmatrix} = 0. \tag{6.21}$$

The solution of constraint forces in (6.5) also requires solving for $\frac{\partial C}{\partial x}$. By definition

$$\frac{\partial C}{\partial x} = \frac{\partial}{\partial x} \left[\bar{x}_1' - \bar{x}_1 - d \begin{pmatrix} c_1^* \\ s_1^* \end{pmatrix} \right], \tag{6.22}$$

but from (6.20) the partials of $\bar{x}_1$ and $\bar{x}_1'$ with respect to vectors $[\theta_1, \theta_2, q_2]$ and $[\theta_1', \theta_2', q_2']^T$ respectively are zero matrices. Thus $\frac{\partial C}{\partial x}$ can be expressed as

$$J^T = \frac{\partial C}{\partial x} = \left[-J_1 \vdots \begin{pmatrix} ds_1^* \\ -dc_1^* \end{pmatrix} \vdots J_1' \right], \tag{6.23}$$

where the Jacobians in inertial coordinates have the usual definitions as in Section 6.1.3. Simulations of such a constrained dynamical system can take advantage of available Jacobian values when calculating the term J.

The model of this simplified RDT structural dynamics is thus shown to include explicitly holonomic constraint forces as a means for coupling its sides.

6.1.4 State Space Formulation

The general equations of motion for both manipulators and RDT type structures, both rigid and flexible, can be written in the form

$$M(x)\ddot{x} + g(x, \dot{x}) = J^T \Gamma(x, u) + Bu \tag{6.24}$$

where x is the $n/2$ by 1 vector of rigid-body and flexure coordinates, $M(x)$ is the positive definite mass matrix, $g(x, \dot{x})$ is all nonlinear terms due to centrifugal, coriolis, and gravity effects, the holonomic constraint expression $C(x) = 0$ represents all closed structural loops, $\Gamma(x, u)$ is a vector of constraint forces or Lagrange multipliers, and B is the control distribution matrix for input vector u. Using the expression derived for

constraint forces $\Gamma(x,u)$ in (6.5), and grouping terms in input u, the system dynamical equation (6.24) can be rewritten as

$$M(x)\ddot{x} + g(x,\dot{x}) + J^T\left[JM^{-1}J^T\right]^{-1}\left\{\dot{x}^T\frac{\partial}{\partial x}(J\dot{x}) - JM^{-1}g(x,\dot{x})\right\}$$

$$= [-J^T(JM^{-1}J^T)^{-1}JM^{-1} + B]u. \tag{6.25}$$

the state space form of (6.25) can be written in more brief form

$$\ddot{x} = f(x,\dot{x}) + D(x)u \tag{6.26}$$

where

$$f(x,\dot{x}) =$$

$$M^{-1}(x)\left\{-g(x,\dot{x}) - J^T(JM^{-1}J^T)^{-1}[\dot{x}^T\frac{\partial(J\dot{x})}{\partial x} - Jg(x,\dot{x})]\right\}, \tag{6.27}$$

$$D(x) = M^{-1}(x)\left\{B - J^T(JM^{-1}J^T)^{-1}JM^{-1}\right\} \tag{6.28}$$

Since matrix M is a function of x, both f and D are nonlinear. The vector f is a nonlinear function of both x and $\dot{x}$ due to expressions $g(x,\dot{x})$ and $\dot{x}^T\frac{\partial}{\partial x}(J\dot{x})$.

6.2 Frequency Shaped Variable Structure Control for RDT

In this research, a frequency shaped sliding mode approach [38] is being considered. The method is applied in two steps. First, a controller with variable structure (VSC) is established according to some switching logic. At this primary design stage the link flexure is treated as a system uncertainty or disturbance to the rigid body motion. The aim of VSC is to guarantee tracking error convergence of each rigid body joint. In the next stage of the control design, the switching surface is selected to act like a set of linear operators with high frequency control penalty. As a result, high frequency modeling uncertainties are less excited.

For the RDT, since no direct actuation of flexure variables is available, there is no design degree-of-freedom to control their deformation directly. However, since the

switching surface of VSC can be chosen arbitrarily, the switching surface can be selected to act like an operator which controls the vibration indirectly. When a nonlinear system enters the sliding mode, its dynamics become those dictated by the switching surface. If the surface dynamics are linear, the linear operator can be devised by applying optimization methods. Moreover, there is a degree-of-freedom for the designer to choose weighting matrices in the performance index, weighting matrices which can be made frequency-dependent based upon RDT structure bandwidth.

6.2.1 The "Switching Surface " as a Linear Operator

In this section we will consider the "switching surface" not to be a hypersurface, but a linear operator representable as linear, time-invariant dynamic system itself, acting on the states. The model is assumed to be the system

$$\begin{bmatrix} \dot{x}_1 \\ \dot{x}_2 \end{bmatrix} = \begin{bmatrix} A_{11} & A_{12} \\ A_{21} & A_{22} \end{bmatrix} \begin{bmatrix} x_1 \\ x_2 \end{bmatrix} + \begin{bmatrix} O \\ B_2 \end{bmatrix} u \tag{6.29}$$

where $x_1 \in R^n$, $x_2 \in r^m$, $u \in R^m$, the matrices are real, of compatible dimension and B_2 is of full rank. The switching surface is

$$\sigma = C(x_1) + x_2 \tag{6.30}$$

where $C(\cdot)$ is a linear operator which has a realization as a system, i.e.,

$$\begin{aligned} \dot{z} &= Fz + Gx_1 \\ y &= Hz + Cx_1 \end{aligned}$$

Here we have assumed that $C(\cdot)$ has an equal number of poles and zeros (or less zeros). Extensions to more zeros can also be made, introducing derivatives of x_1.

The total system is

$$\begin{bmatrix} \dot{z} \\ \dot{x}_1 \\ \dot{x}_2 \end{bmatrix} = \begin{bmatrix} F & G & \vdots & 0 \\ 0 & A_{11} & \vdots & A_{12} \\ \cdots & \cdots & \cdots & \cdots \\ 0 & A_{21} & \vdots & A_{22} \end{bmatrix} \begin{bmatrix} z \\ x_1 \\ \cdots \\ x_2 \end{bmatrix} + \begin{bmatrix} 0 \\ 0 \\ \cdots \\ B_2 \end{bmatrix} u$$

$$\sigma = [H \;\; C] \begin{bmatrix} z \\ x_1 \end{bmatrix} + x_2$$

The equivalent control on the switching surface can be found from using the conditions $\sigma = 0$

$$[H \quad C]\begin{bmatrix} z \\ x_1 \end{bmatrix} + x_2 = 0 \tag{6.31}$$

and $\dot{\sigma} = 0$

$$\begin{aligned} H\dot{z} + C\dot{x}_1 + \dot{x}_2 = \; & HFz + HGx_1 + CA_{11}x_1 + CA_{12}x_2 \\ & + A_{21}x_2 + A_{22}x_2 + B_2u_{eq} = 0 \end{aligned}$$

to give

$$\begin{aligned} u_{eq} = \; & -B_2^{-1}[HFz + (HG + CA_{11} + A_{21})x_1 && (6.32) \\ & + (CA_{12} + A_{22})x_2] && (6.33) \end{aligned}$$

and

$$x_2 = -Hz - Cx_1$$

Thus, u_{eq} can also be expressed as

$$\begin{aligned} u_{eq} = \; & -B_2^{-1}[(HF - CA_{12}H - A_{22}H)z && (6.34) \\ & + (HG + CA_{11} + A_{21} - CA_{12}C - A_{22}C)x_1] \end{aligned}$$

On the switching surface, the reduced order system is

$$\dot{z} = Fz + Gx_1$$

$$\dot{x}_1 = A_{11}x_1 + A_{12}x_2 = A_{11}x_1 + A_{12}(-Hz - Cx_1)$$

Thus, this is a pair of systems in feedback configuration.

Note that if σ is non-dynamic, it is realizable as $y = Cx_1$ which is the standard switching surface representation.

What we have thus accomplished is insertion of a "filter" (dynamics to be defined as required) into the standard switching control.

6.2.2 Frequency-shaped Optimal Sliding Mode

In an earlier work Utkin and Young have shown [43] how a quadratic regulator can be defined to specify behavior of a system in the sliding region. Özgüner and Öz have shown [44] the clear relationship between the choice of weights in the quadratic regulator and the inclination of the hypersurface, in mechanical systems. Thus the formulations above can thus be merged for a frequency weighted variable structure controller which will filter the vibrational modes.

As developed by Utkin and Young, this method called for the minimization of the quadratic cost,

$$J_s = \int_{t_s}^{\infty} (x^T Q x) dt \tag{6.35}$$

where t_s is the time at which sliding mode begins. This problem was interpreted as an LQ optimal regulator problem for the transformed system,

$$\begin{bmatrix} \dot{x}_1 \\ \dot{x}_2 \end{bmatrix} = \begin{bmatrix} A_{11} & A_{12} \\ A_{21} & A_{22} \end{bmatrix} \begin{bmatrix} x_1 \\ x_2 \end{bmatrix} + \begin{bmatrix} 0 \\ B_2 \end{bmatrix} u \tag{6.36}$$

for which the quadratic cost,

$$J_s = \int_{t_s}^{\infty} (x_1^T Q_{11} x_1 + 2 x_1^T Q_{12} x_2 + x_2^T Q_{22} x_2) dt \tag{6.37}$$

is minimized with respect to x_2. The optimal switching surface $s(x_1, x_2) = 0$ is derived from the optimal control solution of this problem to be:

$$x_2 = -Q_{22}^{-1} [A_{12}^T P + Q_{12}^T] x_1 \tag{6.38}$$

where P is the appropriate Riccati equation solution. The above expression also defines the switching line. While sliding mode exists, in the upper row of (6.36) x_2 can be regarded as a vector of operating variables. Consequently, the frequency-shaped optimal sliding mode is realized through replacing (6.37) by

$$J = \frac{1}{2} \int_{-\infty}^{\infty} [x_1^*(j\omega) Q_{11} x(j\omega) + x_2^*(j\omega) Q_{22}(j\omega) x_2(j\omega)] \, d\omega \tag{6.39}$$

where Q_{11} is positive semi-definite, $Q_{22}(j\omega)$ is a positive definite Hermitian matrices for all frequencies. The state weighting matrix $Q_{22}(j\omega)$ is selected to have a high pass filtering property to penalize high frequency control efforts which may excite vibration of higher order flexible modes.

6.2.3 Variable Structure Control Design for the Simplified RDT

According to the state space formulation, it is easy to give a primary VSC design to stabilize the RDT rigid body dynamics if bounds on uncertainties are known. Assuming that the model displacement and velocity are reasonably bounded by

$$-\epsilon_1 \leq q \leq \epsilon_1 \tag{6.40}$$

$$-\epsilon_2 \leq \dot{q} \leq \epsilon_2 \tag{6.41}$$

where ϵ_1 and ϵ_2 are constant vectors with each element being positive. Using Lyapunov design method the VSC design gives global stability conditions for MIMO systems such as the simplified RDT.

Since the simplified RDT dynamics is

$$\ddot{x} = f(x, \dot{x}) + D(x)u \tag{6.42}$$

multiply B^T to both sides of (42), the rigid part can be obtained

$$\ddot{x}_0 = f_0(x, \dot{x}) + D_0(x)u \tag{6.43}$$

where $x_0,\ f_0 \in R^4,\ D_0 \in R^{4\times4},\ x_0 = [\theta_1, \theta_2, \theta_1', \theta_2']^T$.

Because the first two links of the simplified RDT are rigid, and have the same lengths as the constrained link, the first equation of (43) is exactly the same as the third equation of (43) whatever u would be, i.e.

$$\theta_1 \equiv \theta_1'$$

hence the first column (row) of D_0 equals the third column (row), and rank $(D_0) = 3$. Therefore in the VSC design, the rigid dynamics can be further reduced to a 3×3 dynamics as

$$\ddot{x}_r = f_r(x, \dot{x}) + D_r(x)u_r \tag{6.44}$$

where $x_r = [\theta_2, \theta_1', \theta_2']^T,\ u_r = [U_2, 2u_1', u_2']^T$, and $D_r \in R^{3\times3}$ is obtained by eliminating the first column and first row of D_r. In this case

$$\forall\ x\quad D_r(x) = D_r^T(x) > 0.$$

The VSC can be devised by first using Lyapunov direct method to give u_r, then simply letting $u_1 = u_1'$.

i) Switching surface

Select switching surface

$$\sigma = \sigma(x_r, \dot{x}_r, x_{dr}, \dot{x}_{dr}, z) \qquad \sigma \in R^3. \tag{6.45}$$

where x_{dr} is given control goal and z represents frequency shaping manipulation.

Let $\sigma_{\dot{x}_r} = -I_3$, then

$$\begin{aligned} \dot{\sigma} &= \sigma_{\dot{x}_r}\ddot{x}_r + \sigma_{x_r}\dot{x}_r + \sigma_z\dot{z} \\ &= -\ddot{x}_r + \sigma_{x_r}\dot{x}_r + \sigma_z\dot{z} \end{aligned} \tag{6.46}$$

As will be related later on, $\dot{z}$ is a function vector of z and $\dot{x}_r$.

ii) Formulation of uncertainties

The nonlinear vector f_r can be expressed as

$$f_r(x, \dot{x}) = \phi(x, \dot{q}_2)\xi(\dot{x}_r) \tag{6.47}$$

where

$$\xi = [\dot{\theta}_1\ \dot{\theta}_2\ \dot{\theta}_1^2\ \dot{\theta}_1\dot{\theta}_2\ \dot{\theta}_2^2\ \dot{\theta}_1'\ \dot{\theta}_2'\ \dot{\theta}_1'^2\ \dot{\theta}_1'\dot{\theta}_2'\ \dot{\theta}_2'^2]^T,$$

ϕ is a known matrix with each element be.

$$\phi_{ij} = \phi_{ij}(x, \dot{q}_2) \tag{6.48}$$

Consequently

$$\begin{aligned} \dot{\sigma} &= -\phi\xi - D_r u_r + \sigma_{x_r}\dot{x}_r + \sigma_z\dot{z} \\ &= D_r[-D_r^{-1}\phi\xi - u_r + D_r^{-1}\sigma_{x_r}\dot{x}_r + D_r^1\sigma_z\dot{z}] \\ &= D_r(\Theta\eta - u_r) \end{aligned} \tag{6.49}$$

where $\eta = [\xi^T, z^T]^T$, $\Theta = \Theta(x, \dot{q}_2)$ is a coefficient matrix corresponding to the vector η. With the assumption (6.40), (6.41), it is easy to calculate the bounds of Θ off-line, therefore

$$-\Theta_{max} \leq \Theta \leq \Theta_{\mathbf{max}} \tag{6.50}$$

which implies

$$\begin{aligned} \forall \;\; x_r, q_2 \in [-\epsilon_1, \epsilon_1],\; \dot{q}_2 \in [-\epsilon_2, \epsilon_2] \\ |\theta_{ij}(x, \dot{q}_2)| \leq \theta_{ij\,\max} \\ i = 1,2,3 \qquad j = 1, \cdots, 3 + N_2 \end{aligned} \tag{6.51}$$

iii) Lyapunov Function

Now choosing Lyapunov function to be

$$v = \frac{1}{2}\sigma^T D_r^{-1}\sigma \tag{6.52}$$

Substituting (6.49) into the time differential of (6.52) one obtains

$$\dot{v} = \frac{1}{2}\,\sigma^T\,\frac{d}{dt}\,(D_r^{-1})\sigma \;+ \sigma^T\Theta\eta - u_r \tag{6.53}$$

The first term of the right side of (6.53) can be calculated with symbolic computing method. However, note that when a system in sliding mode, $\sigma \approx 0$, therefore it can be neglected in VSC design. The switching control is thus of the form

$$u_r = S\Theta_{\max}|\eta|_1 \tag{6.54}$$

where

$$\begin{aligned} S &= diag(sgn(\sigma_1),\; sgn(\sigma_2),\; sgn(\sigma_3)) \\ |\eta|_1 &= [\,|\eta_1|, \cdots, |\eta_{3+N_2}|\,]^T. \end{aligned} \tag{6.55}$$

The conventional VSC design can also be done by following above design procedures except letting $z = 0$.

6.3 Simulations and Discussion

Since all the parameters of right part of the RDT is same as the left part, system responses of the right part must be exact the same as the left part if same control are applied. Therefore only the simulation results of the left part will be given. Besides, for simplicity only the first flexible mode is considered in the RDT model.

The equations simulated are those of identical two link open-kinematic chains but spatially discretized using the assumed modes method, and suitably modified to include

rungs as given in Section 6.1.3. For augmentation of rapid deployment, torsional springs act between the reference frame and link one, and between links one and two. The simulated system parameters are defined in Table 6.1, and numerical values appear in Table 6.2.

Table 6.1: Simulation Parameter Definitions

I_h	hub inertia
$L_i^{[\prime]}$	length of link $i^{[\prime]}$
$M_i^{[\prime]}$	mass of link $i^{[\prime]}$
d_i	distance between first links of RDT, length of rigid pinned-pinned member
m^*	mass of rung
d_i^*	distance from rung left joint to center of mass
$l_i^{[\prime]}$	spatial variable for link $i^{[\prime]}$
$\alpha_i^{[\prime]}(l_i, t)$	angle of flexure of link $i^{[\prime]}$ at location l_i
$\theta_i^{[\prime]}$	rigid link angle of link $i^{[\prime]}$
$\rho_i^{[\prime]}$	mass density of link $i^{[\prime]}$
$E_i^{[\prime]} I_i^{[\prime]}$	stiffness term for link $i^{[\prime]}$
$\hat{u}_i^{[\prime]}$	input torque at joint $i^{[\prime]}$
$N_i^{[\prime]}$	number of modes of link $i^{[\prime]}$
$M_{hub}^{[\prime]}$	hub mass
$k_{ri}^{[\prime]}$	torsional spring constant at joint $i^{[\prime]}$
$\mu_{ij}^{[\prime]}$	damping of mode j of link $i^{[\prime]}$
$\gamma_{pi}^{[\prime]}$	proportional gain at joint $i^{[\prime]}$
$\gamma_{vi}^{[\prime]}$	derivative gain at joint $i^{[\prime]}$

All simulations are of a stowed RDT type apparatus as in Figure 6.6 suddenly de-

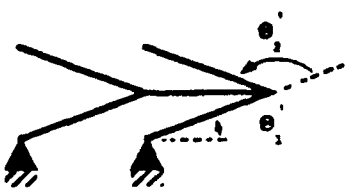

Figure 6.6: Stowed Initial Condition of Simulation

ploying and attempting to reach its final deployed position as in Figure 6.7. The

Table 6.2: Simulation Parameters

i	$1, 1'$	$2, 2'$
$I_{hi}\,[kg \cdot m^2]$	1.0	0.0
$M_{hi}\,[kg]$	2.0	0.0
$L_i\,[m]$	1.0	1.0
$E_i I_i\,[N \cdot m^2]$	∞	8.8778
$M_i\,[kg]$	1.0	1.0
N_i	0	1
$\gamma_{pi}\,[N \cdot m/rad]$	0.0	0.0
$\gamma_{vi}\,[N \cdot m/(rad/s)]$	0.0	0.0
$k_{ri}\,[N/rad]$	10.0	0.1
$\mu_i\,[N \cdot s^2/m]$	0.973	0.973
$d\,[m]$	1.0	0
$d^*\,[m]$	0.5	0
$m^*\,[kg]$	1.0	0

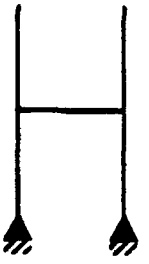

Figure 6.7: Deployed Final Condition of Simulation

numerical values of initial and final conditions of the motion are listed in Table 6.3, page 68. These chosen conditions are somewhat contrived, so as to not generate Jacobian matrices of less than full rank. This loss of rank would cause the matrix $\frac{\partial C}{\partial z} M^{-1} \left(\frac{\partial C}{\partial z}\right)^T$ in (6.5) to become singular, making a solution for Γ, the constraint forces, impossible. Simulations were carried out maintaining the smallest nonzero number possible on the order of 10^{-18} as a measure of numerical accuracy.

In the conventional variable structure control design, the switching surface is

$$\sigma_i = c_i(\theta_{id} - \theta_i) + \dot{\theta}_i \tag{6.56}$$

Table 6.3: Initial and Final Conditions

	θ_1 deg	θ_1' deg	θ_2 deg	θ_2' deg	α_1 m	α_2 m
i.c.	5.0	5.0	175.0	175.0	0	0
f.c.	90.0	90.0	0	0	0	0

where θ_i and θ_{id} $i = 1, 2$ are angles and the desired angles of the two rigid links. c_i is the inclination of the switching line (switching surface). For both the rigid and flexible links, the variable structure control has the form

$$u_i = \left(\sum_{j=1}^{5} k_{ij}\eta_j + \rho_i \right) \mathrm{sgn}(\sigma_i) \quad i = 1, 2 \tag{6.57}$$

where the control gain matrix K is previously calculated according to (6.53),

$$K = \begin{bmatrix} 11 & 11 & 0.7 & 1.5 & 0.8 \\ 4 & 4 & 0.3 & 0.5 & 0.3 \end{bmatrix} \tag{6.58}$$

and $\eta = [\dot{\theta}_1, \dot{\theta}_2, \dot{\theta}_1^2, \dot{\theta}_1\dot{\theta}_2, \dot{\theta}_2^2]^T$. ρ_i is a dither term to reject small disturbances while the system is in sliding mode. A saturation function

$$\mathrm{sat}(s_i) = \begin{cases} 1, & \text{if} \quad s > \delta_i; \\ s_i/\delta_i, & \text{if} \quad |s_i| \leq \delta_i; \\ -1, & \text{if} \quad s_i < -\delta_i. \end{cases} \tag{6.59}$$

is also introduced with $\delta_1 = 0.01$ and $\delta_2 = 0.1$.

Figure 6.8 and Figure 6.9 show the rigid body motion, indicating that set point regulation is achieved in spite of the existence of unknown deformation. Figure 6.10 shows time responses for position and velocity of flexure coordinate α_2 of the end of RDT links. Figure 6.11 and Figure 6.12 show the phaseplane of the first and the second links, respectively. In the simulation the inclination of switching surfaces are set to be $c_1 = 4$, $c_2 = 1.5$, the dither terms are $\rho_1 = 3$, $\rho_2 = 0.3$ respectively.

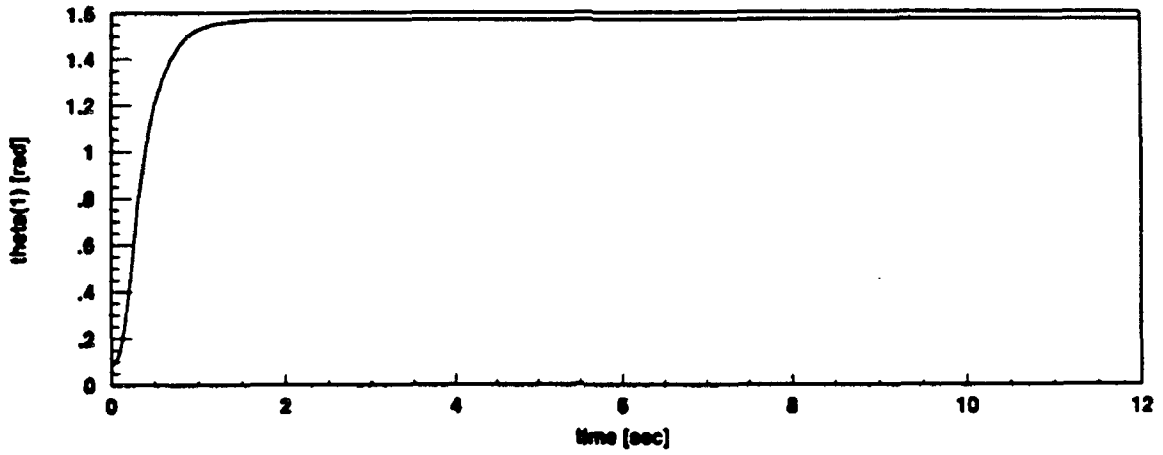

(a) Angular Position (rad)

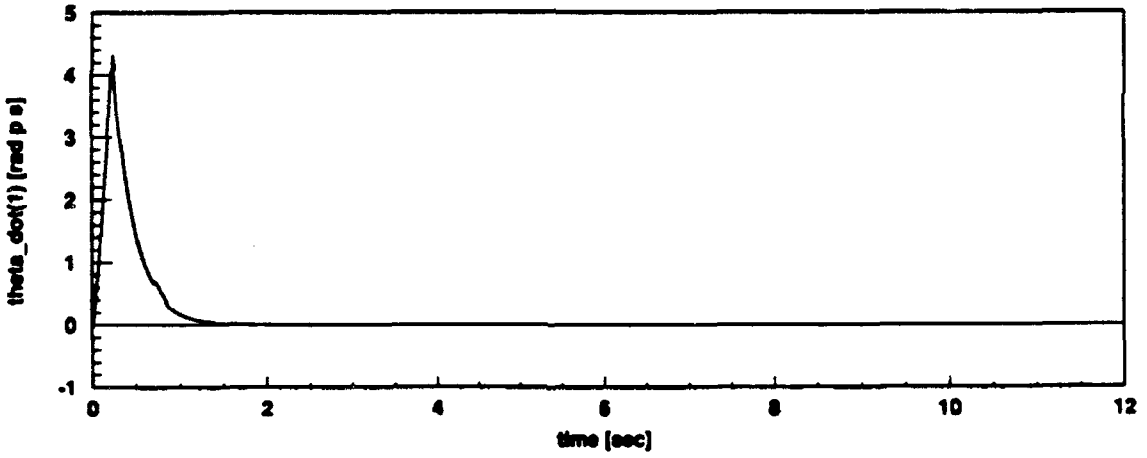

(b) Angular Velocity (rad/sec)

Figure 6.8: Rigid Body Motion of the 1st Link with VSC

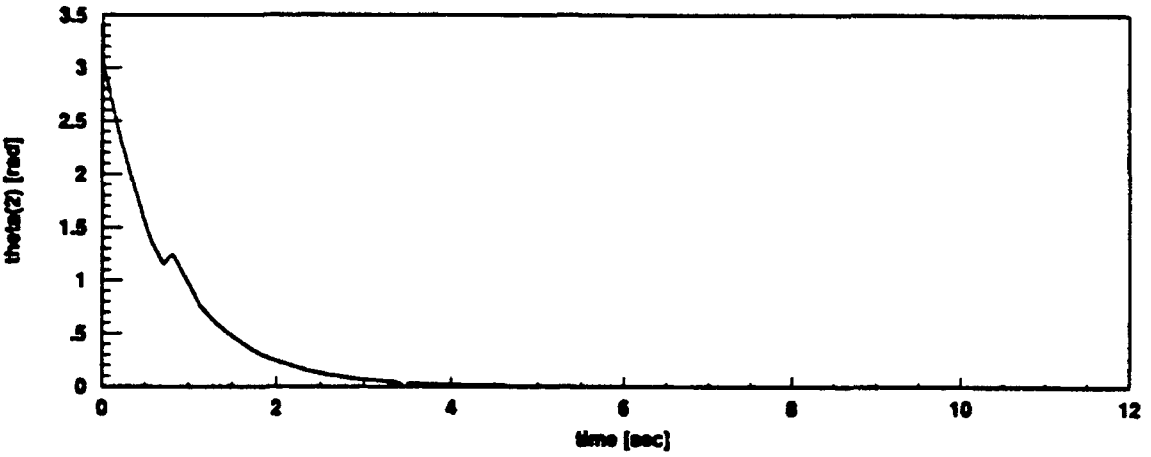

(a) Angular Position (rad)

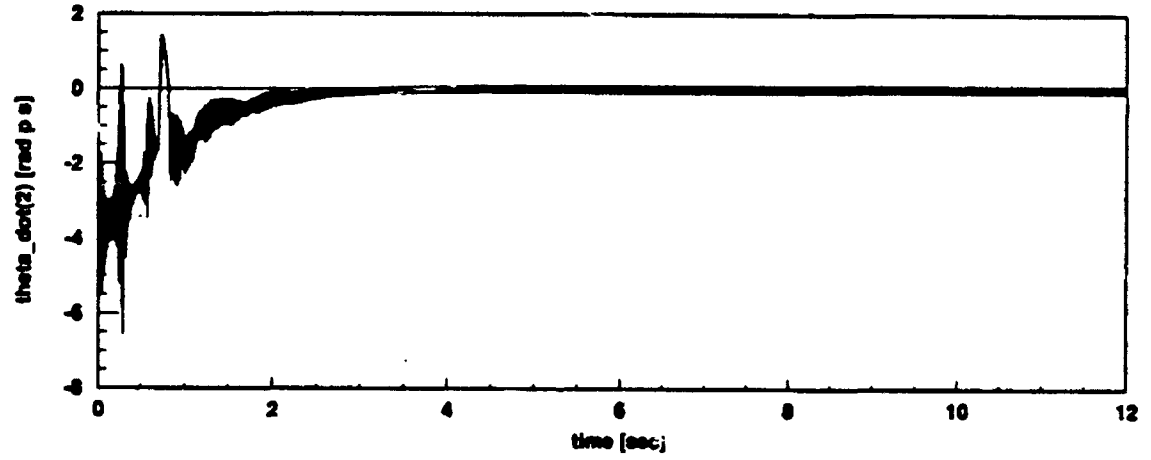

(b) Angular Velocity (rad/sec)

Figure 6.9: Rigid Body Motion of the 2nd Link with VSC

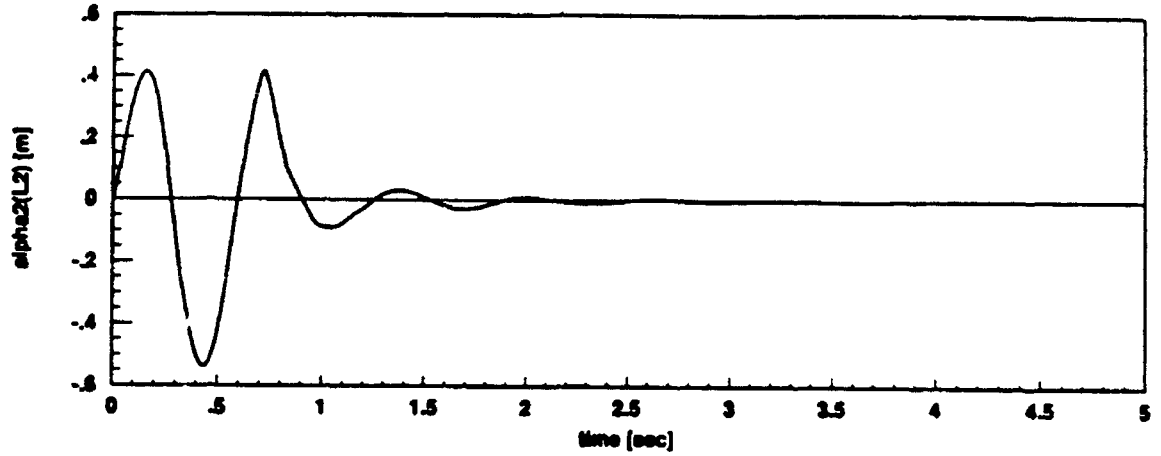

(a) Tip Flexure Deformation (m)

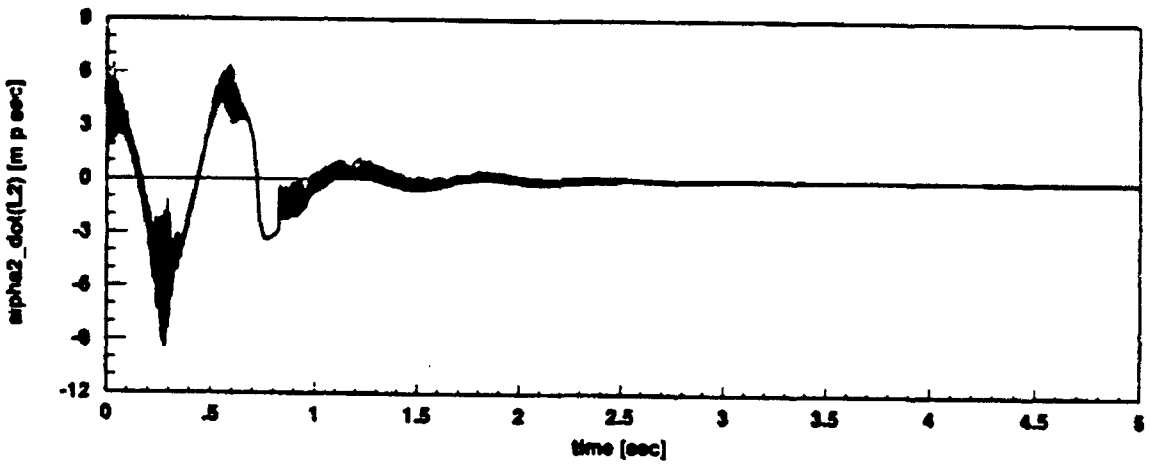

(b) Tip Flexure Velocity (m/sec)

Figure 6.10: End Link Tip Flexure with VSC

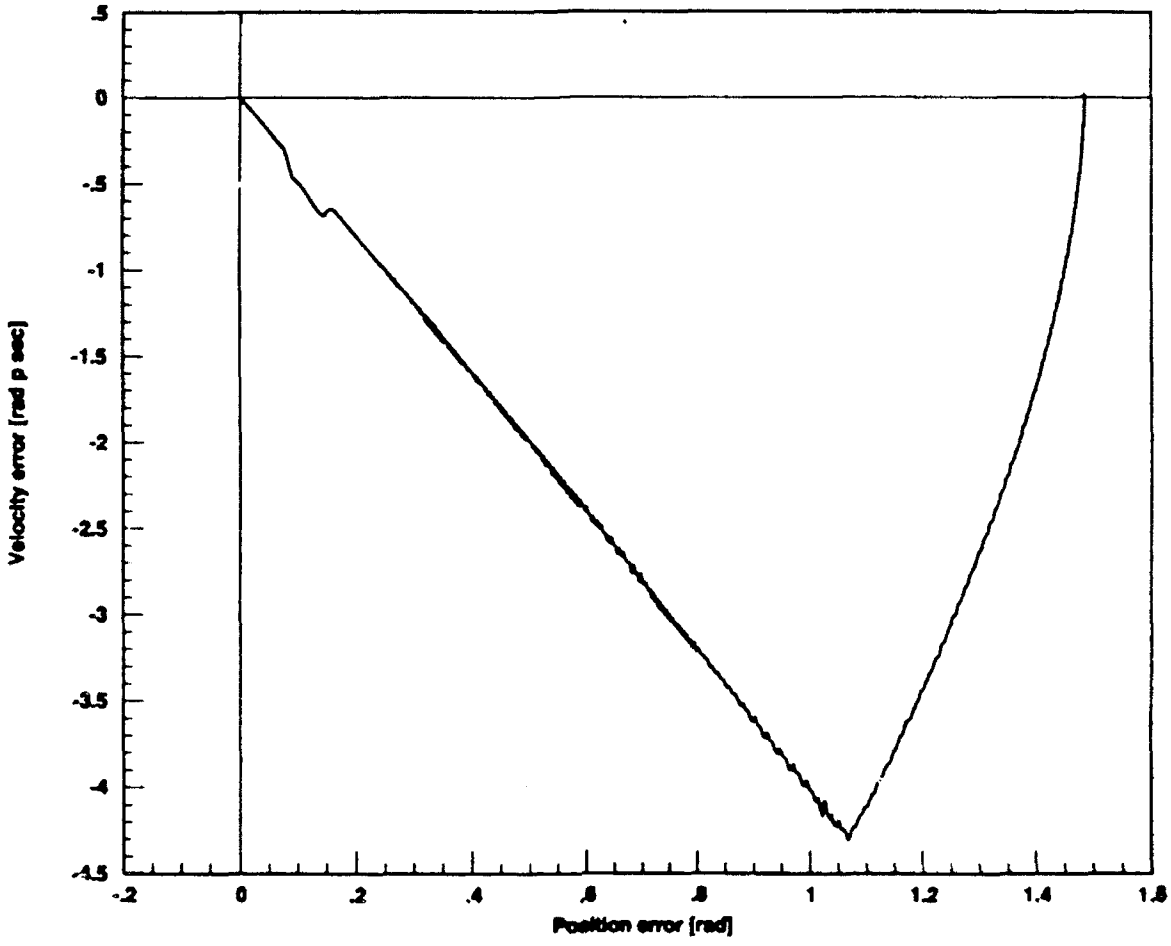

Figure 6.11: Phaseplane of the 1st Link with VSC

In this case, the VSC design for the first two rigid links are the same as those given earlier. As for the flexible link, the variable structure control has the form

$$u_i = \left(\sum_{j=1}^{7} k_{ij}\eta_j + \rho_i \right) \mathrm{sgn}(\sigma_i) \quad i = 1, 2 \tag{6.60}$$

where the control gain matrix K is

$$K = \begin{bmatrix} 11 & 11 & 0.7 & 1.5 & 0.8 & 0.0 & 0.0 \\ 4.4 & 4 & 0.3 & 0.3 & 0.3 & 80 & 12 \end{bmatrix} \tag{6.61}$$

and $\eta = [\dot{\theta}_1, \dot{\theta}_2, \dot{\theta}_1^2, \dot{\theta}_1\dot{\theta}_2, \dot{\theta}_2^2, z_1, z_2]^T$. The switching surface is

$$s_2 = h_1 z_1 + h_2 z_2 + h_3(\theta_{2d} - \theta_2) + \dot{\theta}_2 \tag{6.62}$$

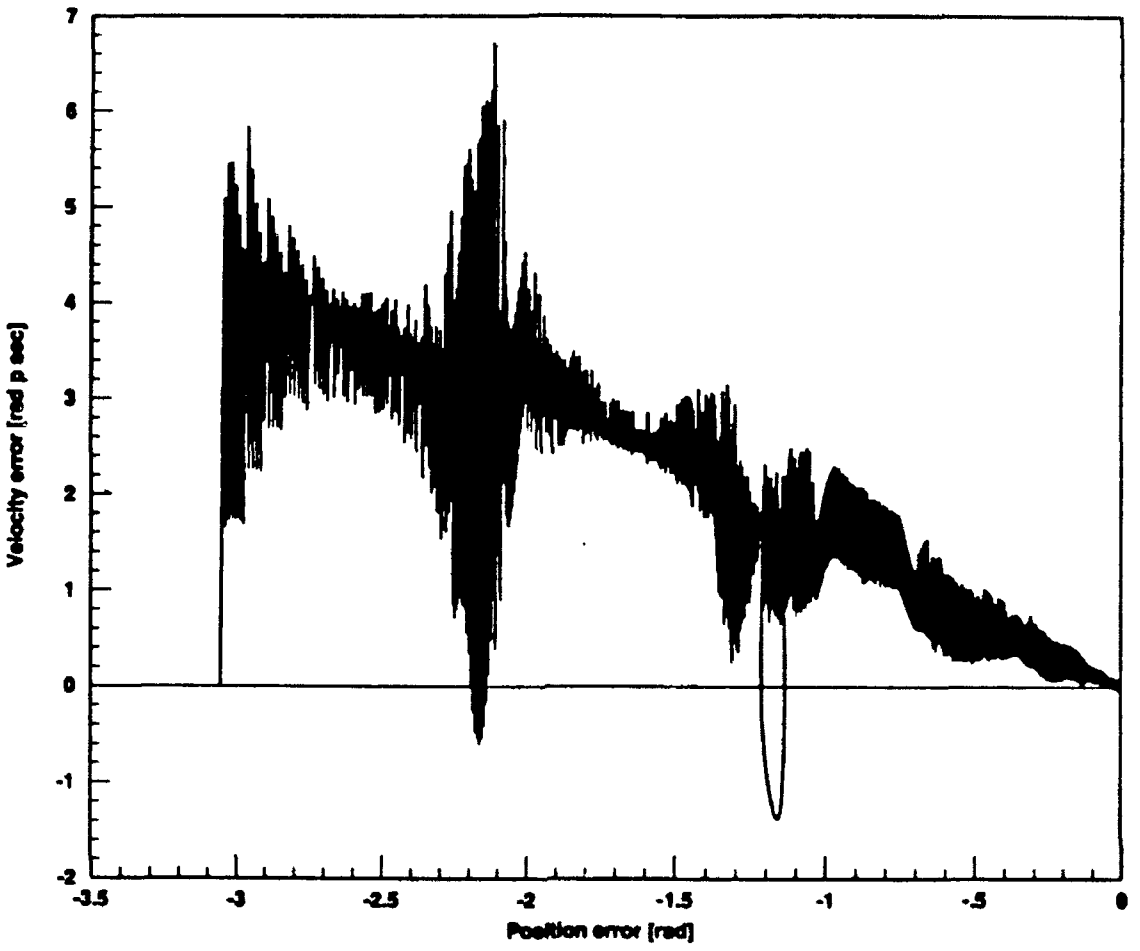

Figure 6.12: Phaseplane of the 2nd Link with VSC

where the states z_1 and z_2 are defined by a state space realization of $Q_{22}(j\omega)$ as follows.

$$\begin{bmatrix} \dot{z}_1 \\ \dot{z}_2 \end{bmatrix} = \begin{bmatrix} 0 & 1 \\ -100 & -20 \end{bmatrix} \begin{bmatrix} z_1 \\ z_2 \end{bmatrix} + \begin{bmatrix} 0 \\ 1 \end{bmatrix} \dot{\theta}_2 \tag{6.63}$$

and $h_1 = -80.18, h_2 = -11.74, h_3 = 0.34$. The high pass filter is selected as

$$Q_{22}(jw) = \frac{10\left(j\omega + \sqrt{10}\right)^2}{(j\omega + 10)^2} \tag{6.64}$$

Results of closed loop system response with frequency-shaped variable structure control follow. The effectiveness of introducing frequency shaping can be found from

Figure 6.13, which shows both position and velocity at the endpoint of the flexible RDT link. It can be observed that he maximum deformation is reduced to about 1/4 of the case without frequency shaping. Figure 6.14 and Figure 6.15 give the phaseplane of the first and the second links respectively.

In order to see how the high pass filter works in sliding mode, once again the conventional VSC is applied to the simplified RDT where inclination $c_2 = 0.5$. Figure 6.16, Figure 6.17 and Figure 6.18, in which the plot data is filtered through a FIR filter, give the phaseplanes for the conventional VSC with $c_2 = 1.5$, $c_2 = 0.5$ and frequency shaped VSC. The one with frequency shaping shows lower switching inclination at beginning and higher switching inclination when position error becomes smaller. In other words, frequency shaped switching surface behaves like a varying surface in terms of tracking error. Therefore it achieves the trade-off between faster convergence nearby equilibrium and lower control action off the equilibrium.

From Figure 6.19 and Figure 6.20 one can observe that, by selecting smaller c_2 the deformation of the flexible link can be reduced as lower as the case with frequency shaping, however, then the rigid body response is in some degree delayed.

Finally, Fast Fourier Transforms are applied to control efforts of both the VSC ($c_2 = 1.5$) and frequency shaped VSC. Comparing Figure 6.21 and Figure 6.22, it is clear that frequency shaping suppressed the control effort which may excite vibrational modes.

Analysis and control issues related to closed chain rigid-flexible mechanical systems are introduced in this chapter. For slewing flexible structures where the vibrational modes are not to be excited, the modeling approach provides a method for simulating constrained flexible structures. The approach of inserting a frequency shaped filter into the design of Variable Structure controllers was pursued for control. A linear operator interpretation of the sliding surface is used together with frequency weighted quadratic regulators in the control design. Through the control design application and simulation of the hybrid rigid-flex RDT example, the validity of the modeling method and effectiveness of proposed control methodology is shown.

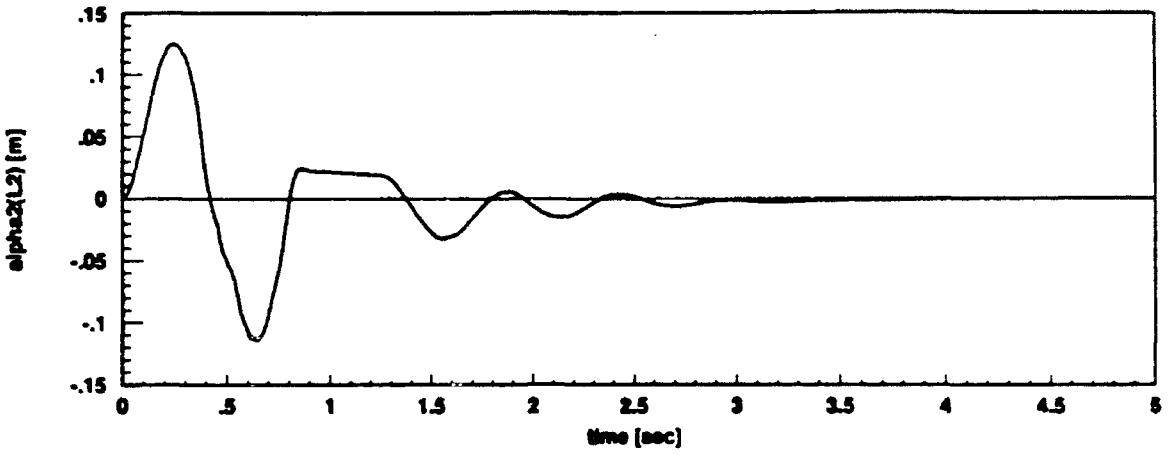

(a) Tip Flexure Deformation (m)

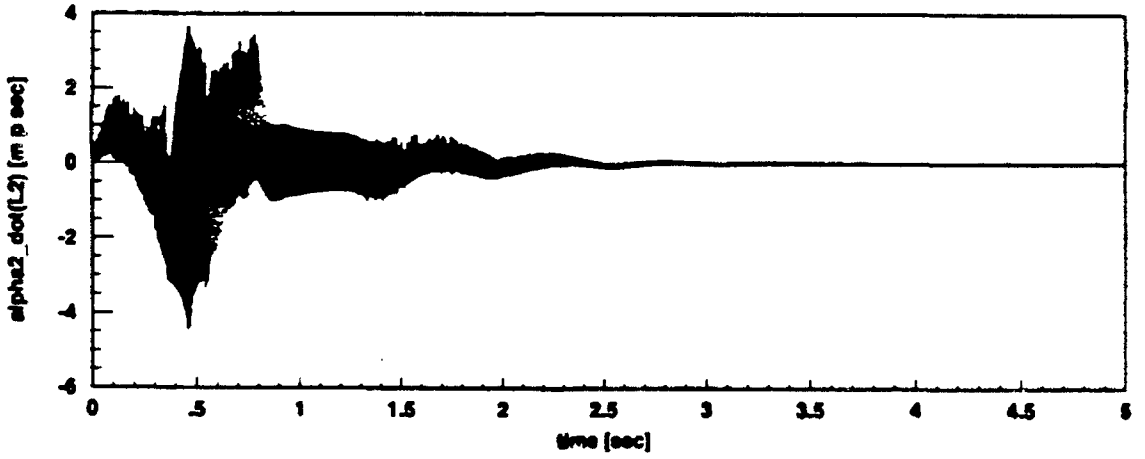

(b) Tip Flexure Velocity (m/sec)

Figure 6.13: End Link Tip Flexure with Frequency Shaped VSC

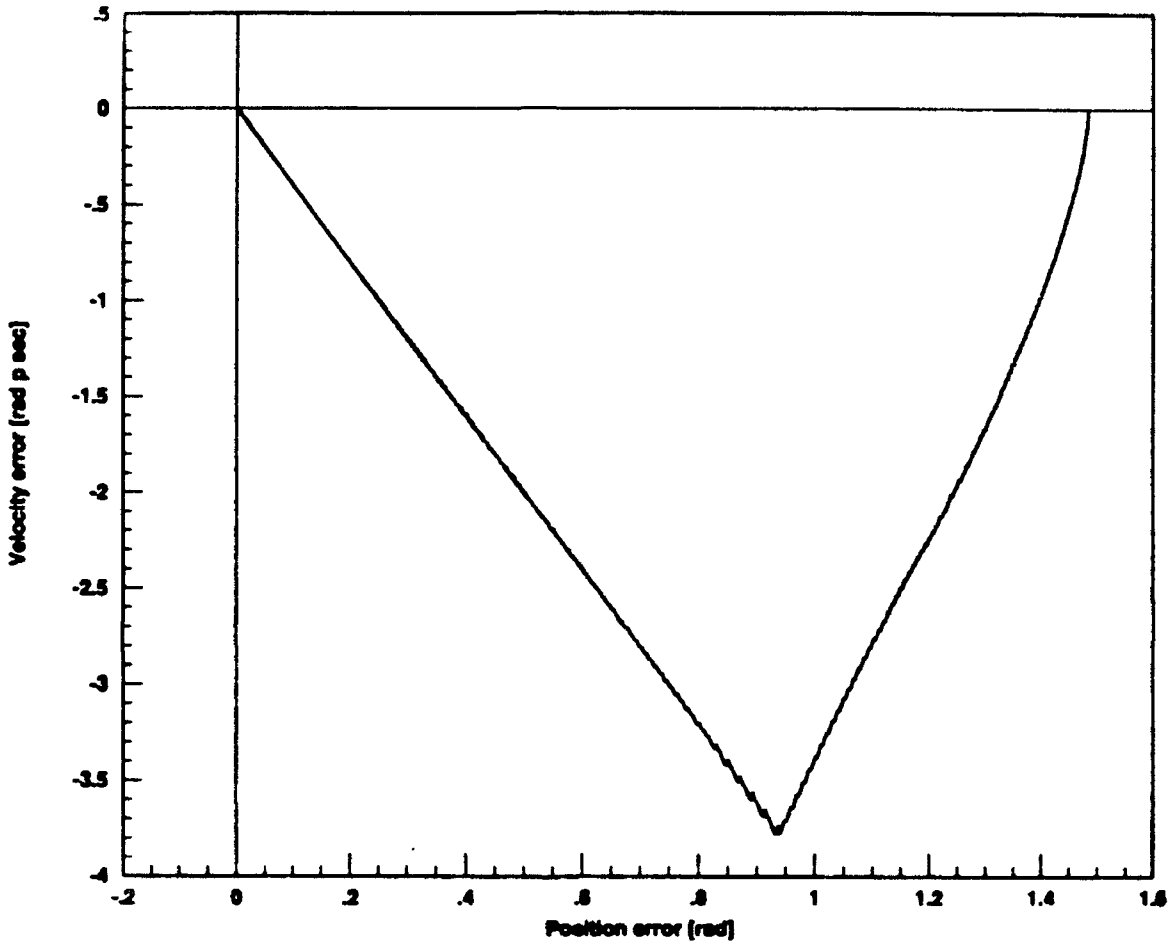

Figure 6.14: Phaseplane of the 1st Link with Frequency Shaped VSC

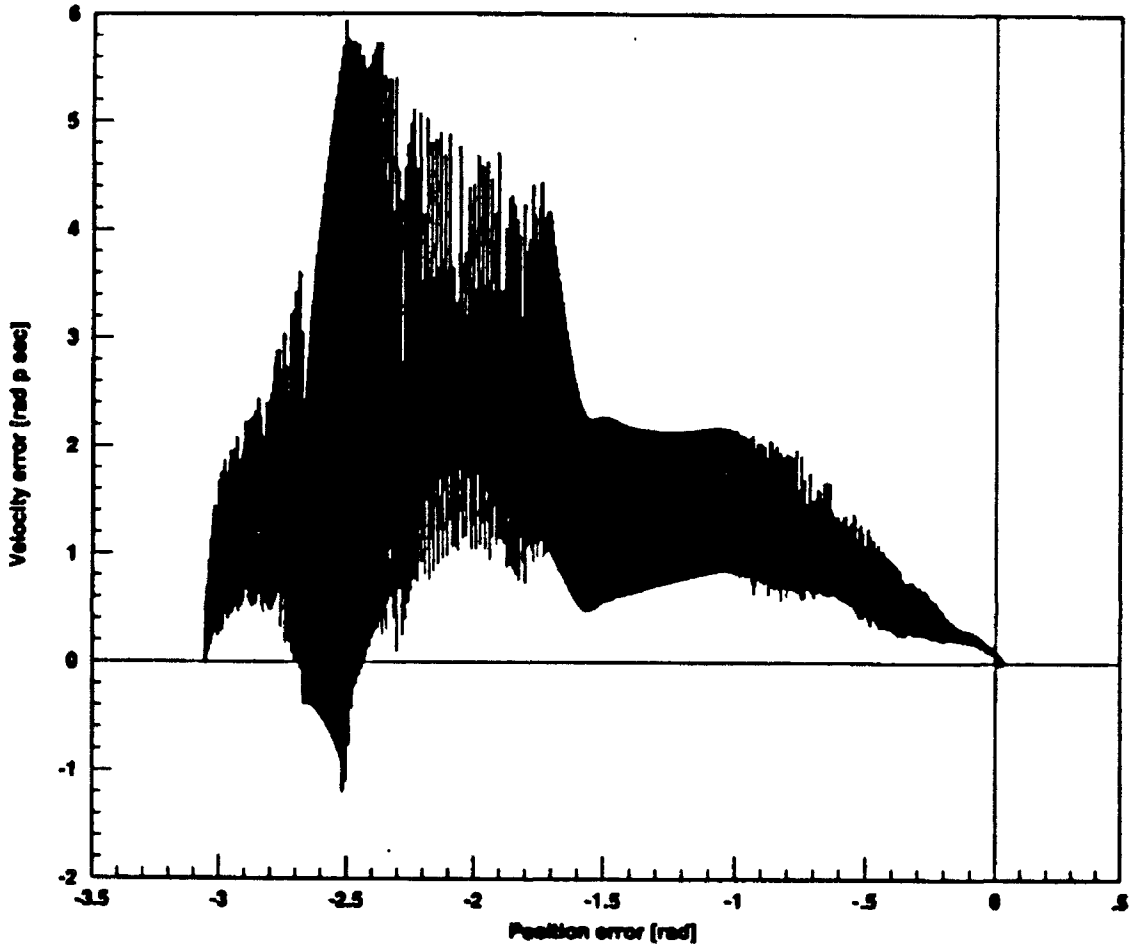

Figure 6.15: Phaseplane of the 2nd Link with Frequency Shaped VSC

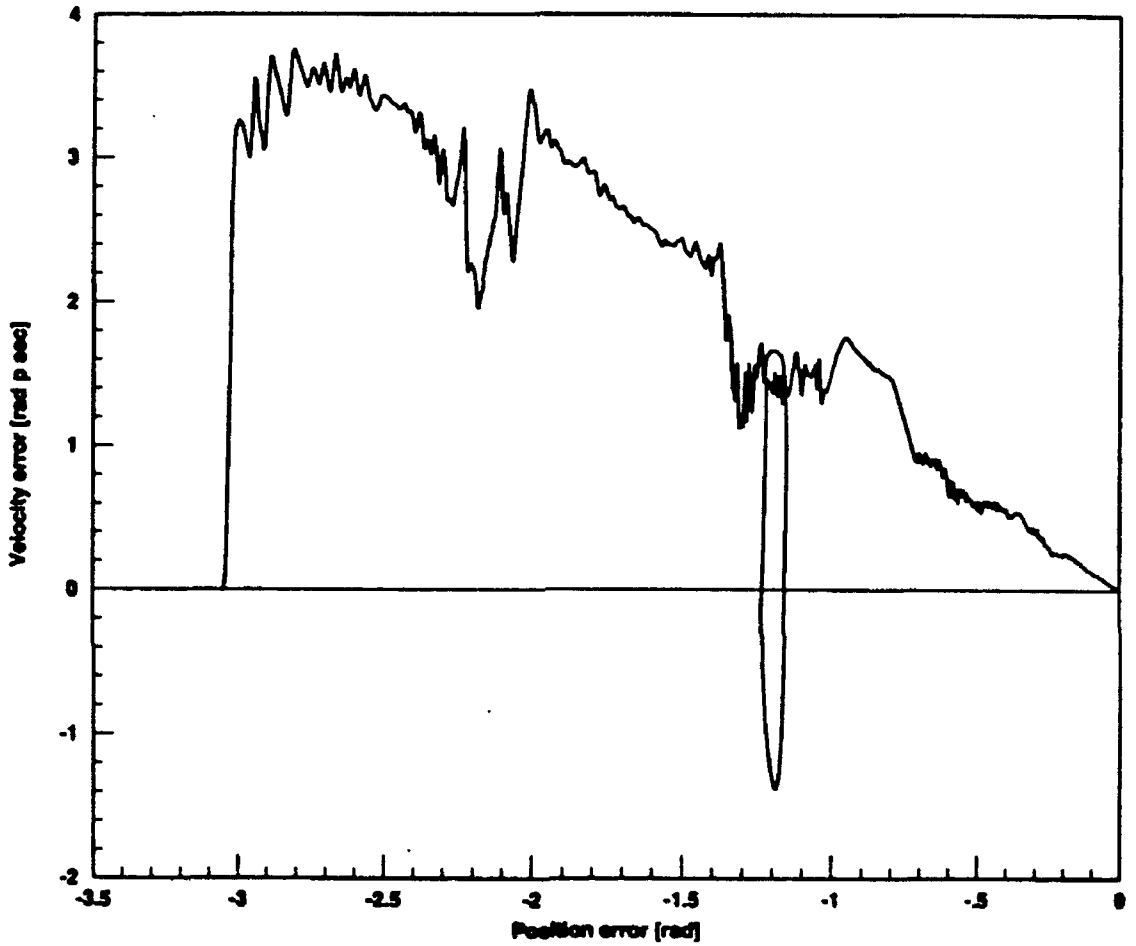

Figure 6.16: Phaseplane of VSC Filtered through FIR ($c_2 = 1.5$)

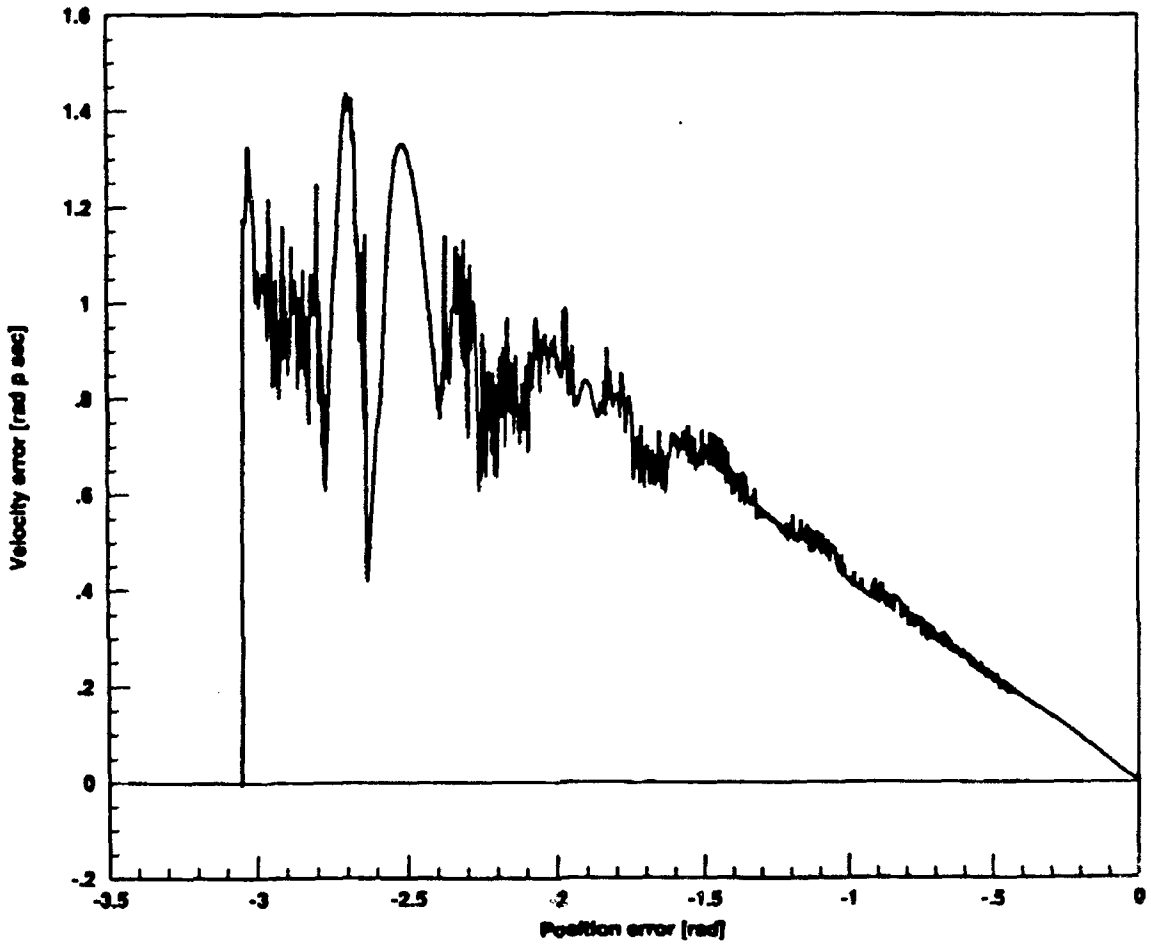

Figure 6.17: Phaseplane of VSC Filtered through FIR ($c_2 = 0.5$)

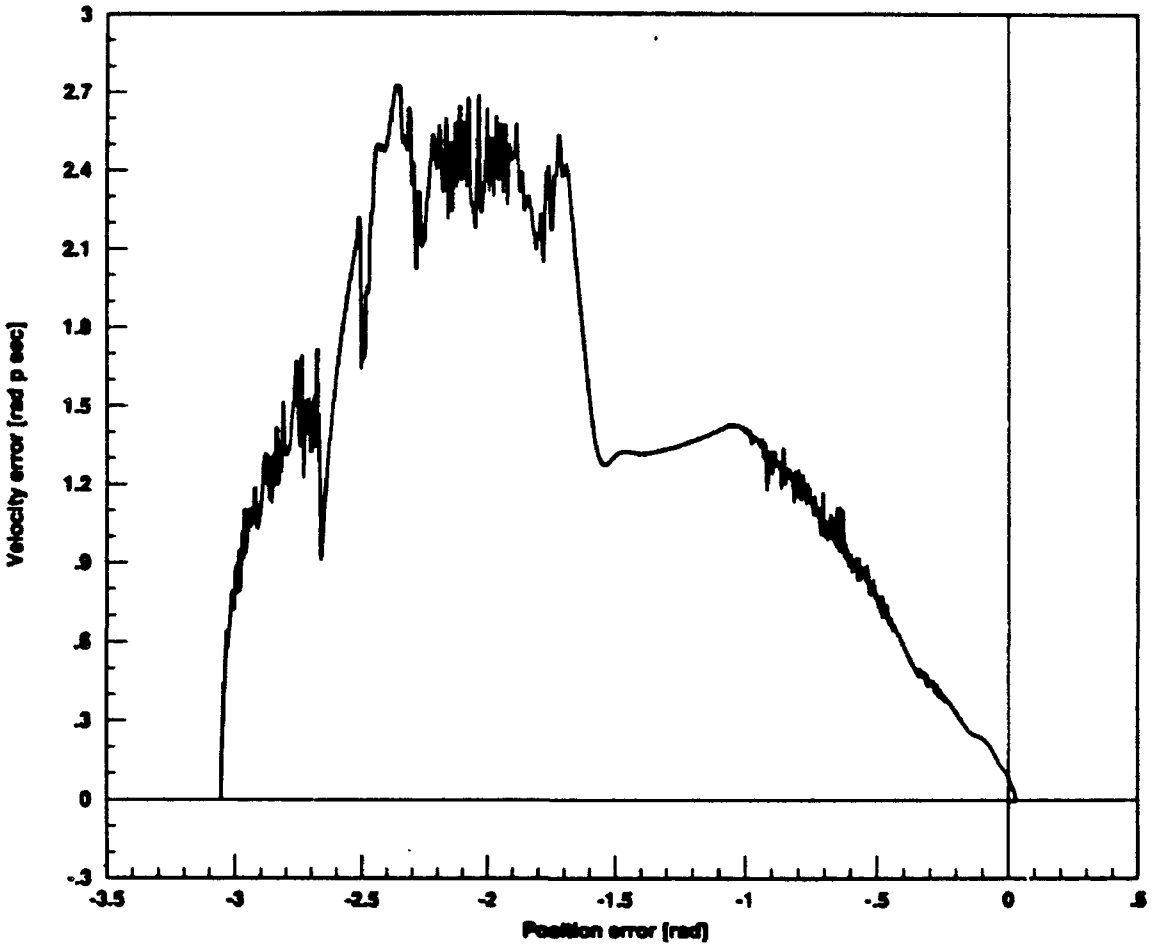

Figure 6.18: Phaseplane of Frequency Shaped VSC Filtered through FIR

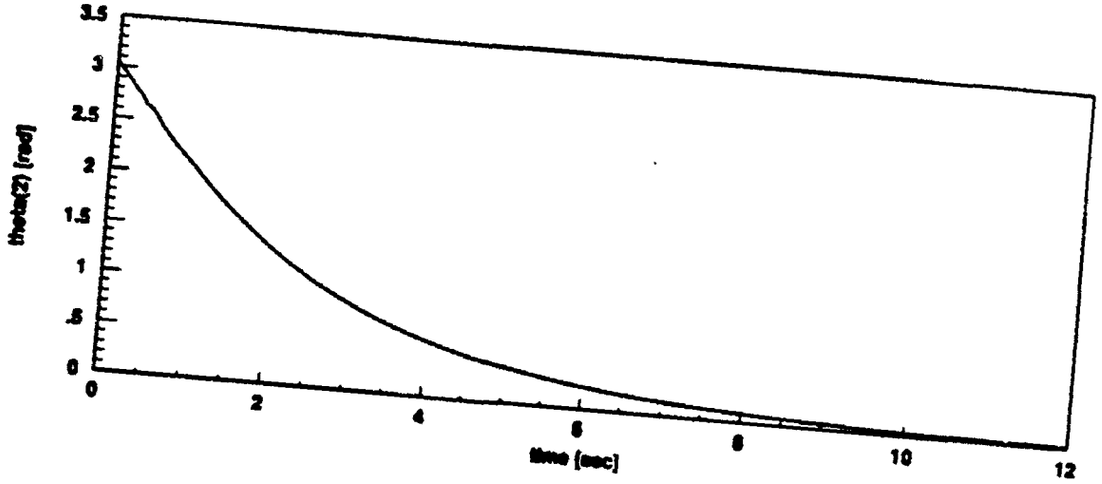

(a) Angular Position (rad)

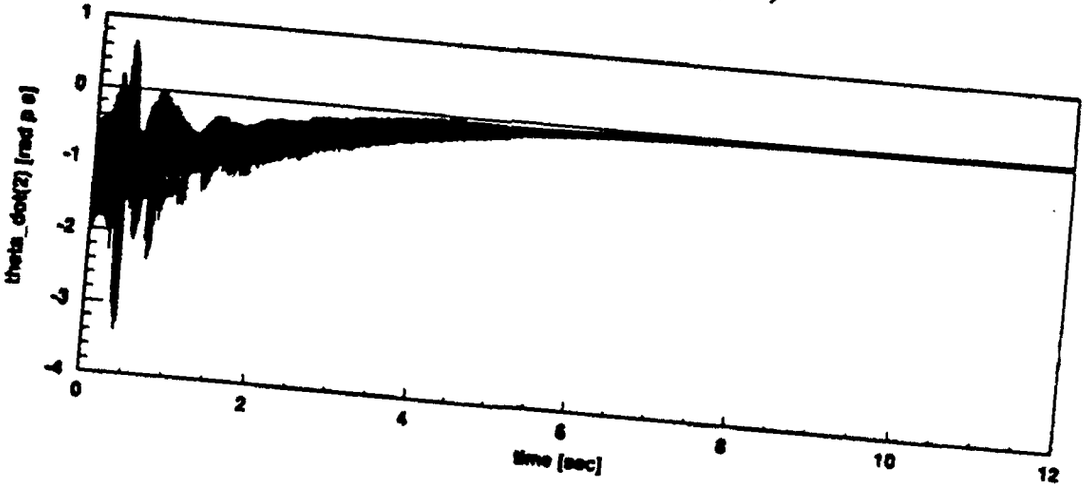

(b) Angular Velocity (rad/sec)

Figure 6.19: Rigid Body Motion of the 2nd Link with VSC ($c_2 = 0.5$)

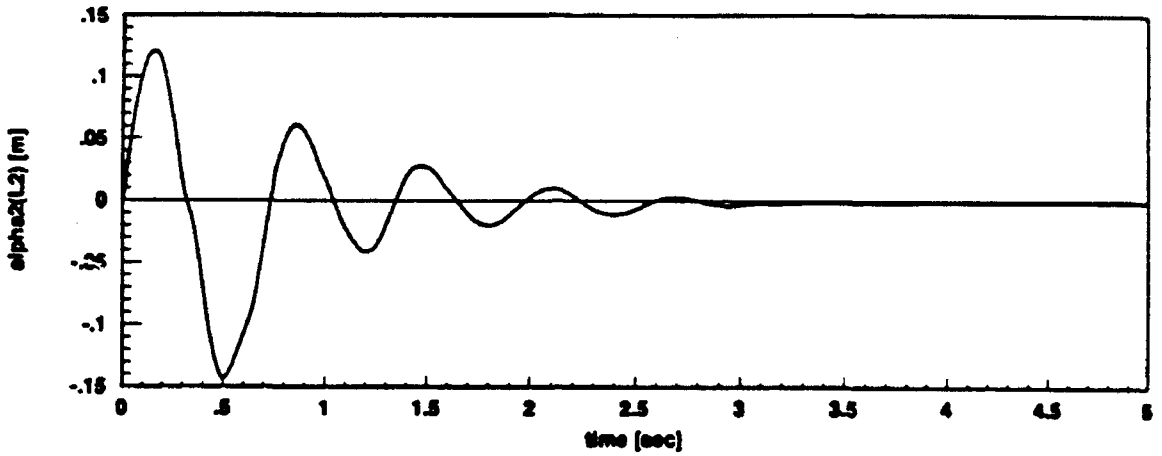

(a) Tip Flexure Deformation (m)

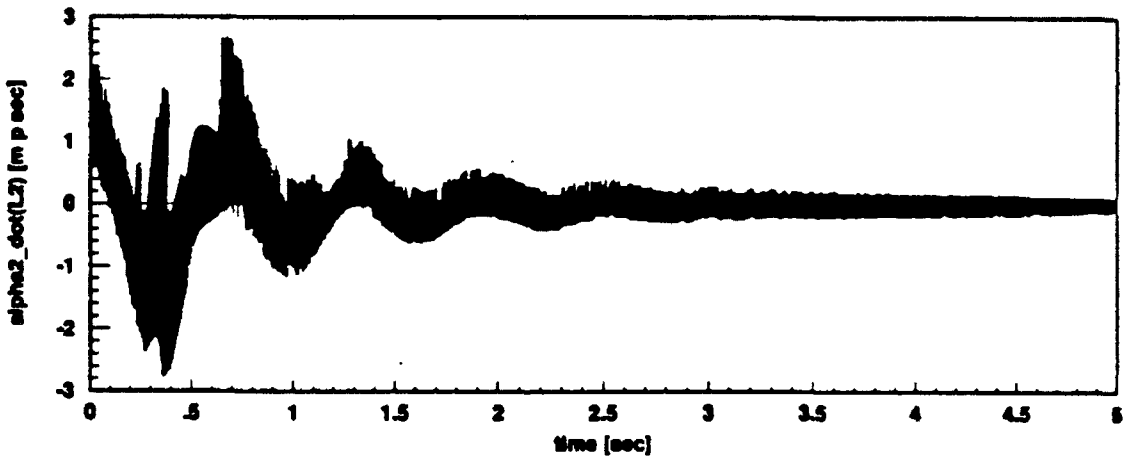

(b) Tip Flexure Velocity (m/sec)

Figure 6.20: End Link Tip Flexure VSC ($c_2 = 0.5$)

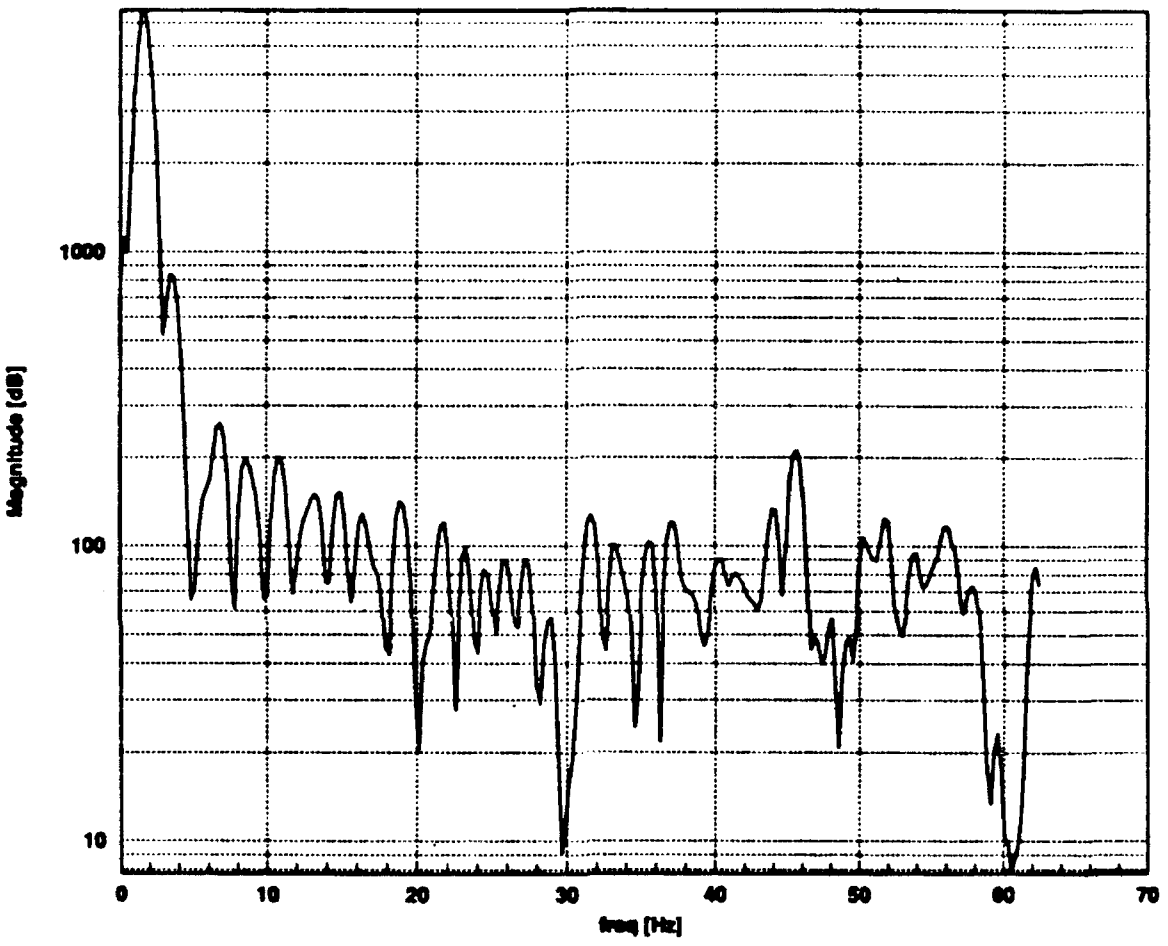

Figure 6.21: FFT of u_2 with VSC ($c_2 = 1.5$)

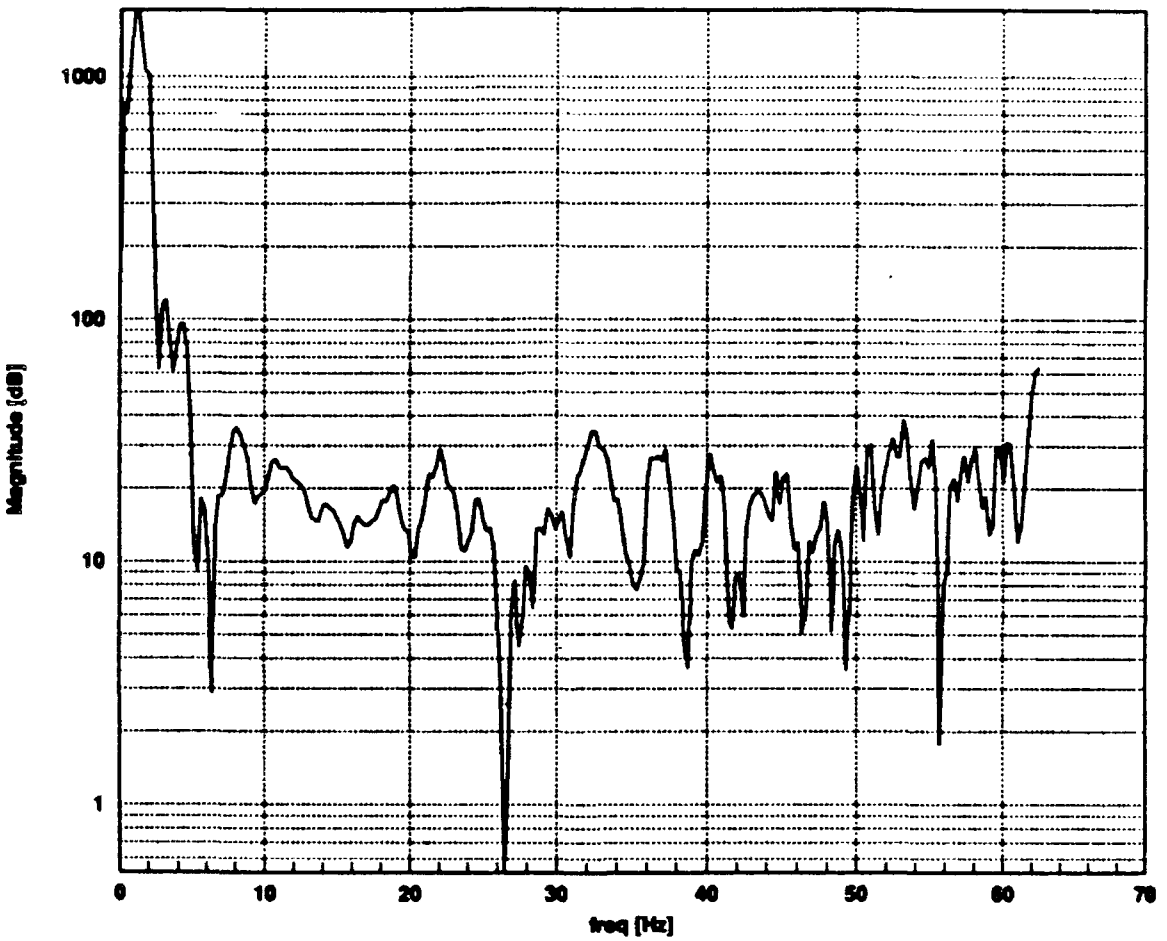

Figure 6.22: FFT of u_2 with Frequency Shaped VSC

7. SLIDING MODE CONTROL IN SAMPLED DATA SYSTEMS

The switching problem in continuous time sliding mode control design has two aspects: switching frequency and magnitude. Although high frequency switching in control is theoretically desirable from the robustness point of view, it is usually hard to achieve in practice due to physical constraints on the system. Even if it is possible, the unmodeled high frequency modes will likely be excited, which in turn deteriorates the performance. As to the chattering magnitude reduction problem, researchers have provided quite a few contributions in this area, however in most, robustness is usually compromised [45, 46].

Sliding mode control for discrete time has been considered for years [47, 48, 49, 50, 51]. To maintain the states on the sliding manifold is never an easy task. Sarpturk *et al.* propose to use the upper and lower bounds of the control to guarantee the convergence of the sliding motion [48]. The difficulty is that the solution is complicated and hard to compute in real time. In some cases, it may not even exist. Furuta implemented the controller by using an equivalent control gain and a switching gain to cope with system parameter variations [47]. The limitations are that the upper bound of the variation magnitude has to be small enough for the method to be applicable and that it does not guarantee exogenous disturbance rejection. Chan solved a servo-system problem successfully by using a similar technique which suffers the same limitations [50].

We study the sliding mode control for discrete-time linear systems resulting from sampling. The switching frequency of discrete time controllers is limited by the value T^{-1}, where T is the sampling period. The use of a discontinuous control law (typically *sign* functions) leads to chattering in the boundary layer of the sliding manifold $\mathcal{S} = \{x : s(x) = 0\}$. Even without disturbances the size of this boundary layer is of order $O(T)$. In order to alleviate chattering, it was proposed to use discrete time equivalent control in the prescribed boundary layer, whose size is defined by the restriction applied to the control variables [49]. This approach results in the motion in $O(T^2)$ vicinity of the sliding manifold. The main difficulty arising in implementation of the proposed control law is that one needs to know the disturbances for calculating the equivalent control. Lack of such information leads to $O(T)$ boundary layer, the same as with discontinuous control.

In this chapter, we introduce a new control based on that concept with robustness. Our approach allows to keep the state in the $O(T^2)$ vicinity of the sliding manifold even in the presence of disturbances. Both internal and external uncertainties are considered. Only the continuous time matching conditions and sufficient smoothness properties are required, which are reasonable constraints in most applications.

Since the system is discretized in time by the sample/hold processes, the control signal space is shrunk from $(L^2_{[0,T]})^m$ to R^m with m being the number of control inputs. Therefore, the controller will inherently be less capable then the continuous one. Sliding mode is originally a continuous time concept, and at first glance, it may not be clear that it will retain its properties in discrete time. Nevertheless, the advantage is that we are able to overcome the chattering problem with considerable robustness against system uncertainties.

7.1 Invariance Condition

Consider a continuous time linear, time-invariant system

$$\dot{x} = Ax + Bu + Ef \tag{7.1}$$

where x is an $n \times 1$ state vector, u is an $m \times 1$ control vector, and f is an $l \times 1$ deterministic disturbance vector. A, B, E are constant matrices of appropriate dimensions.

Assume u is applied through a zero-order-hold. The discretized version of (7.1) can be formulated as

$$x_{k+1} = \Phi x_k + \Gamma u_k + d_k \tag{7.2}$$

where $\Phi = e^{AT}$, $\Gamma = \int_0^T e^{A\lambda} d\lambda B$, $d_k = \int_0^T e^{A\lambda} E f((k+1)T - \lambda) d\lambda$.

The sliding surface is

$$s_k = Cx_k = 0 \tag{7.3}$$

where C is an $m \times n$ matrix and is chosen to meet some stability or performance criterion [52]. To maintain the state on the hyperplane (7.3) at the $(k+1)^{th}$ sampling instant, the equivalent control law is given by

$$u_k^{eq} = -(C\Gamma)^{-1} C(\Phi x_k + d_k) \tag{7.4}$$

assuming $C\Gamma$ is invertible.

Here d_k represents the lumped effect of the disturbance $f(t)$ to the system in the time interval $kT \leq t < (k+1)T$. If the closed loop system behavior does not depend on $f(t)$, we say the controlled system has the property of disturbance invariance and the disturbance is said to be rejectable.

Given that $f(t)$ is bounded, the integration of $f((k+1)T - \lambda)$ multiplied by another bounded function $e^{A\lambda}$ in the sampling interval results in the magnitude of $O(T)$ in

each component of d_k. If no further information is provided and we simply implement the controller u with state feedback alone, the next state x_{k+1} will not be able to reach the sliding surface exactly but will result in

$$s_{k+1} = O(T)^1 \tag{7.5}$$

We will show later that if d_k is known, it is still not rejectable by the control in general unless the discrete time matching condition holds. Unlike continuous time VSC, the matching condition

$$rank[B, E] = rank[B] \tag{7.6}$$

and the boundedness of disturbances is not sufficient for the controller to maintain sliding mode. Rather, it requires some more knowledge about $f(t)$ so that the current disturbance, d_k, can be predicted with accuracy to some extent. It is advantageous to consider the problem in discrete time because through the measurement of the states, the past values of the disturbances can be determined and this will provide the knowledge about the future ones. However, the sampling process will also result in a requirement or a condition stronger than matching.

Lemma 1 For disturbance invariance in the sampled linear system (7.2), it is necessary that the continuous time matching condition (7.6) holds.

Proof. Substituting (7.4) into (7.2) yields the sliding mode equation

$$x_{k+1} = (I - \Gamma(C\Gamma)^{-1}C)(\Phi x_k + \int_0^T e^{A\lambda} E f((k+1)T - \lambda) d\lambda) \tag{7.7}$$

The condition for disturbance invariance is

$$\int_0^T e^{A\lambda} E f((k+1)T - \lambda) d\lambda = \Gamma(C\Gamma)^{-1} C \int_0^T e^{A\lambda} E f((k+1)T - \lambda) d\lambda \tag{7.8}$$

for all possible disturbance functions $f(t)$. The necessary and sufficient condition for (7.8) is the existence of a constant $m \times 1$ vector g_k such that

$$\int_0^T e^{A\lambda} (E f((k+1)T - \lambda) - B g_k) d\lambda = 0 \tag{7.9}$$

In particular, if $f(t) = \bar{f}_k = const.$, for $kT \leq t < (k+1)T$ then $E\bar{f}_k = Bg_k$. Therefore equation (7.6) is a necessary condition for disturbance rejection.

To show that the above is not sufficient, assume (7.6) holds; i.e. there exists an $m \times l$ matrix Λ such that

$$E = B\Lambda \tag{7.10}$$

Equation (7.9) becomes

$$\int_0^T e^{A\lambda} B(\Lambda f((k+1)T - \lambda) - g_k) d\lambda = 0 \tag{7.11}$$

Thus, it yields n equations with m unknowns. Since $m < n$ in general, there exists no solution for g_k. This completes the proof. □

It is important to note why the sampled system does not preserve the disturbance rejection property. This is due to the zero-order-hold which is imposed between consecutive sampling instants to the control channels during the sampling process. A similar hold does not exist in the disturbance channel and as a result, the perfect sliding property is destroyed. The same argument is true for system parameter variations. Although perfect sliding mode is not possible, one can still maintain the states in the vicinity of the sliding surface and retain the satisfying disturbance rejection character.

Lemma 2 If the continuous time matching condition (7.6) holds and $\dot{f}(t)$ is bounded, there exists a control law u_k such that the sliding surface (7.3) can be reached with $O(T^2)$ accuracy.

Proof. Choose $g_k = \Lambda f(kT)$, then the left hand side of equation (7.11) becomes

$$\int_0^T e^{A\lambda} B\Lambda \int_{(k+1)T-\lambda}^{kT} \dot{f}(\sigma) d\sigma d\lambda = O(T^2) \tag{7.12}$$

Since $\dot{f}$ is bounded, equation (7.12) is confirmed. We then apply the control

$$u_k = -(C\Gamma)^{-1} C\Phi x_k - g_k \tag{7.13}$$

to achieve $O(T^2)$ invariance in the sliding equation (7.7) and $s_{k+1} = O(T^2)$. □

If $f(t)$ is measurable or we have its model, then $f(kT)$ can be observed and g_k obtained. Nevertheless, since in general $f(kT)$ will not be known exactly, it is necessary to design g_k in some other way. As a matter of fact, we will show in the next section that the choice $g_k = \Lambda f(kT)$ is satisfying but not optimal. There exists a better solution for g_k that compensates for most of the disturbances without the need for observing $f(t)$.

7.2 Deterministic Systems

7.2.1 Exogenous Disturbances

The major difficulty in maintaining sliding mode for a discrete time system is that the exogenous disturbance d_k is essentially independent of the state x_k; i.e., even if we achieve $s_k = 0$ at the present moment, it is still not guaranteed that $s_{k+1} = 0$ since the unknown d_k will force the state out of the sliding manifold. Therefore, perfect sliding mode is impossible in spite of the knowledge about the disturbances. However, within a certain tolerance, we are able to achieve satisfying system performance by steering the states as close to the sliding manifold as possible. This includes a predictor for d_k and proper choice of the feedback compensator. The rudiments of a one-step disturbance predictor were given by Özgüner and Morgan [35] in the context of a robotics application. Here we rigorously analyze this issue.

The Disturbance predictor

The past values of the disturbances d_i, $i = k-1, k-2, \cdots$ can be computed exactly from the state and control history by considering the discrete time system (7.2). If $f(t)$ possesses some continuity attributes, there will exist a strong correlation between the past and future disturbances.

If $f(t)$ is bounded, then $d_k = O(T)$.

If furthermore $\dot{f}(t)$ is bounded, then the difference

$$d_k - d_{k-1} = \int_0^T e^{A\lambda} E[f((k+1)T - \lambda) - f(KT - \lambda)]d\lambda$$

is of order $O(T^2)$. In the same manner, for bounded $f(t)$, $\dot{f}(t)$, $\cdots$, $f^{q-1}(t)$, we have the prediction for d_k

$$\tilde{d}_k = \sum_{i=1}^{q-1}(-1)^{i-1}\binom{q-1}{i}d_{k-i} \tag{7.14}$$

with $O(T^q)$ error. If one desires to perform p-step ahead prediction, define

$$\bar{d}_j = \begin{cases} d_j & if \quad j \leq k-1 \\ \tilde{d}_j & if \quad j \geq k, \end{cases} \tag{7.15}$$

then

$$d_{k+p-1} = \sum_{i=1}^{q-1}(-1)^{i-1}\binom{q-1}{i}\bar{d}_{k-i+p-1} + O(T^q). \tag{7.16}$$

Therefore we are able to predict d_j, $j \geq k$ with accuracy up to $O(T^q)$ if $f(t) \in C^{(q-1)}$.

Equation (7.16) is actually an incomplete model for disturbances with accuracy depending on the degree of smoothness of $f(t)$. The past values are to accumulate the knowledge base of the unknowns. If $f(t)$ can be measured exactly, such as a reference input signal to the system, no prediction for d_k is necessary.

Sliding Mode with $O(T^q)$ Accuracy

It is understood that the discrete time sliding surface (7.3) can not be reached exactly due to the effect of unknown disturbances. Nevertheless, it is possible to reach a higher accuracy if appropriate disturbance prediction process is employed.

Theorem 1 If $f(t) \in C^{(q-1)}$, $q \geq 2$, and (7.6) holds, then the control law

$$u_k = -(C\Gamma)^{-1}C\Phi x_k - (C\Gamma)^{-1}C\tilde{d}_k \tag{7.17}$$

will lead to sliding motion such that $s_{k+1} = O(T^q)$ for $k \geq q$ and x_k in the $O(T)$ boundary layer of the sliding surface (7.3).

The proof is straight forward by direct substitution. As to the intersample system behavior, an $O(T^2)$ error is inevitable. This is an inherent limitation of the discrete time controller since the control signal space does not cover the disturbance range space. To further increase the accuracy in between samples, more degrees of freedom should be added to the control.

Additional Switchings

To improve accuracy in between consecutive samples, we insert r additional switchings by letting

$$u(t) = u_k^i, \;\; (k + \frac{i}{r})T \leq t < (k + \frac{i+1}{r})T, \;\; i = 0, \ldots r-1$$

The equations for the expanded system becomes

$$x_{k+1} = \Phi x_k + \sum_{i=0}^{r-1} \Phi^{\frac{r-1-i}{r}} \Gamma_r u_k^i + d_k \tag{7.18}$$

where $\Gamma_r = \int_0^{\frac{T}{r}} e^{A\lambda} d\lambda B$. The intersample disturbance d_k^i can be estimated by

$$\tilde{d}_k^i = (\sum_{j=0}^{r-1} \Phi^{\frac{j}{r}})^{-1} \tilde{d}_k$$

with $O((\frac{T}{r})^2)$ error. Each intermediate state value x_k^i will be estimated by

$$\tilde{x}_k^{i+1} = \Phi^{\frac{1}{r}} \tilde{x}_k^i + \Gamma_r u_r^i + \tilde{d}_k^i \quad i = 0, \cdots, r-2$$

with $\tilde{x}_k^0 = x_k$. To reach sliding mode with $O((\frac{T}{r})^2)$ in the intersample period and $O(T^q)$ at each sampling instant, choose

$$u_k^i = -(C\Gamma_r)^{-1} C\Phi^{\frac{1}{r}} \tilde{x}_k^i - (C\Gamma_r)^{-1} C\tilde{d}_k^i, \quad i = 0, \ldots r-2$$
$$u_k^{r-1} = -(C\Gamma_r)^{-1} C[\Phi x_k + \textstyle\sum_{i=0}^{r-2} \Phi^{\frac{r-1-i}{r}} \Gamma_r u_k^{i-1} + \tilde{d}_k]$$

We have

$$s_{k+1} = O(T^q), \quad s_k^i = O((\frac{T}{r})^2), \quad i = 1, \ldots, r-1 \tag{7.19}$$

The main characteristic feature of systems with sliding modes is the motion on the manifold which can be reached in finite time [53]. During that motion, the continuous-time finite-dimensional systems with discontinuous control variables possess the property of disturbance rejection. However, implementation proves to be more difficult than expected. We can mention three crucial facts that disappoint one trying to implement real systems with sliding modes: first, the chattering of the control variable which excites the neglected high frequency modes and in many cases can not be allowed by the physical nature of the actuator; second, the lack of full information on the system state which is needed to design the appropriate switching function (the use of linear observers for estimating state variables unfortunately eliminate the disturbance rejection); third, direct discrete time implementation of the switching control law leads to additional chattering caused by the sampling delay. [54, 38] proposed a possible solution to the first problem, both the first and second problems are addressed in [45].

The third problem can be released by using the approach proposed in [53]. The concept of discrete time sliding mode provides the motion on the manifold at the

sampling instants with $O(T^2)$ error, while at other moments, it leads to the motion only in $O(T)$-vicinity of the desired manifold, which is not sufficient in many cases. Even if the disturbance can be measured in discrete time with continuous time matching condition, it generally can not be rejected because there is no matching in the corresponding discrete time system. The solution of all these issues is obtained by using the disturbance prediction algorithms proposed here.

It is shown that for sufficiently smooth disturbances even without matching condition in discrete time, the desired accuracy $O(T^q)$ of disturbance rejection in the sliding manifold can be achieved not at every sampling moment but every rT sampling intervals. We can say that there is rth order discrete time sliding mode. To obtain $O(T^q)$ disturbance rejection at every T-instant we should have additional $r-1$ switchings of control during that interval. If the system has internal uncertainties, only one step ahead prediction is allowed due to discontinuity in the control law; nevertheless, exact sliding mode can be achieved asymptotically.

8. NEURAL CONTROL OF FLEXIBLE SYSTEMS WITH PARTIALLY KNOWN DYNAMICS

In this chapter, the use of neural nets for simultaneous modeling and control in an optimal control setting is investigated for systems with partially known dynamics. Specifically, we consider the case where the unknown portion is related to flexibility. Systems with a high degree of flexibility fall into the general class of distributed parameter systems whose motion is described by hybrid systems of integrodifferential equations. For the class of plants considered in this chapter, the known part of the dynamics is represented by a simple analytical model and a neural net-based model is used to estimate the unknown part of the dynamics. A novel approach is given where neural nets are used in concert with conventional control methodologies to achieve high performance for both trajectory tracking and vibration damping. The control strategy is a two-part control scheme: one part is model-based, using the known dynamics and conventional optimal control techniques, the second component of the control scheme is neural net-based. These strategies are applied to a one-link flexible manipulator. Flexible link manipulators are of extreme interest to researchers interested in space-based robot applications and other robotic applications with weight and power constraints. However, flexibility leads to highly complex system models, resulting in more complication for controller design. In this chapter, we show that for a one-link flexible manipulator, a control design can be achieved that provides accurate slewing while minimizing vibration of the manipulator. It is further shown that the control design can adapt to variations of the manipulator payload, resulting in accurate slewing and small tip vibrations for a wide range of payload variations.

Neural networks possess many of the necessary qualifications for implementation of the identification and control strategies. For the identification stage, neural nets can be implemented with supervised learning rules to learn the nonlinear dynamics of the unknown plant. The neural net performs a nonlinear mapping from input space to output space while also giving the necessary nonlinear interpolation that is desired, such that the nonlinear dynamics of the process are stored in weight space of the neural net. For the control neural net, the control signal needed to produce the desired result is not known *a priori* and therefore must be generated using an unsupervised learning control strategy. Unsupervised learning rules exploit some key features of the backpropagation algorithm since backpropagation calculates partial derivatives during the training process. These derivatives are used to minimize a cost function based on output error and control expenditure.

There have been several examples of the use of neural nets for control. General control ideas were discussed in [55] for completely unknown nonlinear systems, and adaptive neural controllers were demonstrated in [56] for a simple linear plant. There have also

been many examples of neural nets applied to robot control. In fact, in [57], there is an example of a neural net-based controller implemented on a real rigid-link robot system, where a neural net is used for payload estimation and the payload estimate is used as a parameter in the feedforward controller. This scheme results in payload-invariant trajectory tracking. While there is a multitude of literature concerning rigid link robotic control using neural nets, there is relatively little concerning the control of flexible link manipulators.

Almost all *real* plants can be characterized as a system with partially known dynamics since one can never fully realize a real plant with a mathematical model. There exist a number of techniques available for control of linear systems with either unknown or partially known dynamics. Adaptive controllers [58] can be designed using a standard model structure with unknown parameters, but these systems are fraught with limitations. These types of systems assume a structured uncertainty, where the uncertainty is reduced using stability theory and parameter estimation techniques. However, systems of this type could become unstable due to excitation of unmodeled dynamics. Moreover, a plant is seldom completely linear, and there are few model structures that can accommodate a reasonably large class of nonlinear systems. For this application, we assume that the rigid dynamics are well known, but the nonlinear flexible dynamics are not known, and therefore must be learned from input/output data.

The control strategy proceeds as follows for slewing control of the one-link flexible robot. A model-based control is implemented based on the rigid dynamics of the system. The unmodeled flexible dynamics are learned using a neural network as a predictor, and a corrective control signal is synthesized using a second neural net for control. This method was used by Iiguni, *et al.* [59] in which the authors presented a strategy for control of linear systems with a low degree of uncertainty and small additive nonlinearity using what was referred to as a nonlinear regulator. We extend this method to plants with a high degree of nonlinearity and apply it to the flexible robot problem.

The chapter is organized as follows. We begin with a discussion of flexible manipulator modeling issues to better understand the control strategies implemented. In Section 8.2, neural net modeling for the described class of systems is discussed simultaneously with the problem of controller design. Simulations are given in Section 8.3 for the flexible manipulator with fixed dynamics and a constant payload, then the problem is complicated by varying the payload, resulting in a system with variable dynamics. The ability of the controller to adapt to this disturbance is investigated via simulation.

8.1 General Aspects of Flexible Manipulator Models

Flexible robots possess the attractive properties of (1) light weight, resulting in systems with smaller actuators for lower energy consumption, and (2) mobility for fast response as compared to heavier rigid counterparts. Modeling of flexible robots is difficult due to the infinite dimensional nature of the distributed parameter systems and the difficulty in modeling the structural flexibility of the link. The dynamical equations of motion can be described mathematically using integro-partial differential equations (PDEs) with the appropriate boundary conditions. The methods known for modeling flexible robots are many and are addressed in a variety of works, using methods such as the Euler-Newton method with finite element models [60], the Euler-Lagrange method [61], or Hamilton's principle [62]. The model used for the simulations of this work is obtained from a distributed parameter model via the assumed modes method. The parameters are derived from the Ohio State University single-link flexible manipulator [63]. Experimental identification results obtained for this structure [64] demonstrate that only one mode is dominant in the identified model for transverse motion of the manipulator. Therefore, a one-mode expansion is used in the simulations.

In flexible robots, if the payload is allowed to be variable, then both the rigid dynamics and the flexible dynamics change as a function of payload. In addition, the boundary conditions assumed initially may not be valid as the payload varies. This presents a difficult chore for the control designer as we shall see in the section that follows. Alternately, one can assume little or no knowledge of the plant and use robust control techniques and model the unknown dynamics as a disturbance. While this is a viable alternative, we have chosen to use model-based control methods that are between the two extremes, where we assume partial knowledge of system dynamics.

There has been much recent interest in the problem of slewing control for flexible manipulators. The resulting control strategies can be complex and difficult to implement. To ease the computational burden and implementation difficulties, we introduce the neural net-based composite control strategy described herein. Using a one-step-ahead prediction of the system outputs, we can form a control signal for predictive control. In addition, the estimation error in the identification neural net is used for training of the neural net for corrective control which is trained based on an unsupervised learning strategy.

Conventional system identification techniques have also been used to determine the model of a flexible link manipulator (see [65] for example). A potential problem with this approach, however is that a model structure must be assumed *a priori*, and thus, modeling errors are built in for the infinite dimensional system being considered. Furthermore, most identification techniques are based on linear system models,

introducing further difficulties for the highly nonlinear systems being considered. Further uncertainties exist due to the difficulties associated with modeling drive system mechanics estimating physical parameters, in addition to the difficulty of accurately modeling the flexible dynamics. Our alternative approach offers several advantages over conventional methods in this paradigm, since neural nets can be used to learn nonlinear system dynamics. The neural net learns the nonlinear flexible dynamics from input/output data, which allows for a more exact representation than one using a linearized model or approximations of the nonlinear system dynamics.

8.2 Modeling and Control Strategy

8.2.1 Simulation Model for a Flexible One-Link Manipulator

Distributed parameter systems are characterized as having an infinite number of modes. For control applications, we describe the system using approximations that are finite-dimensional state-space representations. Starting with a Hamiltonian formulation, we use an assumed modes representation of the flexure variable α for insertion into the system equations to obtain a finite-dimensional representation of the dynamics. The resulting equations are programmed on a computer to model the one-link flexible manipulator shown in Figure 8.1. In this case, the link is modeled as clamped at the hub and as a mass with an inertia is at the free end. The resulting mode shapes are referred to as CLTI mode shapes (cantilever with tip inertia). A detailed derivation of the equations can be found in [15] or in [66] for a two-link flexible manipulator. The terms used to obtain the dynamical equations of the manipulator are defined in Table 8.1. In addition, the subscript notation of Equation (8.1) is used to denote a partial derivative. For example, the second partial of a with respect to t is given as $a_{tt} = \partial^2 a / \partial t^2$.

The equations for the flexible link manipulator can be written as

$$EI\alpha_{\ell\ell\ell\ell} + \rho\alpha_{tt} + \rho\ell\ddot{\theta} = \rho\alpha\dot{\theta}^2, \quad \ell \in [0, L], \quad t > 0 \tag{8.1}$$

$$[I_h + \frac{1}{3}\rho L^3 + \rho\int_0^L \alpha^2 d\ell]\ddot{\theta} + \rho\int_0^L \ell\alpha_{tt} d\ell = u \tag{8.2}$$

The assumed modes method requires that the flexure be expanded as

$$\alpha(\ell, t) = \sum_{j=1}^{N} \phi_j(\ell) q_j(t) \tag{8.3}$$

where j is the mode number, ϕ is the mode shape, and q is the modal displacement. The CLTI mode shapes have been used previously by [67] to model a link with a

Table 8.1: Parameters of the One–Link Manipulator

I_h	Hub inertia
I_p	Payload inertia
L	Length of link
EI	Stiffness term
ρ	Mass density of link
M	Mass of hub
M_p	Mass of payload
ℓ	Spatial variable for link
$\alpha(\ell,t)$	Flexure of link at location ℓ
θ	rigid link angle of link
u	Input torque at hub

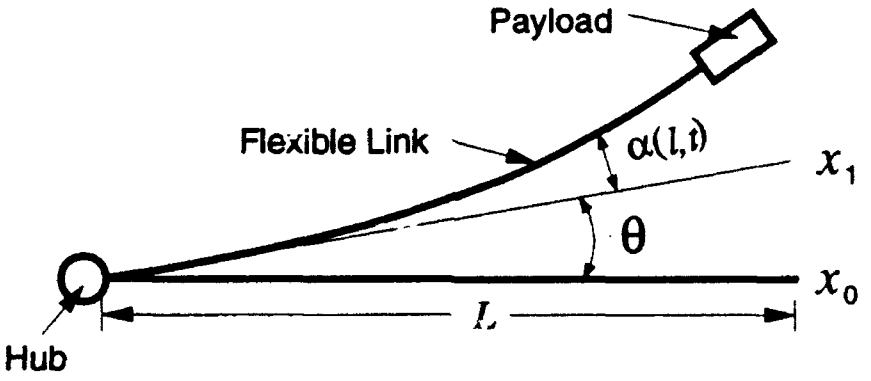

Figure 8.1: The Flexible One–Link Manipulator

payload, and have also been used in [66] to model the first link of a two-link system as a link with an attached link as the payload. The boundary conditions are

$$\alpha(0,t) = 0, \quad \alpha_\ell(0,t) = 0 \tag{8.4}$$

$$EI\alpha_{\ell\ell}(L,t) = -(M_pO_p^2 + I_p)\ddot{\alpha}_\ell(L,t) - M_pO_p\ddot{\alpha}(L,t) \tag{8.5}$$

$$EI\alpha_{\ell\ell\ell}(L,t) = M_p\ddot{\alpha}(L,t) + M_pO_p\ddot{\alpha}_\ell(L,t) \tag{8.6}$$

where M_p is the mass of the payload, I_p is the mass moment of inertia of the payload, and O_p is the distance from the endpoint of the link to the center of mass of the payload. The first boundary condition represents the clamped boundary condition at the hub. The next two boundary conditions correspond to the mass plus inertia at the end of the link. In this chapter, the above equations are simplified since the

payload is modeled as a point mass at the tip, so that I_p and O_p are equal to zero. The CLTI mode shape equations can be found in [66].

The resulting model is of the form

$$\mathcal{M}(X)\ddot{X} + KX + F(X, \dot{X}) = U \tag{8.7}$$

where $X = [\theta \;\; q_1 \;\; q_2 \;\cdots\; q_N]^T$, and N is the number of modes retained in the model from flexural effects of the link. The following expressions can be defined in terms of the variables of the above approximation:

$$A_j \triangleq \int_0^L \rho \ell \phi_j(\ell) d\ell \tag{8.8}$$

$$B_j \triangleq \int_0^L \rho \phi_j^2(\ell) d\ell \tag{8.9}$$

$$C_j \triangleq \phi(L) \tag{8.10}$$

$$\frac{\partial^4 \phi_j}{\partial \ell^4} \triangleq \lambda_j \phi_j \; . \tag{8.11}$$

This allows for the calculation of the terms

$$\int_0^L \alpha d\ell, \quad \int_0^L \ell \alpha d\ell, \quad \text{and} \quad \int_0^L \alpha^2 d\ell \; . \tag{8.12}$$

Substitution of (8.3) into (8.1) and (8.2) results in an ordinary differential equation for the rigid body motion motion and a partial differential equation for the flexure equation. To convert the flexure equation into an ordinary differential equation, we multiply through by ϕ_k and integrate from 0 to L. Since the ϕ_k's are orthogonal (the integral from 0 to L is an inner product, *i.e.*, the ϕ_k's belong to the space $\mathcal{L}_2[0, L]$), all the terms drop out except the $\phi_k \phi_k$ integral, so that N differential equations remain.

The resulting rigid body motion (θ) and flexure (α) equations are respectively:

$$[I_h + \frac{1}{3}\rho L^3 + \sum_{j=1}^{N} B_j q_j^2]\ddot{\theta} + \sum_{j=1}^{N} A_j \ddot{q}_j = u \tag{8.13}$$

$$A_k \ddot{\theta} + B_k \ddot{q}_k + EI \frac{\lambda_k}{\rho} B_k q_k - B_k q_k \dot{\theta}^2 = 0, \quad k = 1, 2, \ldots, N \tag{8.14}$$

For the simulations, we let $N = 1$ and use the parameters of Table 8.2.

8.2.2 Modeling and Identification

To predict the flexible manipulator outputs, we use our knowledge of the rigid dynamics to form a model of the known part of the plant and use a neural net to learn

Table 8.2: Physical Parameters of the One–Link Manipulator

E	6.8944×10^{10} N/m^2
I	3.3339×10^{-11} m^4
A	1.5875×10^{-4} m^2
I_h	1.6640×10^{-5} kg-m^2
L	1.0 m
ρ	0.4847 kg/m
M	0.4847 kg

the unmodeled flexible dynamics. Let x^p be the output of the plant which we wish to estimate, x^r the output of the known system, and $\hat{x}^f$ be the output of the neural net, which when added to x^r yields a prediction of the plant output. Thus for the one-step-ahead predictor, we have

$$\hat{x}^p_{k+1} = x^r_{k+1} + \hat{x}^f_{k+1} \tag{8.15}$$

where $\hat{x}^p_{k+1}$ is the prediction of the plant output and $\hat{x}^f_{k+1}$ is the predicted state of the unknown dynamics at time $k+1$. The known dynamics are a nonlinear function of prior states and inputs described by the function f,

$$x^r_{k+1} = f(x^r, u^p) \tag{8.16}$$

and the unknown dynamics are a nonlinear function of the prior plant outputs, rigid dynamic model outputs, and prior inputs, described by the function g,

$$\hat{x}^f_{k+1} = g(x^p, x^r, u^p) \tag{8.17}$$

where u^p_k is the input to the plant at time k. Thus, we assume that the unknown dynamics can be driven by the states of the known dynamics, but not vice-versa. We impose the following system constraints in the form of assumptions on the structure of the plant and the models.

Assumption 8.2.1 The plant to be controlled is completely stabilizable and detectable.

Assumption 8.2.2 The dynamics given by $f(\cdot)$ is stabilizable and describes the plant to a sufficient degree such that the controller designed to stabilize the known dynamics also stabilizes the plant.

Assumption 8.2.3 The unknown dynamics given by $g(\cdot)$ is stable.

Assumption 8.2.1 gives us a starting point for the plants to be considered. See [68] for details on stability of nonlinear systems. Although Assumption 8.2.2 is not a necessary condition for identification, it is provided since identification proceeds much better with a stable plant. (In [69], an unstable inverted pendulum was identified using a "human-in-the-loop" to provide stability when necessary.) Assumption 8.2.3 is given since if the unmodeled dynamics are unstable, then plant states may blow up before an appropriate model can be found and the subsequent controller designed.

The identification stage is a neural net training process using a supervised training rule as shown in Figure 8.2. In this stage, the neural identifier produces the signal $\hat{x}^f$ representing the unmodeled flexible dynamics and uncertainties to produce a signal which "corrects" the output from the known dynamics to subsequently provide an accurate estimate of the plant outputs.

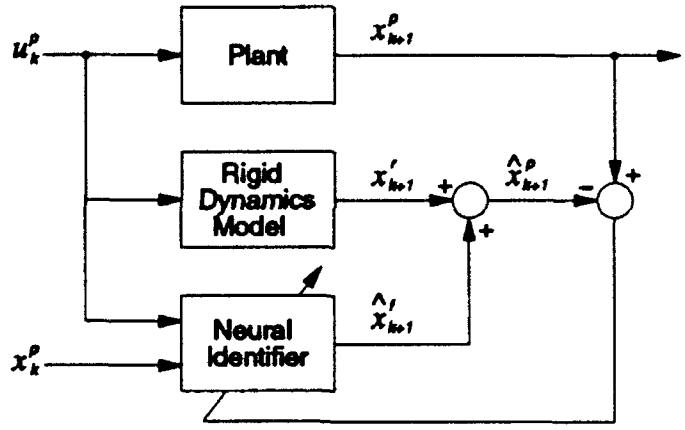

Figure 8.2: Identification Stage Using Neural Nets

The predicted signal (8.15) is compared with the plant output to form the error signal used to train the neural net identifier. The neural net identifier receives as input both the reference signal for control and a regression of the output of the plant. It uses these signals to produce an output $\hat{x}^f_{k+1}$, which is trained based on minimization of the error from the supervised training algorithm. The error function is

$$E_{k+1} = \|x^p_{k+1} - \hat{x}^p_{k+1}\|^2 \tag{8.18}$$

where $\|\cdot\|$ is the standard L_2 norm. The backpropagation algorithm [70] adjusts the weights at each time k by the update rule

$$w_{i,j}^m(k+1) = w_{i,j}^m(k) + \eta \frac{\partial E_{k+1}}{\partial w_{i,j}^m} \tag{8.19}$$

where η is the learning rate and $w_{i,j}^m$ is the weight connecting node i in layer m with node j of layer $m+1$. Differentiation of (8.18) yields

$$\begin{aligned} \frac{\partial E_{k+1}}{\partial w_{i,j}^m} &= -(x_{k+1}^p - \hat{x}_{k+1}^p)^T \frac{\partial \hat{x}_{k+1}^p}{\partial w_{i,j}^m} \\ &= -(x_{k+1}^p - \hat{x}_{k+1}^p)^T \frac{\partial g(x_k^p, x_k^r, u_k^p)}{\partial w_{i,j}^m} \end{aligned} \tag{8.20}$$

To calculate $\partial g(x_k^p, x_k^r, u_k^p)/\partial w_{i,j}^m$ the backpropagation algorithm is used since this quantity is calculated during training. It is equal to the quantity $\delta_j z_i$, where

$$\delta_j = \begin{cases} x_j^p(1-x_j^p)(x_j^d - x_j^p) & \text{(output nodes)} \\ z_j(1-z_j)\sum_k \delta_k w_{kj} & \text{(hidden nodes)} \end{cases} \tag{8.21}$$

where z_j is the output of a hidden node.

8.2.3 Controller Design

With the plant identified, we proceed to controller design. In Figure 8.3, the overall system architecture is given in terms of a control block and an identification block. It is seen that the control signal is composed of two parts: one part is based on conventional model-based control, so that any conventional controller design can be chosen for this part. The output of the conventional controller is given by u^r. The second component comprising the control signal is the contribution due to the neural network for control, indicated by u^f. Both u^f and u^r are formed using the error signal as input, calculated as the difference between the desired trajectory at time $k+1$ and the projected next state at time $k+1$. This is a predictive control scheme where it is desired to know at time k what the output is likely to be at time $k+1$ in order to take appropriate control action at time k. The two components of the control are combined for the composite plant input,

$$u_k^p = u_k^r + u_k^f. \tag{8.22}$$

Since the signal u_k^f is not known *a priori*, it is generated using an unsupervised training rule for the neural net. Unsupervised learning rules exploit some key features of the backpropagation algorithm since backpropagation calculates partial derivatives during the training process. The output of the neural net under unsupervised training is found by adjusting the weights to minimize a performance function.

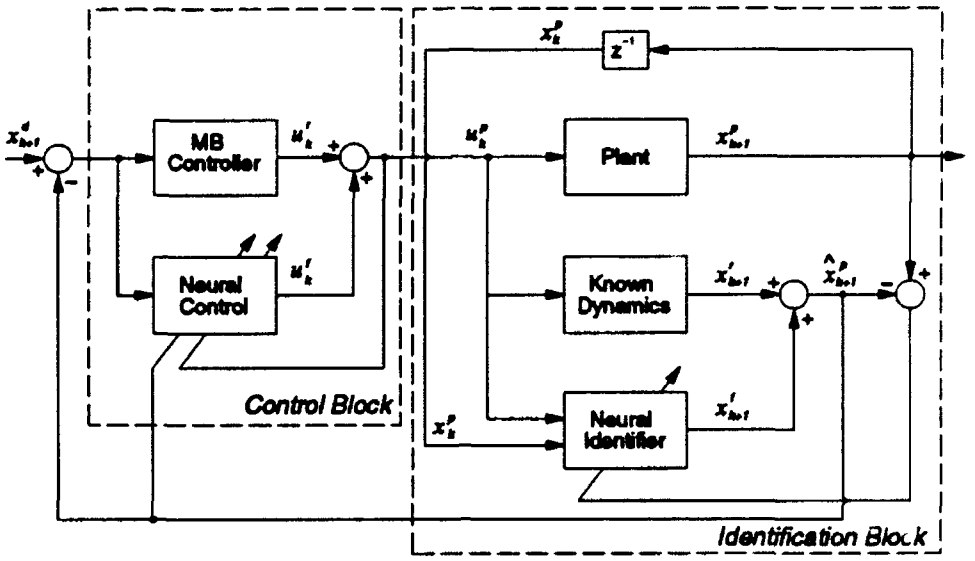

Figure 8.3: Identification and Control Using Neural Nets

In the proposed configuration, the control strategy is derived by a model-based predictive controller where the model used for controller design is the rigid dynamics of the manipulator. The estimated next state is subtracted from the desired state to produce a prediction error which drives the system to the next state. A close look at the rigid dynamics equations reveals that in the absence of a gravity term, the system is linear. Therefore, without loss of generality, we will assume that the gravity term is zero (which is the case for space-based robots). This is a valid assumption since we can always add a feedforward controller to perform gravity compensation separately. Now since the known dynamics is a linear system, we can use any conventional linear control technique to achieve the desired controller design. We will choose the linear quadratic regulator (LQR) and proceed with a brief discussion of the LQR.

Consider a linear time-invariant system described by

$$x_{k+1} = Ax_k + Bu_k \tag{8.23}$$

where $x \in \mathbb{R}^n$ is the state, $u \in \mathbb{R}^m$ is the control and A, B are known matrices. A linear control law of the form

$$u = -Kx \tag{8.24}$$

is sought. Instead of choosing K to achieve some prespecified closed loop poles, we choose K to minimize a cost function J, which is quadratic in both state and input:

$$J = \sum_{k=0}^{\infty} x_k^T Q x_k + u_k^T R u_k \tag{8.25}$$

with Q, R symmetric. If we wish to follow a prespecified state trajectory x_d, then (8.25) becomes

$$J = \sum_{k=0}^{\infty} (x_k - x_k^d)^T Q (x_k - x_k^d) + u_k^T R u_k. \tag{8.26}$$

Without x_d, the control objective is to bring the state to the origin.

The optimal control is given by minimizing (8.25) to obtain

$$\begin{aligned} u_k &= -K x_k \\ &= -(R + B^T P B)^{-1} B^T P A x_k \end{aligned} \tag{8.27}$$

where P is the steady state solution of the algebraic Riccati equation:

$$P = A^T P A - A^T P B (R + B^T P B)^{-1} B^T P A + Q \tag{8.28}$$

The unique solution to (8.28) exists and leads to a stable closed loop system if and only if (A, B) is stabilizable (provided by Assumption 8.2.2) and $(Q^{1/2}, A)$ is detectable (see [71] for LQR details).

Although the LQR has well known robustness properties, one cannot expect it to work well when there is unmodeled dynamics not included in the mathematical description of the plant. Thus a corrective control, provided by the neural network is needed to improve the tracking of the system. A similar methodology was pursued in [59], in which the authors presented a strategy for control of linear systems with a low degree of uncertainty and small additive nonlinearity using what was referred to as a nonlinear regulator.

The problem here is to synthesize the corrective control signal that is used to compensate for system flexibility and other unmodeled dynamics. Since there is not a training signal u(desired) from which we can generate an error signal as in supervised learning schemes, we instead use a neural net with an unsupervised training algorithm as in [72, 69]. Referring to Figure 8.3, it is obvious that when the linear system perfectly describes the plant, the control signal u^r is the optimal control. Thus, we desire an error function for training that when minimized forces the neural net output to be zero when the linear model is an exact representation of the plant. A candidate error function is given by

$$E_c = (x_{k+1}^p - x_{k+1}^d)^T P (x_{k+1}^p - x_{k+1}^d) + u_k^{pT} R u_k^p \tag{8.29}$$

since it is easily shown [59] that the control produced by (8.27) minimizes this function at each time k. This is done by taking the partial of (8.29) with respect to u_k^p to yield the control strategy given in Equation (8.27). However, at time k, the plant state x_{k+1}^p is not available, so we must use $\hat{x}_{k+1}^p$ which results in the following error function for training the neural net:

$$E_c = (\hat{x}_{k+1}^p - x_{k+1}^d)^T P(\hat{x}_{k+1}^p - x_{k+1}^d) + u_k^{pT} R u_k^p. \tag{8.30}$$

This function is used to adjust the weights of the neural net in the following way. The weights of the neural net for control are indicated by q to distinguish from the weights w in the neural identifier and use the following update rule:

$$q_{i,j}^m(k+1) = q_{i,j}^m(k) + \eta \frac{\partial E_c}{\partial q_{i,j}^m} \tag{8.31}$$

To compute $\partial E_c / \partial q_{i,j}^m$ use Equations (8.15) and (8.22) to get

$$\begin{aligned} \frac{\partial E_c}{\partial q_{i,j}^m} &= \hat{x}_{k+1}^{pT} P \frac{\partial \hat{x}_{k+1}^p}{\partial q_{i,j}^m} + u_k^{pT} R \frac{\partial u_k^p}{\partial q_{i,j}^m} \\ &= \left[\hat{x}_{k+1}^{pT} P \left(B + \frac{\partial g(x_k^p, x_k^r, u_k^p)}{\partial u_k^p} \right) + u_k^p R \right] \frac{\partial h(x_k^p)}{\partial q_{i,j}^m} \end{aligned} \tag{8.32}$$

where $g(\cdot)$ is the mapping performed by (8.17) in the neural identification stage, and $h(\cdot)$ represents the mapping performed by the control neural net. The quantity $\partial h(x_k^p)/\partial q_{i,j}^m$ is calculated from the backpropagation algorithm similar to the calculation for $\partial g(x_k^p, x_k^r, u_k^p)/\partial w_{i,j}^m$ since all of the necessary quantities are involved in the backpropagation training process. The quantity $\partial g(x_k^p, x_k^r, u_k^p)/\partial u_k^p$ is calculated from the neural network used for identification and from the weights $w_{i,j}^m$ in that network. All of these quantities are easily extracted from the backpropagation training rule.

8.3 Neural Control Examples on a One–Link Flexible Robot

In this section, several examples are given to demonstrate the effectiveness of the proposed strategy. We first present both identification and control results for a system that operates in a constant environment using a nominal value for a payload added to the tip equal to 0.20 kg, which is about 41% of the link weight. Secondly, we present results for which we vary the payload over the range 0 to 70% of the link mass. Payload invariant slewing control is demonstrated and some of the difficulties encountered in implementation are discussed in detail.

8.3.1 Constant Environment

We begin with the identification stage for the system of Figure 8.2. The first step in the identification process is to collect data that can be used to train the neural network. The simulation model previously described is used in parallel with a model of the rigid dynamics, and the signals x^p and x^r are stored using several different inputs at u^p. The signals indicated by x are vectors with elements of hub angle and hub angular velocity, so that $x \triangleq [\theta \quad \dot{\theta}]^T$. In order to limit the amount of data for the neural network, the motion of the manipulator is limited to slews in the first quadrant, so $0 \leq \theta \leq 90$ degrees. Initially, a white noise input was used as an input to the system and data was collected and applied to the neural network for training. Then, the loop was closed using state feedback and data was collect for a variety of slews in the allowable range of inputs. This data was applied to the neural net which was previously trained using white noise inputs. Thus, the first stage of the identification process can be thought of as a "coarse" training process, and the second stage can be thought of as a "fine" tuning process, where the neural net weights were adapted to learn the dynamics for slewing maneuvers.

For this application, using a model structure for the neural net of order two, we chose a neural net with five inputs and two outputs. Two hidden layers with 15 and 10 nodes respectively are used, and the notation $\mathcal{N}_{5,15,10,2}$ is used for a shorthand means of stating the neural net topology. The backpropagation algorithm used for training in the identification stage is a version of the *Neural Shell, V2.01* [73] which is a program that was written first for use on Sun Computers and later optimized by Ahalt and his students for use on the Ohio Supercomputer Cray Y-MP8/864. The results of the identification process are shown in Figure 8.4 for the neural net outputs of position and velocity. This plot is validation process where a 45 degree slew is commanded and the outputs of the plant and the prediction of the plant outputs are recorded. Also shown is the position without the neural net contribution. The benefit is obvious, as the variance of the estimation error is very small for both position and velocity ($\sigma^2 = [0.00196 \quad 0.00854]$).

The control objective is to slew the arm along a desired trajectory as indicated by x^d, while minimizing arm vibrations. The model based controller in the block of Figure 8.3 is LQR control using hub angle state feedback. The weighting functions were chosen to put more emphasis on the output error term and less on control expenditure. However, we must limit the size of the feedback gains since large gains cause more flexure of the manipulator resulting in more vibrations of the tip. The results for a slew from 0 degrees to 45 degrees are shown in the plots of Figure 8.5. The dashed line represents the manipulator *tip* position and the solid line is the hub angle position, both measured in degrees. The top plot is the output of the system with LQR state feedback control only, and the middle plot is the output of the system

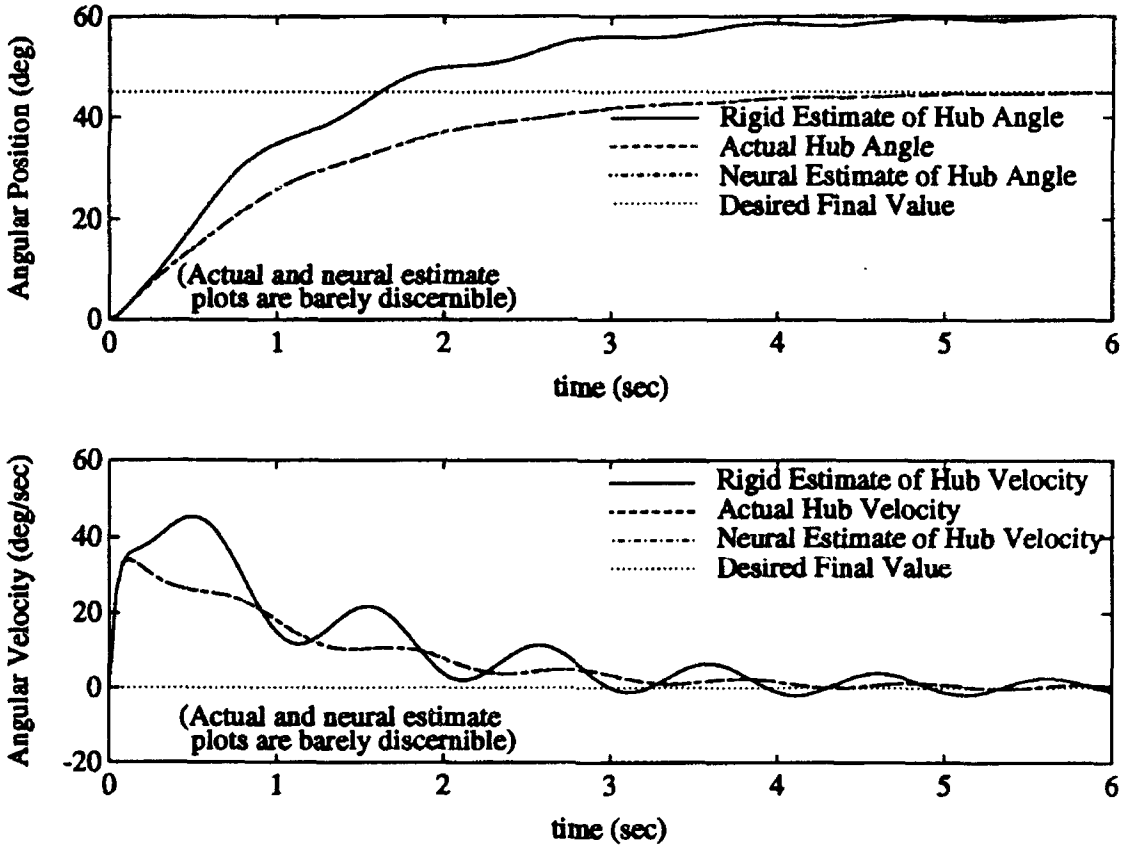

Figure 8.4: Identification Results for System with Nominal Payload

with the addition of neural control. The control signal follows in the bottom plot. The neural net achieves the desired effect, since an increase in damping reduces tip vibrations significantly. Note that the fundamental modal frequency changes to reflect the increase in damping of the flexible modes.

8.3.2 Payload Variation

We now turn our attention to the problem where a payload at the tip of the manipulator is permitted to vary. The effect of adding a mass at the tip is that both the rigid and flexible dynamics change as a function of payload. Since the controller is designed with a fixed gain for the rigid dynamics, the control is no longer valid if the dynamics change. Again, to compensate for this effect, a neural net is added to the control loop, but now it is asked to perform more of the control effort. In addition, since the dynamics of the rigid body system has changed, the neural identifier must

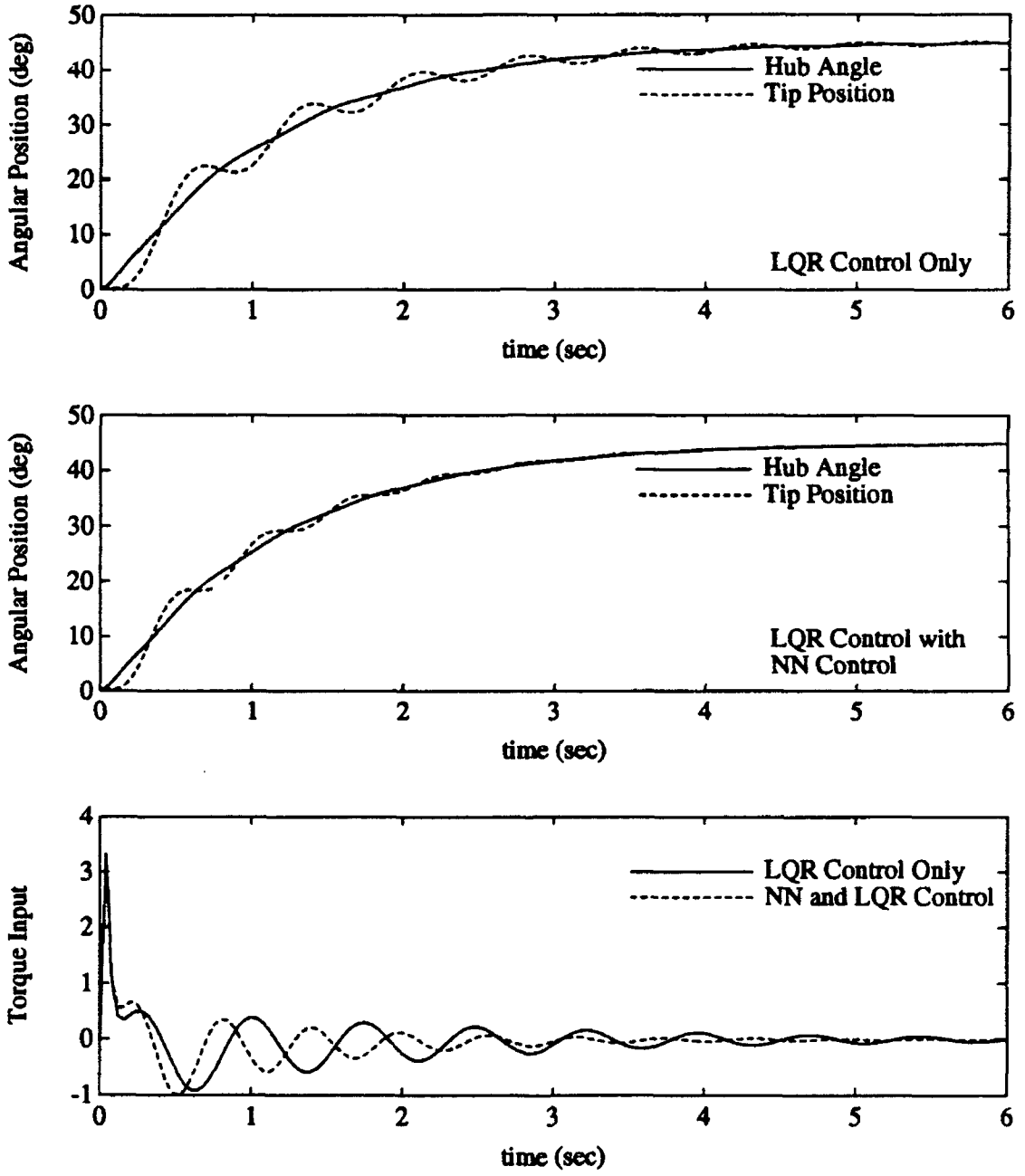

Figure 8.5: Flexible One–Link Manipulator: Position with LQR Control (top), Position with LQR and Neural Net Control (middle), and Control Signal (bottom)

also be able to compensate for this variability.

Consider again the identification neural network, which performs the mapping $g(\cdot)$ to compensate for the unmodeled flexible dynamics as

$$\hat{x}^f_{k+1} = g(x^p, x^r, u^p) \tag{8.33}$$

where the output of the neural net, $\hat{x}^f$ is a function of the plant output x^p, the rigid dynamics x^r and the plant input, u^p. It can be observed both analytically from the dynamical equations of motion and experimentally that by varying the tip mass, one varies the fundamental frequency of the flexible dynamics. Simulations were performed to determine the modal frequencies for various payloads. The results are displayed in Table 8.3.

Table 8.3: Modal Frequency as a Function of Payload

Payload Mass (kg)	0 kg	0.05 kg	0.10 kg	0.15 kg	0.20 kg	0.25 kg	0.30 kg	0.35 kg
% of Link Mass	0%	10.3%	21.6%	31.0%	41.3%	51.6%	61.9%	72.2%
Frequency (Hz)	1.3481	1.1323	0.9908	0.8966	0.8188	0.7592	0.7140	0.6705

The table shows that as the tip mass increases, the modal frequency of the manipulator decreases. The neural identifier in the constant payload case was trained to learn the dynamics for a single frequency. The variable payload case is much more challenging since the identifier must learn a continuously variable modal frequency over the range defined in Table 8.3 which results in an identifier that effectively performs a "modal selection process". A critical condition on the mapping process is that the mapping must be ***well conditioned***. A well conditioned mapping is one where the mapping from input to output defines a unique one-to-one mapping. For example, if the manipulator output and the rigid dynamics output error exhibits a similar response to both a 0.10 kg payload and a 0.30 kg payload, then the neural net will not be able to discern the difference for the corrective response action since there will be ambiguities in the mapping. Fortunately this is *not* the case, since not only the modal frequency changes as a function of payload but also the error between the rigid dynamics output and the actual plant output varies in direct proportion to payload variation.

To achieve accurate identification, the neural net training data is selected using data from a variety of payload cases, then the neural net can interpolate the results to output the desired response. A new configuration is implemented for the identification stage to give the neural net more information, specifically with respect to the modal frequency. An accelerometer is included as an additional measurement at the tip of the manipulator and used as input to the neural net. For first bending mode vibrations,

placement at the tip of the manipulator gives maximal output response [64]. Thus, the neural identifier is changed to accept another input as shown in Figure 8.6, where the accelerometer input at time k is denoted by $\ddot{q}_k$.

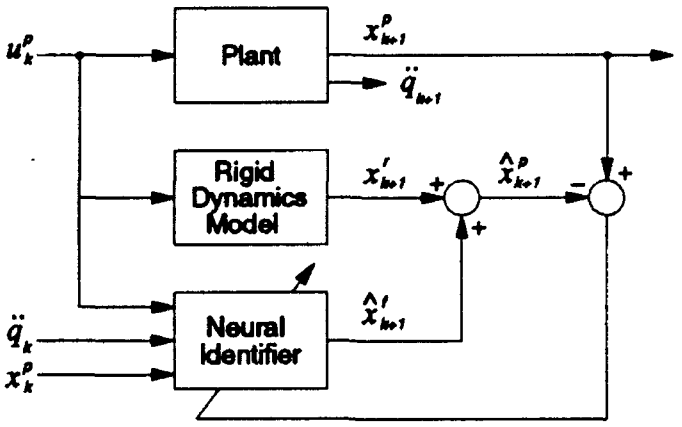

Figure 8.6: Identification Block with Accelerometer Input

Using experimental data from each of the payload cases of Table 8.3, the identification neural net was trained to learn the new flexible dynamics as a function of payload. The neural topology was changed to reflect the new information required for identification. There are four variables used for input to the identifier and assuming a model structure of order two, a delayed version of each input is also used to give the neural net a total of eight inputs. Since the neural net has more information to learn, a larger topology is used, with two hidden layers of size 30 and 20, respectively. The number of outputs remains at two, so that the neural net topology is $\mathcal{N}_{8,30,20,2}$. The result of identification for a payload that is 23% of the link mass is identical to the results shown in Figure 8.4 where the estimation error variances in this case are $\sigma^2 = [0.00375 \quad 0.00986]$ for position and velocity respectively. Similar results were verified for several payload variations.

The neural net provides an excellent means of identification for both position and velocity. Note that the 23% value use for the payload is not part of the training data set, so the neural net performs the required interpolation with a high degree of accuracy. Thus, since the neural net can perform the required identification, the neural net controller is designed in the same manner as previously discussed. However, since the LQR feedback is designed for a plant with nominal payload, the neural net is asked to perform more of the task for control which results in slightly longer training time to achieve the desired tracking. This can be illustrated by way of example.

Consider the following experiment. The flexible link moves from a rest position to a desired position with the nominal value of 0.20 kg payload, and the neural net for control adjusts the weights in the control loop to achieve the desired tracking as in the

previous example. In the new position, a mass is added to the link tip, and the link is then slewed to a new position during which time the neural net collects the data over the latest motion to adjust the weights to compensate for the new load. The manipulator does not perform well over the second slew, but it adjusts the weights using the unsupervised learning control scheme such that during subsequent motion with the same payload, performance continues to improve until a desired performance specification is met.

This procedure is depicted in Figure 8.7. The manipulator starts at rest where it is assumed that training has been completed for the nominal case. The manipulator moves through a 45 degree slew and the tip mass is changed to 0.30 kg (61.9% of link mass). The manipulator moves in the same direction by 25 degrees to a rest position of 70 degrees. Although the manipulator did not dampen vibrations well, subsequent maneuvers show that the control neural net is adjusting to compensate for the disturbance. The manipulator is moved back to 45 degrees and back again to 70 degrees to show how performance continues to improve. The control neural net trains itself on-line and improves its vibration damping characteristics with each slew. This can be seen when the manipulator moves through a slew of -45 degrees to the final position of 25 degrees. It was also found that if the mass is later changed back to the nominal value, the training time for the procedure is reduced slightly, but not enough to say that the neural net "remembers" the control for the original case, since the neural net adjusts itself to compensate for the most recent payload.

This plot shows that the neural net can achieve payload-invariant tracking with on-line training and a minimal amount of information known about the system dynamics or the payload. Real-time implementations of such an approach are dependent upon how much the payload changes from the nominal value. If there is a small change in the payload, then the neural net can easily adjust itself in one slew. If the payload size doubles, then several slews may be necessary to achieve the desired tracking specifications. To determine the ability of this control scheme to adjust to real situations, we investigated several different payload variations for a slew of 0 to 45 degrees (Trial 1), then back to 0 degrees (Trial 2). The maneuver was held constant at 45 degree slews and the payload was varied in order to make valid comparisons of training time. The results are shown in Table 8.4, where a +20% variation of the payload means that the payload changed from 0.20 kg to 0.24 kg. The first column is the percent variation of the payload, with the payload varied over the entire range of Table 8.3. The figure of merit used for comparison is the sum-squared value of the tip deflection, since we are trying to minimize vibration at the tip. Let $\alpha(L,k)$ be the tip deflection at time k, so that the sum-squared value is given by J as

$$J = \sum_{k=1}^{N} \alpha(L,k)^2 \,. \tag{8.34}$$

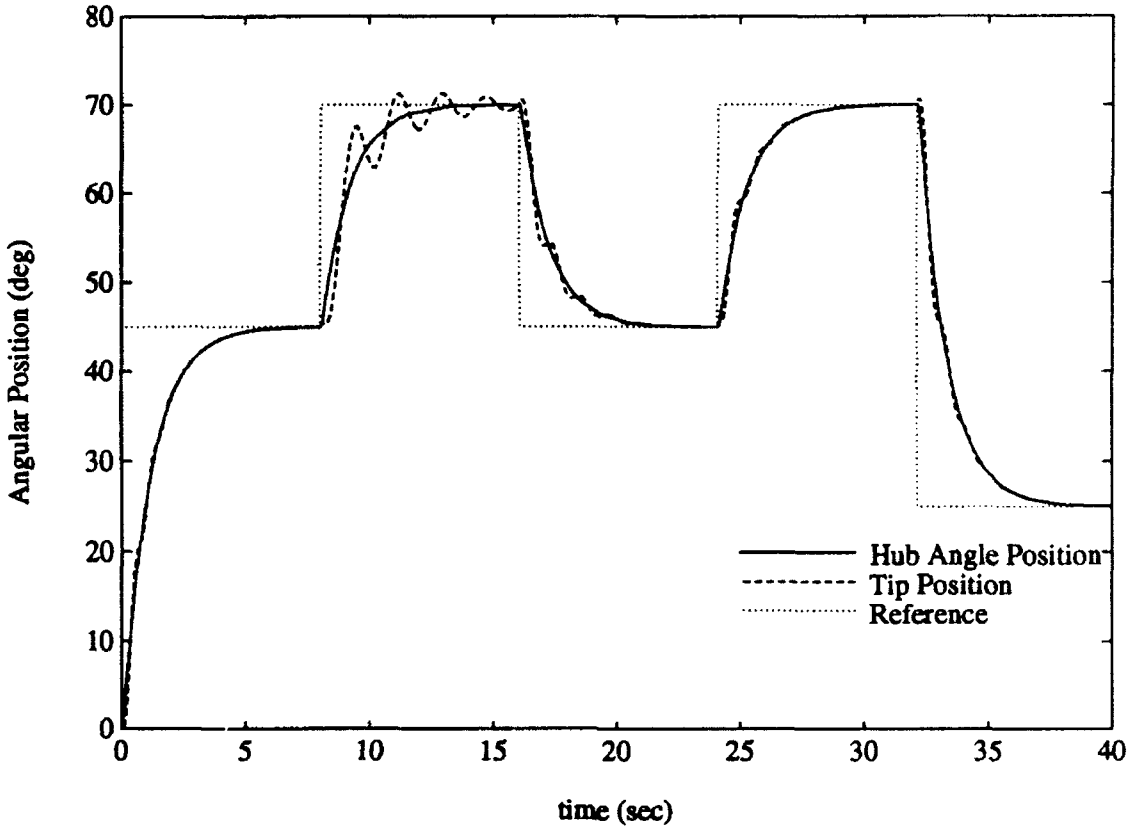

Figure 8.7: Slewing Maneuvers with Variable Payload

In Table 8.4 the value of J is given for a slew from 0 to 45 degrees(Trial 1), then for a slew back to 0 degrees (Trial 2) in columns 2 and 3, respectively. Note that for large deviations of the payload in the positive direction, more than two slewing maneuvers might be necessary to control vibrations at the tip.

The simulations clearly illustrate how we can take advantage of partial knowledge of plant dynamics to control a system using a combination of conventional controllers and neural-based control. The strategy outlined for the new control scheme was demonstrated on a flexible one-link manipulator in which the rigid body dynamics were assumed known and the flexible dynamics were learned by a neural identifier. A control scheme using conventional control was used for control of the rigid dynamics and a neural controller was used to provide a corrective control to compensate for the unmodeled dynamics. The overall effect is to minimize tip vibration of the manipulator. This is demonstrated first for the case of a constant payload chosen with a nominal value, then for the case where the payload was varied. On-line training of

Table 8.4: Effect of Payload Variation on Training Time

Payload (% change)	Trial 1	Trial 2
0%	0.0299	0.0285
+10%	0.0388	0.0351
−10%	0.0342	0.0325
+20%	0.0513	0.0378
−20%	0.0421	0.0352
+30%	0.1100	0.0391
−30%	0.0805	0.0380
+50%	0.4733	0.0823
−50%	0.1317	0.0420
+100%	1.2564	0.1100
−100%	0.1678	0.0422

the control neural net showed that control could be achieved in a minimum number of arm movements for reasonable changes of the payload.

9. APPLICATIONS

The structures we consider for application of the previously discussed techniques are space structures that contain flexible components for which we wish to minimize vibrations. These structures also exhibit rotational and translating capabilities which result in nonlinear behavior.

9.1 Spacecraft

One of these structures is a rigid hub that can translate in two dimensions as well as rotate in one dimension. Attached to this hub is a flexible beam that exhibits planar vibrations. This structure represents a coupling of linear vibration characteristics with nonlinear slewing behavior and is illustrated in Figure 9.1.

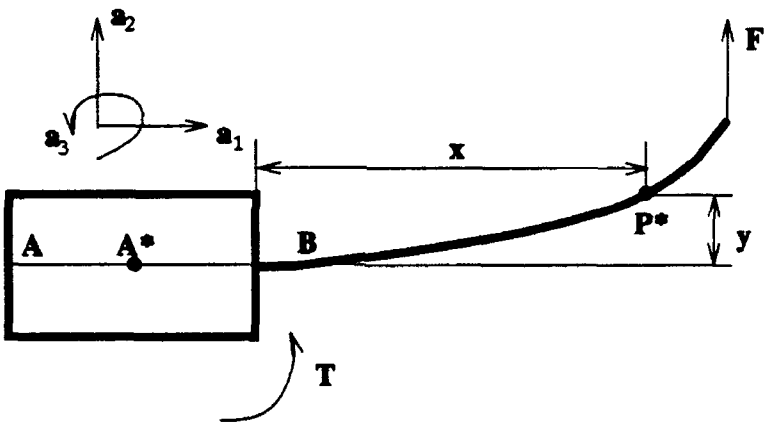

Figure 9.1: Spacecraft with rigid hub and attached flexible appendage.

Equations of motion can be derived for this spacecraft by modeling the beam as clamped at the hub and free at the other end. Then using the assumed modes method we retain one mode in the model (more modes can be handled quite easily). We also ignore gravity in this model. Let u_1, u_2, u_3 be the velocity of A^* (center of mass of hub A) in a_1, a_2, a_3 direction, respectively. Let u_4 and q_1 be the modal velocity and modal displacement, respectively, of the flexible beam B. The control variables are T and F which are the torque produced by the hub motor and the force produced by the jet at the beam's endpoint, respectively. All other parameters appearing in the model are constants representing masses, moments of inertia, stiffness constants, and various other physical quantities that will not be discussed further for the sake of brevity.

The equations of motion can then be written as

$$\begin{bmatrix} m_A+m_B & 0 & -E_1q_1 & 0 & 0 \\ 0 & m_A+m_B & bm_B+e_B & E_1 & 0 \\ E_1q_1 & -(bm_B+e_B) & -(b^2m_B+2(e_B+I_B+J_3)) & -(bE_1+F_1) & 0 \\ 0 & E_1 & bE_1+F_1 & G_{11} & 0 \\ 0 & 0 & 0 & 0 & 1 \end{bmatrix} \begin{bmatrix} \dot{u}_1 \\ \dot{u}_2 \\ \dot{u}_3 \\ \dot{u}_4 \\ \dot{q}_1 \end{bmatrix} =$$

$$\begin{bmatrix} (m_A+m_B)u_2u_3+2E_1u_3u_4+(bm_B+e_B)u_3^2 \\ -(m_A+m_B)u_1u_3+E_1u_3^2q_1 \\ E_1u_2u_3q_1+(bm_B+e_B)u_1u_3 \\ -E_1u_1u_3+G_{11}u_3^2q_1-H_{11}q_1 \\ u_4 \end{bmatrix} + \begin{bmatrix} 0 & 0 \\ 0 & 1 \\ -1 & -(b+L) \\ 0 & \phi_1(L) \\ 0 & 0 \end{bmatrix} \begin{bmatrix} T \\ F \end{bmatrix} \tag{9.1}$$

which is a fifth order nonlinear time-varying ordinary differential equation. The outputs can be chosen to be any of the five states, thus they will ordinarily be linear functions. By choosing two outputs (say, hub rotation, u_3, and tip displacement, q_1), we obtain a two-input, two-output nonlinear system. The first input/output port could be restricted to hub information only (u_1, u_2, u_3), and the second input/output port could be restricted to beam endpoint information only (u_4 and q_1). This decentralization constraint would be desirable for a real spacecraft of the type in Figure 9.1 because of the difficulty in exchanging information between the two ports. Thus, the results of the previous section could be applied to this structure. This represents one of our priorities for future work.

9.2 Optical Tracking System

In this section, the algorithm of Section2.4 is applied to an optical tracking system[74, 1, 2]. The system, shown in Figure 9.2, consists of two motors with mirrors mounted

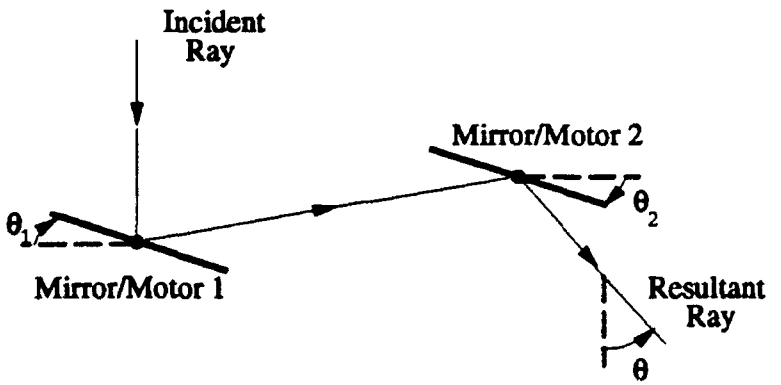

Figure 9.2: Optical tracking system example.

on them. It is desired to slew a ray of light by an angle θ^d. The geometry of the system indicates that the desired individual angles of rotation for each motor $y_i^d = \theta_i^d$ are related to the desired angle of slew by

$$2(\theta_1^d - \theta_2^d) = \theta^d \tag{9.2}$$

which becomes our constraint equation (2.48). Since our constraint is linear, the equations (2.49) and (2.53) become much simpler. The dynamics of the optical system consist of two linear coupled subsystems. Thus, there are two input/output channels with each subsystem being first order. For simplicity the Q and R matrices in the servocompensator cost criterion (2.33) are chosen to be the identity matrices of order 4 and 2 respectively.

The output of each subsystem is the angle produced by the motor for that mirror, and the input to each subsystem is the torque generated by the motor (i.e., the motor dynamics are ignored here for simplicity). Then the dynamical equations of the mirror system are

$$\begin{bmatrix} \dot{x}_1 \\ \dot{x}_2 \end{bmatrix} = \begin{bmatrix} 0 & 1 \\ 0 & -314.16 \end{bmatrix} \begin{bmatrix} x_1 \\ x_2 \end{bmatrix} + \begin{bmatrix} 1 & 0 \\ 0 & 1 \end{bmatrix} \begin{bmatrix} u_1 \\ u_2 \end{bmatrix} \tag{9.3}$$

$$\begin{bmatrix} y_1 \\ y_2 \end{bmatrix} = \begin{bmatrix} 1 & 0 \\ 0 & 1 \end{bmatrix} \begin{bmatrix} x_1 \\ x_2 \end{bmatrix} \tag{9.4}$$

where the data are taken from [74]. The desired slewing angle θ^d was chosen to be 30 degrees ($\pi/6$ radians) which implies from (9.2) that the difference between the two individual mirror angles should be 15 degrees.

The algorithm in the last section was implemented on CTRL-C using the negative gradient of J as the search direction with a stepsize of $\epsilon = 1$. The algorithm converged quite rapidly. Indeed, after one iteration the norm of the gradient was 0.0033 and after two iterations it was 0.0032. The optimal choice of setpoints was $\theta_1^d = 14.95°$ and $\theta_2^d = -0.05°$. The optimal decentralized PI control laws turned out to be

$$u_1 = 1.002x_1 + 0.998 \int_0^t (y_1(\tau) - \theta_1^d)\, d\tau \tag{9.5}$$

$$u_2 = 1.0x_2 + 1.0 \int_0^t (y_2(\tau) - \theta_2^d)\, d\tau \tag{9.6}$$

with the setpoints from above, and the optimal cost was $J^* = 0.0093$. This example, though quite simple, illustrates the method and its fast convergence. The above algorithm could be implemented on-line for this particular example which would eliminate the need to compute the setpoints *a priori*. The primary point of the example is that using this algorithm allows one to compute the setpoints in an optimal manner instead of *ad hoc*. That is, the output objectives of each mirror are chosen to minimize the given performance criterion while taking into account the dynamics of the system. Among the infinite set of feasible mirror settings, the one solved for above is optimal with respect to the quadratic performance criterion.

9.3 LIVE

One structure which we have considered in our research is an experiment that has been built at Ohio State. It is a flexible truss cantilevered at the top, with two large panels attached to the bottom. The panels can rotate and can induce vibrations in the truss. This configuration is depicted in Figure 9.3 which shows the Large Interconnected Vibration Experiment from The Ohio State University (LIVE from OSU). Figure 9.4 illustrates the hardware dedicated to the experiment. Again, decentralized control techniques will be utilized here with the panels representing one subsystem and the truss representing the other subsystem. The coupling of the panel rotation with the truss vibrations will result in coupled nonlinear subsystems. In the immediate future, the structure will be modeled using the finite-element method and controlled using the approaches presented above and in the sequel.

9.4 Sampled Variable Structure Control for Flexible Structures

A general slewing structure with flexibility can be described as:

$$M(\theta, q)\begin{pmatrix} \ddot{\theta} \\ \ddot{q} \end{pmatrix} + G(\theta, \dot{\theta}, q, \dot{q}) = Bu \tag{9.7}$$

where θ is a vector of rigid modes, q is a vector of flexible modes, and u is the control with the same dimension as θ.

Our goal is to steer the controlled variables θ from the initial state $(\theta_0, \dot{\theta}_0)$ to the desired steady state $(\theta_d, 0)$ with as small deformation of the structure q as possible. A discrete time variable structure control, or sampled sliding mode, approach is conducted in the controller design for θ. We shall formulate the problem in a linearized model around the steady state value. The higher order terms as well as the unmeasured flexible modes q will be treated as disturbances. Thus, a linear system with exogenous disturbances together with parameter variations in both the system and control matrices results.

This is a quite general VSC problem. In addition to solving for a robust controller against those uncertainties mentioned above, several practical considerations, such as chattering reduction, sampling frequency, disturbance prediction, and control variable saturation, etc. are also included in this report. It is found that the proposed technique is well suited for digital implementation of sliding mode control. On the other hand, the frequency shaping technique, which we have developed during the last three years, has not been added to the approach here yet.

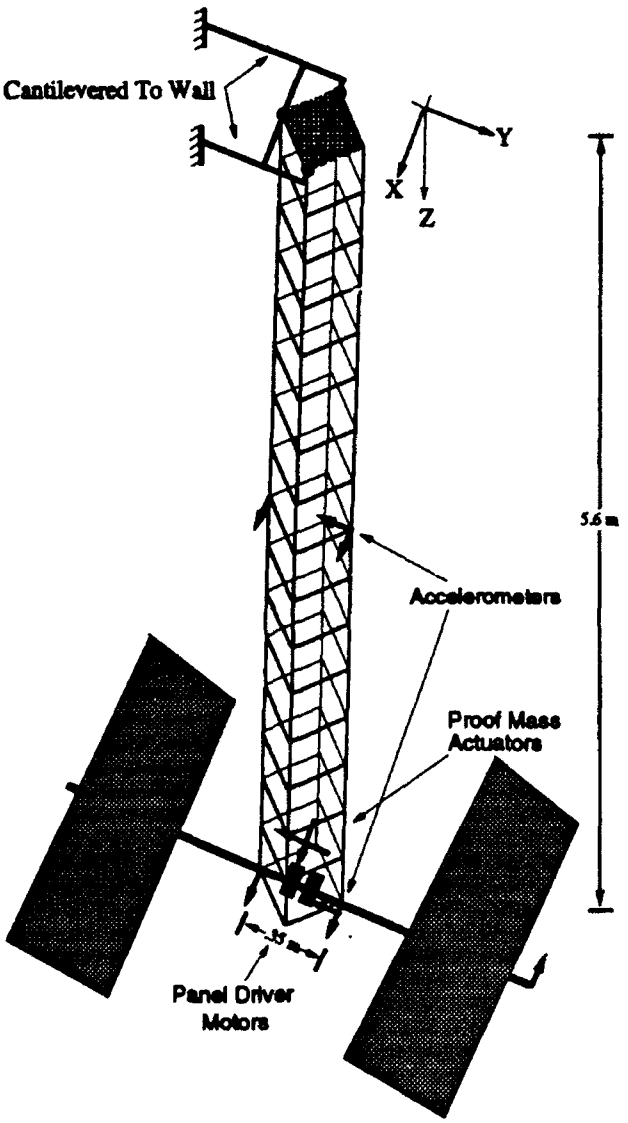

Figure 9.3: Ohio State flexible truss with attached panel assembly.

LIVE

Flexible Truss Controller Setup

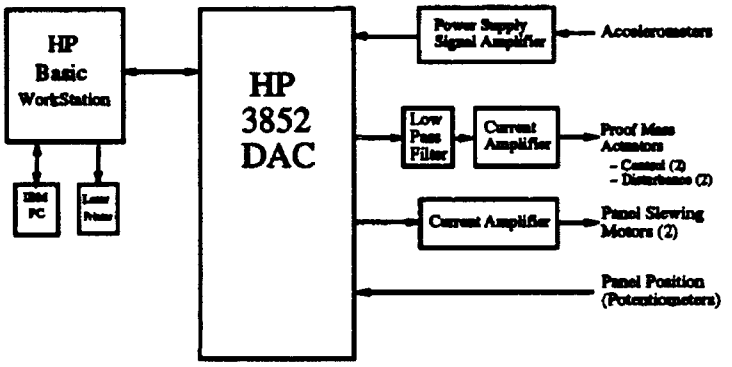

HP 3852 DAC Features

High Speed 68020 Processor with Numerical Coprocessor

256 K bytes On Board Memory

100 Khz A/D Converter with 24 Channel Multiplexer

4 Channel D/A Converter (Current and Voltage Output)

HPIB Communications Interface

Programmable in High Level Language

Prioritized Multitasking and Interrupt Capability

Figure 9.4: Block diagram of hardware configuration for LIVE.

9.4.1 Linearized System Model

The desired steady state solution can be obtained by solving

$$G(\theta_d, 0, q_{ss}, 0) = Bu_{ss} \tag{9.8}$$

Rewrite (9.7)

$$\begin{pmatrix} \ddot{\theta} \\ \ddot{q} \end{pmatrix} = h(\theta, \dot{\theta}, q, \dot{q}) + l(\theta, q)Bu \tag{9.9}$$

where $h(\theta, \dot{\theta}, q, \dot{q}) = -M^{-1}(\theta, q)G(\theta, \dot{\theta}, q, \dot{q})$ and $l(\theta, q) = M^{-1}(\theta, q)B$ assuming M is always invertible. Note that if q_{ss} and u_{ss} satisfy (9.8), then

$$h(\theta_d, 0, q_{ss}, 0) + l(\theta_d, q_{ss})Bu_{ss} = 0 \tag{9.10}$$

Define

$$\begin{aligned} e &= \theta - \theta_d \\ \epsilon &= q - q_{ss} \\ \tilde{u} &= u - u_{ss} \end{aligned}$$

The linearized system is obtained as:

$$\ddot{e} = a_1(\theta_d, 0, q_{ss}, 0)e + a_2(\theta_d, 0, q_{ss}, 0)\dot{e} + b(\theta_d, q_{ss})\tilde{u} + g(e, \dot{e}, \epsilon, \dot{\epsilon}, \tilde{u}) \tag{9.11}$$

where $a_1 = \frac{\partial h}{\partial \theta} + \frac{\partial l}{\partial \theta}$ and $a_2 = \frac{\partial h}{\partial \dot{\theta}}$ evaluated at the desired steady state point with $g(0, 0, 0, 0, 0) = 0$.

In the standard state space formulation,

$$\dot{x} = Ax + B\tilde{u} + H(x, \epsilon, \dot{\epsilon}) \tag{9.12}$$

$H(x, \epsilon, \dot{\epsilon})$ is the lumped representation of the parameter changes $\Delta A(x, \epsilon, \dot{\epsilon})$, $\Delta B(x, \epsilon, \dot{\epsilon})$, and unknown disturbances $f(t)$ due to ϵ, $\dot{\epsilon}$ and the neglected higher order terms in the linearization process.

An important property of H is that

$$H \longrightarrow 0 \quad as \quad e \to 0, \dot{e} \to 0, \epsilon \to 0, \dot{\epsilon} \to 0 \tag{9.13}$$

9.4.2 Numerical Example

We adopt an identical example of a single flexible robotic link as [38] and implement sliding mode control by using both continuous time design and sampled VSC design. The dynamic model is of the form:

$$\begin{bmatrix} J_1 + m_1 q^2 & b_{11} \\ b_{11} & m_1 \end{bmatrix} \begin{bmatrix} \ddot{\theta}_1 \\ \ddot{q}_1 \end{bmatrix} + \begin{bmatrix} 2m_1 q_1 & 0 \\ 0 & -m_1 q_1 \end{bmatrix} \begin{bmatrix} \dot{\theta}_1 \dot{q}_1 \\ \dot{\theta}_1^2 \end{bmatrix} + \begin{bmatrix} 0 \\ \mu_1 \dot{q}_1 + k_1 q_1 \end{bmatrix} + \begin{bmatrix} 0.5 m_1 l_1 \cos\theta_1 - a_{11} q_1 \sin\theta_1 \\ a_{11} \cos\theta_1 \end{bmatrix} g = \begin{bmatrix} u_1 \\ 0 \end{bmatrix}, \tag{9.14}$$

in which θ_1 is the angular displacement of the rigid mode, the end deflection is

$$p_1(t) = (h_1[l_1^2 + h_2 l_1^2(1 - l_1)])q_1(t).$$

We shall approximate the tip position by measuring the arc length of the rigid link together with the deflection length, i.e.,

$$L = \pi\theta_1 + p_1 \tag{9.15}$$

The following link parameter values are used.

$l_1 = 1m$	$J_1 = 0.4847Kg - m^2$	$a_{11} = 0.377Kg$
$\mu_1 = 0.373N - sec/m$	$m_1 = 0.4847Kg$	$b_{11} = 0.242Kg - m$
$k_1 = 28.7N/m$	$h_1 = 2.02$	$h2 = 0.6237$
$g = 9.8m/sec^2$		

The desired angular displacement set point is $\theta_1^d = \frac{\pi}{4}$. Steady state deflection and control input are obtained by solving

$$\begin{cases} (0.5 m_1 l_1 \cos\theta_1^d - a_{11} q_1^{ss} \sin\theta_1^d) g = u_1^{ss} \\ k_1 q_1^{ss} + a_{11} g \cos\theta_1^d = 0 \end{cases}$$

They are

$$q_1^{ss} = -0.0910 \quad u_1^{ss} = 1.9172$$

The linearized system has system matrices as in (9.12)

$$A = \begin{bmatrix} 0 & 1 \\ a_1 & 0 \end{bmatrix}; \quad B = \begin{bmatrix} 0 \\ b \end{bmatrix}$$

where

$$a_1 = \frac{(0.5m_1 l_1 \cos\theta_1^d - a_{11} q_1^{**} \sin\theta_1^d)g}{(J_1 + m_1(q_1^{**})^2)m_1 - b_{11}^2} \quad and \quad b = \frac{m_1}{(J_1 + m_1(q_1^{**})^2)m_1 - b_{11}^2}$$

The numerical values are

$$A = \begin{bmatrix} 0 & 1 \\ 0.3731 & 0 \end{bmatrix}; \quad B = \begin{bmatrix} 0 \\ 2.7182 \end{bmatrix}$$

Choose the sliding surface to be

$$s(t) = Ce - s(0)e^{-2t} = [1 \quad 1]e - s(0)e^{-2t}$$

with initial condition

$$\theta_1(0) = 0 \quad \dot{\theta}_1(0) = 0.1 \quad q_1(0) = -0.1787 \quad \dot{q}_1(0) = -0.1$$

The continuous time sliding mode design yield the following controller

$$\tilde{u} = -(CB)^{-1}Ae - Ksgn(s)$$

where K is selected to bound over all uncertainties.
The sampled sliding mode control law is

$$u_k = -(C\Gamma)^{-1}C\Phi x_k - (C\Gamma)^{-1}Cd_{k-1} + (C\Gamma)^{-1}s(0)e^{-2kT}$$

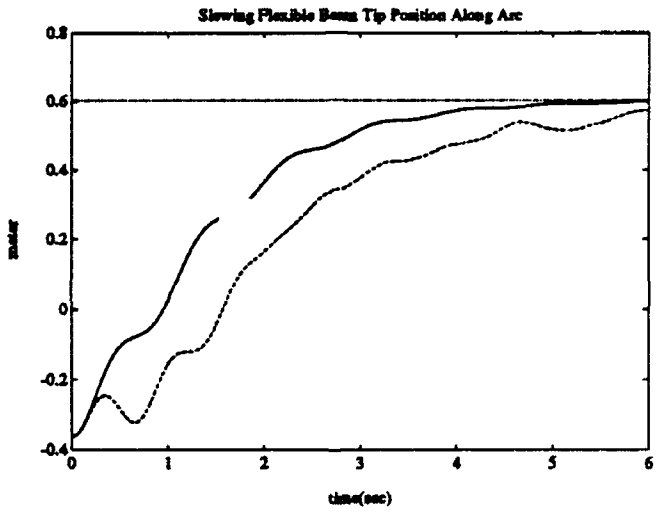

Figure 9.5: Comparison between Sampled VSC and the Discrete Implementation of Continuous Time VSC

10. CONCLUSION

The main thrust of this project has been to consider the control of interconnected rigid and flexible structures. Due to the fact that we distributed our attention to different modelling, analysis and design techniques, we have obtained many new results in different areas.

Conclusions obtained from individual aspects of our report are listed below, as they correspond to the chapters in this report:

In **Chapter 2** the work on the concept of *relegation* was outlined. We have provided the basis for assigning control tasks to multiple coupled systems so that some some total criterion is minimized. This approach will provide a systematic way of optimal regulation of coupled substructures, some flexible, some not, for vibration damping and slewing purposes.

Chapter 3 was on our initial work on *circuit analogies*. We believe this to be one of the most innovative ideas emerging from this project with many implications related to the design and implementation of "smart structures".

Chapter 4-6 all develop techniques that are useful in analyzing and controlling coupled nonlinear systems. Singular perturbation and sliding mode techniques are specifically applied to slewing, coupled flexible structures. Although these techniques are not new, they each had to be extended and various theoretical problems had to be resolved before they could be advocated for use in this area.

Chapter 6 furthermore develops modeling and control of closed–chain structures, where participants in a kinematic loop are all flexible. This is a very hard problem in its own right which, to our knowledge, had not been addresssed before.

In **Chapter 7** we provided initial results on the control of sampled systems with the sliding–mode control technique. The research has been very favorably reviewed by experts in the field. (In fact, the graduate student developing these ideas was rewarded with an Ohio State University Presidential Fellowship based on the letters of recommendation of external reviewers of his research work. This highly innovative approach is presently being further developed.

Finally in **Chapter 8** the utilization of neural networks for the identification and control was considered. This also was quite innovative, and was one of the first examples of the utilization of neural networks in the flexible structures/vibration damping domain.

The structure LIVE is a highly versatile hardware configuration that is still being developed, and will be a good test bed for future control verification studies.

REFERENCES

[1] Ü. Özgüner, "Decentralized/relegated control," in *Proceedings of the 1988 American Control Conference*, (Atlanta, Georgia), 1988.

[2] Ü. Özgüner and D. A. Schoenwald, "The concept of relegation for decentralized control," in *Proceedings of the 1990 IFAC World Congress*, (Tallin, Estonia), August 1990.

[3] D. A. Schoenwald and Ü. Özgüner, "Relegation for decentralized control of coupled systems," in *Proceedings of the 27th Annual Allerton Conference on Communication, Control, and Computing*, (Monticello, Illinois), pp. 421–428, September 1989.

[4] J. C. Geromel and J. Bernussou, "An algorithm for optimal decentralized regulation of linear quadratic interconnected systems," *Automatica*, vol. 15, pp. 489–491, 1979.

[5] J. C. Geromel and J. Bernussou, "Optimal decentralized control of dynamic systems," *Automatica*, vol. 18, no. 5, pp. 545–557, 1982.

[6] F. Khorrammi, S. Tien, and Ü. Özgüner, "DOLORES: a software package for analysis and design of optimal decentralized control," in *Proceedings of the 40th National Aerospace and Electronics Conference*, (Dayton, OH), May 1988.

[7] F. Khorrami and Ü. Özgüner, "Frequency-shaped cost functionals for decentralized systems," in *Proceedings of the IEEE Conference on Decision and Control*, (Austin, TX), December 1988.

[8] W. S. Levine, T. L. Johnson, and M. Athans, "Optimal limited state variable feedback controllers for linear systems," *IEEE Transactions on Automatic Control*, vol. AC-16, no. 6, pp. 785–793, 1971.

[9] P. V. Kokotović, W. R. Perkins, J. B. Cruz, and G. D'Ans, "ϵ-coupling method for near optimum design of large-scale linear systems," in *Proceedings of the IEE*, vol. 116, May 1969.

[10] Ü. Özgüner and W. R. Perkins, "A series solution to the Nash strategy for large-scale interconnected systems," *Automatica*, vol. 113, pp. 313–315, 1977.

[11] M. W. Spong, K. Khorasani, and P. V. Kokotović, "An integral manifold approach to the feedback control of flexible joint robots," *IEEE Transactions on Robotics and Automation*, vol. RA-3, no. 4, pp. 291–300, 1987.

[12] B. Siciliano and W. J. Book, "A singular perturbation approach to control of lightweight flexible manipulators," *International Journal of Robotics Research*, vol. 7, no. 4, pp. 79–90, 1988.

[13] S. Nicosia, P. Tomei, and A. Tornambè, "Nonlinear control and observation algorithms for a single-link flexible robot arm," *International Journal of Control*, vol. 49, pp. 827–840, 1989.

[14] A. De Luca and B. Siciliano. "Trajectory control of a non-linear one-link flexible arm," *International Journal of Control*, vol. 50, no. 5, pp. 1699–1715, 1989.

[15] F. Khorrami, *Asymptotic perturbation and Lyapunov stability based approaches for control of flexible and rigid robot manipulators.* PhD thesis, The Ohio State University, Columbus, OH, 1988.

[16] D. A. Schoenwald, Ü. Özgüner, and H. Chan, "An analysis of distributed vibration control of flexible manipulators using integral manifolds," in *Proceedings of the 28th IEEE Conference on Decision and Control*, (Tampa, FL), pp. 2095–2100, 1989.

[17] D. A. Schoenwald and Ü. Özgüner, "Control of flexible robotics via singular perturbations and distributed vibration damping," Control Research Laboratory Technical Report #1062-W92-R, Department of Electrical Engineering, The Ohio State University, Columbus, OH, 1992.

[18] X. Ding, T. J. Tarn, and A. K. Bejczy, "A novel approach to the dynamics and control of flexible robot arms," in *Proceedings of the 27th IEEE Conference on Decision and Control*, (Austin, TX), pp. 52–57, December 1988.

[19] F. Khorrami and S. Zheng, "Vibration control of flexible-link manipulators," in *Proceedings of the 9th American Control Conference*, (San Diego, CA), pp. 175–180, 1990.

[20] V. A. Sobolev, "Integral manifolds and decomposition of singularly perturbed systems," *Systems & Control Letters*, vol. 5, pp. 1169–1179, 1984.

[21] B. Siciliano, W. J. Book, and G. De Maria, "An integral manifold approach to control of a one link flexible arm," in *Proceedings of the 25th IEEE Conference on Decision and Control*, (Athens, Greece), pp. 1131–1134, 1986.

[22] B. Siciliano, A. J. Calise, and V. R. P. Jonnalagadda, "Optimal output fast feedback in two-time scale control of flexible arms," in *Proceedings of the 25th IEEE Conference on Decision and Control*, (Athens, Greece), pp. 1400–1403, 1986.

[23] P. V. Kokotović, H. K. Khalil, and J. O'Reilly, *Singular Perturbation Methods in Control: Analysis and Design.* London: Academic Press, 1986.

[24] A. G. Chassiakos and G. A. Bekey, "On the modelling and control of a flexible manipulator arm by point actuators," in *Proceedings of the 25th IEEE Conference on Decision and Control*, (Athens, Greece), pp. 1145–1150, December 1986.

[25] E. Barbieri, *Modelling and control of planar flexible structures with application to an optical-tracking system.* PhD thesis, The Ohio State University, Columbus, OH, 1988.

[26] T. Bailey and J. E. Hubbard, Jr., "Distributed piezoelectric-polymer active vibration control of a cantilever beam," *Journal of Guidance and Control*, vol. 8, no. 5, pp. 605–611, 1985.

[27] S. E. Burke and J. E. Hubbard, Jr., "Active vibration control of a simply supported beam using a spatially distributed actuator," *IEEE Control Systems Magazine*, vol. 7, no. 4, pp. 25–30, 1987.

[28] S. E. Burke and J. E. Hubbard, Jr., "Distributed actuator control design for flexible beams," *Automatica*, vol. 24, no. 5, pp. 619–627, 1988.

[29] E. F. Crawley and J. de Luis, "Use of piezoelectric actuators as elements of intelligent structures," *Proceedings of the AIAA Guidance, Navigation, and Control Conference*, vol. 25, no. 10, pp. 1371–1385, 1987.

[30] D. A. Schoenwald and Ü. Özgüner, "On combining slewing and vibration control in flexible manipulators via singular perturbations," in *Proceedings of the 29th IEEE Conference on Decision and Control*, (Honolulu, Hawaii), 1990.

[31] S. Yurkovich, A. P. Tzes, and K. L. Hillsley, "Controlling coupled flexible links rotating in the horizontal plane," in *Proceedings of the 9th American Control Conference*, (San Diego, CA), pp. 362–367, 1990.

[32] R. Wynn, H. Robertshaw, and C. Horner, "An analytical study of a six degree-of-freedom active truss of use in vibration control," in *Proc. AIAA/ASME/ASCE/AHS/ASC 31st Structures, Structural Dynamics, and Materials Conf.*, (Long Beach, CA), April 1990.

[33] S. Matunaga, K. Miura, and M. Natori, "A construction concept of large space structures using intelligent/adaptive structures," in *Proc. AIAA/ASME/ASCE/AHS/ASC 31st Structures, Structural Dynamics, and Materials Conf.*, (Long Beach, CA), April 1990.

[34] K. K. D. Young, "Controller design for a manipulator using theory of variable structure systems," *IEEE Transactions on Systems, Man, and Cybernetics*, vol. SMC-8, pp. 101–109, Feb. 1978.

[35] R. Morgan and Ü. Özgüner, "A decentralized variable structure control algorithm for robotic manipulators," *IEEE Trans. Robotics and Automation*, vol. RA-1, no. 1, pp. 57–65, March 1985.

[36] J. J. E. Slotine and S. Sastry, "Tracking control of nonlinear systems using sliding surfaces, with application to robotic manipulators," *Int. J. of Control*, vol. 38, pp. 465–492, 1983.

[37] U. Özgüner, S. Yurkovich, and F. Al-Abbass, "Decentralized variable structure control of a two–arm robotic system," *Journal of Robotic Systems*, vol. 4, pp. 377–395, June 1987.

[38] K. Young and Ü. Özgüner, "Frequency shaped sliding mode synthesis," in *Proc. International Workshop on Variable Structure System and Their Applications*, 1990.

[39] U. Özgüner, S. Yurkovich, and F. Al-Abbass, "Decentralized variable structure control of a two–arm robotic system," in *Proceedings of the IEEE International Conference on Robotics and Automation*, (Raleigh, NC), Mar. 1987.

[40] H. Hemami, "A state space model for interconnected rigid bodies," *IEEE Transactions on Automatic Control*, vol. AC-27, Apr. 1982.

[41] H. Hemami and B. F. Wyman, "Modeling and control of constrained dynamic systems with application to biped locomotion in the frontal plane," *IEEE Transactions on Automatic Control*, vol. AC-24, Aug. 1979.

[42] M. A. Boesch, "Design and modeling aspects of a rapid deployment truss structure," Master's thesis, The Ohio State University, Columbus, OH, December 1990.

[43] V. Utkin and K. Young, "Methods for constructing discontinuous planes in multidimensional variable structure systems," *Automation and Remote Control*, vol. 31, pp. 1466–1470, 1978.

[44] H. Öz and Ü. Özgüner, "Variable structure system conytol of flexible spacecraft," in *Proceedings of the AIAA/AAS Astrodynamics Conference*, (Seattle, WA), 1984.

[45] K. Young and S. Drakunov, "Sliding mode control with chattering reduction," in *Proceedings of the 1992 American Control Conference*, (Chicago, IL), pp. 1291–1292, June 1992.

[46] H. Kwatny and T. Siu, "Chattering in variable structure feedback systems," in *10th World Congress on Automatic Control Preprints*, (Munich), pp. 385–400, 1987.

[47] K. Furuta, "Sliding mode control of a discrete system," *Systems and Control Letters*, vol. 14, pp. 145–152, 1990.

[48] S. Sarpturk, Y. Istefanopulos, and O. Kaynak, "On the stability of discrete-time sliding mode control systems," *IEEE Trans. Automat. Contr.*, vol. AC-32, no. 10, pp. 930–932, October 1987.

[49] V. Utkin and S. Drakunov, "On discrete-time sliding modes," in *Preprints of IFAC Workshop on Nonlinear Control*, (Capri, Italy), 1989.

[50] C. Chan, "Servo-systems with discrete variable structure control," *Systems and Control Letters*, vol. 17, pp. 321–325, 1991.

[51] H. Sira-Ramirez, "Nonlinear discrete variable structure systems in quasi-sliding mode," *Int. J. Control*, vol. 54, no. 5, pp. 1171–1187, 1991.

[52] V. Utkin and K. Young, "Methods for constructing discontinuity planes in multidimensional variable structure systems," *Automation and Remote Control*, vol. 39, pp. 1466–1470, 1979.

[53] S. V. Drakunov and V. I. Utkin, "Sliding modes in dynamic systems," *International Journal of Control*, vol. 55, no. 4, pp. 1029–1037, 1992.

[54] Ü. Özgüner and K. Young, "Frequency shaped variable structure control," in *Proceedings of the 1990 American Control Conference*, (San Diego, CA), May 1990.

[55] W. Li and J.-J. E. Slotine, "Neural network control of unknown nonlinear systems," in *Proceedings of the American Control Conference*, (San Diego, CA), pp. 1136–1141, 1990.

[56] M.-S. Lan, "Adaptive control of unknown dynamical systems via neural network approach," in *Proceedings of the American Control Conference*, (Pittsburgh, PA), pp. 910–915, 1989.

[57] M. B. Leahy, Jr., M. A. Johnson, and S. K. Rogers, "Neural network payload estimation for adaptive robot control," *IEEE Transactions on Neural Networks*, vol. 2, pp. 93–100, Jan. 1991.

[58] K. J. Åström and B. Wittenmark, "On self-tuning regulators," *Automatica*, vol. 9, pp. 185–199, 1973.

[59] Y. Iiguni, H. Sakai, and H. Tokumaru, "A nonlinear regulator design in the presence of system uncertainties using multilayered neural networks," *IEEE Transactions on Neural Networks*, vol. 2, pp. 410–417, July 1991.

[60] D. Schoenwald, J. T. Feddema, G. R. Eisler, and D. J. Segalman, "Minimum-time trajectory control of a two-link flexible robotic manipulator," in *Proceedings of the IEEE International Conference on Robotics and Automation*, (Sacramento, CA), pp. 100–105, Apr. 1991.

[61] W. J. Book, "Recursive lagrangian formulation of flexible manipulator arms," *International Journal of Robotics Research*, vol. 3, pp. 87–101, Oct. 1984.

[62] R. H. Canon and E. Schmitz, "Initial experiments on the end-point control of a flexible one-link robot," *International Journal of Robotics Research*, vol. 3, no. 3, pp. 62–75, 1984.

[63] E. Barbieri and Ü. Özgüner, "Unconstrained and constrained mode expansions for a flexible slewing link," *Transactions of the ASME*, vol. 110, pp. 416–421, Dec. 1988.

[64] P. T. Kotnik, S. Yurkovich, and Ü. Özgüner, "Acceleration feedback for control of a flexible manipulator arm," *Journal of Robotics*, vol. 5, no. 3, pp. 181–196, 1988.

[65] A. P. Tzes, *Self-Tuning Controllers for Flexible Link Manipulators.* PhD thesis, The Ohio State University, Columbus, OH, Aug. 1990.

[66] D. Schoenwald and Ü. Özgüner, "An analysis of distributed vibration control of flexible manipulators using integral manifolds," in *Proceedings of the IEEE Conference on Decision and Control*, (Tampa, FL), Dec. 1989.

[67] C. M. Oakley and R. H. Cannon, Jr., "End-point control of a two-link manipulator with a very flexible forearm: Issues and experiments," in *Proceedings of the American Control Conference*, (Pittsburgh, PA), pp. 1381–1388, 1989.

[68] A. Isidori, *Nonlinear Control Systems.* Communications and Control Engineering Series, Berlin: Springer-Verlag, 2nd ed., 1989.

[69] G.-J. Wang and D. K. Miu, "Unsupervising adaption neural network control," in *Proceedings of the International Joint Conference on Neural Networks*, vol. 3, pp. 421–428, *1990.*

[70] D. E. Rumelhart, G. E. Hinton, and R. J. Williams, *Parallel Distributed Processing: Explorations in the Microstructure of Cognition, Volume 1: Foundations.* Cambridge, MA: MIT Press, 1986.

[71] M. Athans, "The role and use of the stochastic Linear-Quadratic-Gaussian problem in control systems design," *IEEE Transactions on Automatic Control*, vol. AC–16, pp. 529–552, Dec. 1971. Special issue with several other papers on the quadratic regulator problem.

[72] M. I. Jordan, "Generic constraints on underspecified target trajectories," in *Proceedings of the International Joint Conference on Neural Networks*, vol. 1, (Washington, DC), pp. 217–225, 1989.

[73] S. C. Ahalt, P. Chen, and C.-T. Chou, "The Neural Shell: A neural network simulation tool," in *Tools for Artificial Intelligence*, (Herndon, VA), pp. 118–124, Nov. 1990.

[74] E. Barbieri, Ü. Özgüner, and S. Yurkovich, "Vibration compensation in optical tracking systems," *Journal of Guidance and Control*, vol. 12, May 1989.

A. List of Publications Based on Project

Chapters in Books

1. "Variable Structure Control of Flexible Manipulators", in *Variable Structure Control for Robotics and Aerospace Applications*, Elsevier, 1993, Ed: D. Young. (D. Young, Ü. Özgüner and J-X. Xu)
2. "Variable Structure Control of Redundant Mechanisms", in *Variable Structure Control for Robotics and Aerospace Applications*, Elsevier, 1993, Ed: D. Young. (D. Young, J-X. Xu and Ü. Özgüner)

Journal Publications

1. "Synthesis of Feedback Linearization and Variable Structure Control with Neural Net Compensation," *Asia-Pacific Engineering Journal (Part A)*, Vol.2, No.1, pp17-29, 1992, (J-X. Xu, J. Donne and Ü. Özgüner).
2. "Neural Control of Flexible Systems with Partially Known Dynamics," *Modelling and Scientific Computing, Special Issue on: Neural Networks for Identification and Control of Dynamical Systems*, to appear 1993, (J. Donne, J-X. Xu and Ü. Özgüner).
3. "Frequency Shaped Sliding Mode Synthesis", *International Journal of Control*, to appear 1993, (D. Young and Ü. Özgüner).

Conference Publications and Presentations

1. "Relegation for Decentralized Control of Coupled Systems", *Proc. 1989 Allerton Conference*, Monticello Ill., September 1989, (D. Schoenwald and Ü. Özgüner).
2. "An Analysis of Distributed Vibration Control of Flexible Manipulators Using Integral Manifolds", *Proceedings of the IEEE Conference on Decision and Control*, Tampa, FL (December 1989). (D. Schoenwald and Ü. Özgüner)
3. "Frequency Shaped Sliding Mode Synthesis", (D. Young and Ü. Özgüner), Workshop on Variable Structure Systems Control, Yugoslavia, April 1990.
4. "Frequency Shaped Variable Structure Control", (D. Young and Ü. Özgüner), Proc. 1990 ACC, San Diego, CA, May 1990.
5. "The Concept of Relegation for Decentralized Control", (Ü. Özgüner and D. Schoenwald), Proc. of the 1990 IFAC Congress, August 1990, Talinn, Estonia.

6. "Modeling and Control of Rapid Deployment Truss Structure Systems", *28th Annual Allerton Conference on Communication, Control and Computing*, October 1990, (M. Boesch, K. Xu and Ü. Özgüner).

7. "On Combining Slewing and Vibration Control in Flexible Manipulators Via Singular Perturbations", *Proceedings of the 29th IEEE Conference on Decision and Control*, Honolulu, Hawaii, December 1990 (D. Schoenwald and Ü. Özgüner).

8. "Dynamic Modeling and Control of a Rigid–Flexible Closed–Chain Structure," *Proceedings of the 8th VPI&SU/AIAA Symposium on Dynamics and Control of Large Space Structures*, Blacksburgh, VA (May 1991) (J-X. Xu, Ü. Özgüner and K. D. Young).

9. "Variable Structure Control of Rigid–Flexible Closed–Chain Systems," Proc. 1991 ACC, Boston MA, June 1991. (J-X. Xu, Ü. Özgüner and K. D. Young).

10. "Modeling and Control of Large Space Structures Using Circuit Analogies," Proc. 1991 Guidance, Navigation and Control, New Orleans, LA, Aug. 1991. (L. Lenning and Ü. Özgüner).

11. "Synthesis of Feedback Linearization and Variable Structure Control with Neural Net Compensation," Proc. 1991 IFAC Symp. on DIS & 1991 IEEE International Symp. on Intelligent Control, Arlington VA, Aug. 1991. (J-X. Xu, J Donne and Ü. Özgüner).

12. "The Intelligence Between Sensing and Actuation for Smart Structures," Conf. on *Active Materials and Adaptive Structures,* Nov. 1991, Alexandria VA, (Ü. Özgüner and L. Lenning). Proceedings: G. Knowles Ed., pp. 824–830, Institute of Physics Publishing, 1992.

13. "Some Issues in Decentralized Control of Nonlinear Systems," 30th IEEE CDC, December 1991, Brighton, England. (D. Schoenwald and Ü. Özgüner).

14. "Vibration Suppression in Flexible Structures," Proc. NASA Workshop on *Distributed Parameter Modeling and Control of Flexible Aerospace Systems*, Williamsburg, Virginia, June 1992, (S. Drakunov and Ü. Özgüner)

15. "Optimization of Nonlinear System Output via Sliding–Mode Approach," IEEE Workshop on *Variable Structure and Lyapunov Control of Uncertain Dynamical Systems,* September 1992, University of Sheffield, UK, (S. Drakunov and Ü. Özgüner)

16. "Vibration Suppression in Flexible Structures via the Sliding–Mode Control Approach," IEEE Workshop on *Variable Structure and Lyapunov Control of Uncertain Dynamical Systems,* September 1992, University of Sheffield, UK, (S. Drakunov and Ü. Özgüner)

17. "Decentralized Sliding-Mode Observers for Interconnected Nonlinear Systems," IEEE Workshop on *Variable Structure and Lyapunov Control of Uncertain Dynamical Systems,* September 1992, University of Sheffield, UK, (S. Drakunov, Ü. Özgüner and D. Schoenwald)

18. "Experiments on a Truss-Panel Structure," Proc. 1992 ACC, Chicago IL, June 1992. (Ü. Özgüner and K. Redmill).

19. "Robust Feedback Linearization of Uncertain Nonlinear Systems," Proc. 1992 ACC, Chicago IL, June 1992. (D. Schoenwald and Ü. Özgüner).

20. "Neural Control of Flexible Systems with Partially Known Dynamics," Proc. 1992 IEEE International Symposium on Intelligent Control, Glasgow, Scotland, UK, August 1992, (J. Donne, J-X. Xu and Ü. Özgüner).

21. "A Decentralized Approach for Autonomous Structural Control," *Autonomous Structural Control Symposium*, August 1992, USAF Academy, Colorado.

22. "Variable Structure Control in Sampled Systems," *NSF/OAI Workshop on Variable Structure Control*, October 1992, Brook Park, OH.

23. "Optimal Control of Feedback Linearizable Systems," Proc. 1992 CDC, Tucson Arizona, (D. Schoenwald and Ü. Özgüner).

24. "Vibration Suppression in Flexible Structures via the Sliding-Mode Control Approach," Proc 1992 CDC, Tucson Arizona, (S. Drakunov and Ü. Özgüner).

25. "Distributed Hierarchical Architecture for Structural Control," Proc. North American Conf. on *Smart Structures and Materials*, 1-4 Feb. 1993, Albuquerque, New Mexico.

26. "Use of Neural Networks and Sliding Modes in Vibration Damping," Proc. North American Conf. on *Smart Structures and Materials*, 1-4 Feb. 1993, Albuquerque, New Mexico.

Under Review

1. "Robust Stabilization of Nonlinear Systems with Parametric Uncertainty," submitted to *IEEE Trans AC*, 1993, (D. Schoenwald and Ü. Özgüner).

2. "Optimal Control of Feedback Linearizable Systems," submitted to *IEEE Trans AC*, 1993, (D. Schoenwald and Ü. Özgüner).

3. "Decentralized Control of Uncertain Systems Via Sensitivity Models," submitted to *Automatica*, 1993, (D. Schoenwald and Ü. Özgüner).

4. "The Concept of Relegation for Decentralized Control," submitted to *Automatica*, 1993, (D. Schoenwald and Ü. Özgüner).

5. "Flexible Manipulator Control Using Integral Manifolds and Distributed Vibration Damping," submitted for publication, 1993, (D. Schoenwald and Ü. Özgüner).

B. List of Students Supported

David Schoenwald	Ph.D.	- completed Dissertation title: "Analysis and Design of Robust Decentralized Controllers for Nonlinear Systems," 1992 (partial support from Ohio Aerospace Institute)
Peter Dix	M.S.	- completed Thesis title: "Vibration Control for Large Space Structures Using Traveling Wave Modeling," 1990 (partial support from AFWL)
Mathew Boesch	M.S.	- completed Thesis title: "Design and Modeling Aspects of a Rapid Deployment Truss Structure," 1990 (partial support from LLNL)
Layne Lenning	M.S.	- completed Thesis title: "Circuit Analogies for Modeling and Control of Large Flexible Structures," 1991 presently continuing towards Ph.D.
Wu-Chung Su		- presently continuing towards Ph.D.